NTNU – Trondheim
Norwegian University of
Science and Technology

Arctic Coastal Erosion

Thomas Gerard Dormoy

Geotechnics and Geohazards
Submission date: June 2014
Supervisor: Steinar Nordal, BAT
Co-supervisor: Read Lubbad, BAT

Norwegian University of Science and Technology
Department of Civil and Transport Engineering

Thomas Dormoy

Arctic Coastal Erosion

Numerical tools for thermal analysis of the erosion process in arctic coast

Master's thesis in Geotechnical Engineering

Trondheim, June 2014

Supervisor : Steinar Nordal

Norwegian University of Science and Technology
Faculty of Engineering Science and Technology
Department of Civil and Transport Engineering

NTNU – Trondheim
Norwegian University of
Science and Technology

Abstract

With the recent increase of interest in Arctic, the need rises for new tools for understanding the typical mechanisms of this very unique and so vulnerable area. The coast, which concentrates nearly all of the human activities, is in the front line and probably the most critical part of the system. Trough the past decades, mappings of the Arctic's shorelines point out huge erosion rates and show the threat of a climate change upon the coast.

Recent studies seem to link those tremendous moves to the annual thermal variations within the soil. However, the mechanisms of thermal abrasion that are suggested to be at the hearth of the process are not yet completely understood.

In answer for the need of numerical models for thermal analysis of the erosion process, this thesis proposes a toolbox specially designed, based on literature review and fieldwork data. Trough the chapters, the reader shall find essential tools for estimations of the heat transfer into a soil and complete understanding of the physical mechanisms behind. Critical parameters that influence the erosion process are highlighted.

To assess the operational deployment of those tools, a thermal analysis of a site has been performed. The conclusions demonstrate the capacity of numerical models to underline the critical gears of the heat transfers, and hopefully will help understanding the erosion processes of this particular place.

Preface

This thesis is the outcome of my yearlong stay at Trondheim, at the final stage of my civil engineer training. After four years spent in Lyon at the National Institute of Applied Sciences (INSA), I decided to explore new fields of application for my competences. This led me to the Norwegian University of Science and Technology (NTNU), Trondheim, where I discovered Arctic technologies and coastal engineering. Into the first four months I was in Norway, I became fascinated by the huge challenges faced by researchers and engineers in the Artic field and aspired at bring my modest contribution. Trough this paper, I hope to demonstrate the wide knowledge and skills this adventure brought me. However, this adventure would not have been possible without the immense help and encouragement from many professors, students, friends and family. I would like to write my acknowledgment to them.

Steinar Nordal, you are as good a supervisor as I could have had. Your enthusiasm and guidance, not only during those last 22 weeks but also trough my first months in Trondheim, where invaluable. It was your doing to push me toward SAMCoT and the incredible people I met there. To Raed Lubbad also, my co-supervisor who introduced me to coastal engineering and managed to fascinate me with this field completely new to me. Thank you both.

Emilie Guegan, my thesis would not have any purpose if not for you. You are an infinite source of knowledge in your field, and completely mind-blowing when you share them. I hope to return the favor by bringing my modest contribution to your work. It has been a pleasure working with you.

I have been fortunate to meet and work with some of the most advanced searchers in the Artic Technology field, whose discussions and ideas where of great help. Anatoly Sinitsyn, you made my fieldwork in Longyearbyen a great moment and the collection of data would have not be possible of not for the spadesful of snow you removed. Nina Ganicheva, thank you for protecting me against the polar bear. Anateneh Tsegaye, you “champion”, I am grateful for the mind-blowing discussions and inexhaustible questioning.

A thank you must also go out to NTNU, SAMCoT and UNIS, for their unfailing support and the tools they provided me.

And last but not least, I would acknowledge my friends, family, and all other colleagues whose name have not been mentioned here. If not for you, I would not have enjoyed this adventure so much !

Trondheim, June 2014

Contents

List of figures

page

List of tables

1. Introduction

1.1. Motivation

This Master Thesis has been written in order to support research activities in Arctic area, and in particular the Research Based Innovation Centre "Sustainable Arctic Coastal and Marine Technology" (SAMCoT) hosted at the Norwegian University of Science and Technology (NTNU), Trondheim, Norway. SAMCoT activities are divided in 6 work packages :

- WP 1 : Collection and analysis of field data and properties
- WP 2 : Material modeling
- WP 3 : Fixed structures in ice
- WP 4 : Floating structures in ice
- WP 5 : Ice management and design philosophy
- WP 6 : Coastal technology

This paper belongs to WP 6, Coastal technology, and more specifically the task 6.1 of the work package : Erosion Rates and Mechanisms in Coastal Permafrost.

Recent interest in Artic area, motivated by the huge potential for industry as well as the great vulnerability to climate change, leads to an increased need for tools for understanding the specific mechanisms at work. In particular, the need for a thermal analysis numerical tool was emphasized by PhD candidate E. Guegan, at the front line of the research in the field.

The Master started 27th January and will be submitted the 30th of June.

1.2. Background

Because of the harsh conditions in arctic areas, including the lack of a terrestrial transportation network and the huge dependence to the sea for supplying, the large majority of human activities are concentrated in coastal areas. Thus, the high vulnerability of the shore to erosive processes, especially in a context of rapid climate change and warming of permafrost, represents a critical concern for the economy and well being of the arctic communities.

Arctic coasts vary greatly in morphology and geological history but are characterized by the presence of permafrost and sea ice. Sea ice and shorefast ice generally protect the shoreline by limiting wave-based erosion however, during ablation tall fast ice can facilitate erosion by blocking outflow of water leading to outwashing of storm ridges (Rodzik and Zagorski, 2009). Shorefast ice can also lead to abrasion (Caline, 2010). However, the most impressive mechanism, which shall be studied in this paper, is thermal abrasion.

During their investigation of 61 000 km of Artic coasts, Lantuit et al. (2012) reported an average erosion rate of 0,5 m/year. This average is derived from a number of regional rates of which Svalbard is the lowest and the American Beaufort Sea the highest, returning 0 m/yr and 1.15 m/yr, respectively. Erosion rates up to 2m/year have been evidenced in the Beaufort Sea (Jorgenson and Brown, 2005). This difference is suggested to come directly from the observation that Svalbard coasts have an "overwhelmingly rocky nature" with "virtually no visible ground ice" whereas the American Beaufort Sea has extensive unconsolidated coastlines containing massive ground ice thereby contributing through active layer detachments and retrogressive thaw slumping (Lantuit et al., 2012, Lantuit et Pollard, 2008).

If the monitoring of the coastal zone started few decades ago the understanding of the physical and mechanical processes behind it is a much more recent research interest. While both thermal and mechanical action are commonly accepted to work simultaneously on the erosion processes, most of the studies consider waves action as the main eroding forces and limit the erosion period to the sea-ice free period of the year (Guegan, submitted). Meanwhile, this study will focus on the thermal processes leading to the thawing slope instability.

1.3. Objectives

The primary objective of this Master thesis is to develop a tool for thermal analysis of arctic shores. This tool shall be based on TempW, a Finite Element Method calculation software made available by the University Center in Svalbard (UNIS).

In the second chapter, a global presentation of the different erosion mechanisms shall be made. The third and fourth chapter shall present the specific parameters and physical laws that rule heat transfer in the soil. Particular attention shall be observed for thermal conductivity estimations and the soil characteristics that can influence the temperature changes trough it. The fifth chapter shall describe succinctly how thawing affects slope stability. Unfortunately, no time was left to perform a proper slope stability analysis. The sixth and seventh chapters shall present the numerical tools that will be developed and tested. The sixth chapter will focus on new hand calculation tools, while the seventh will focus on TempW. In the eighth and ninth chapters will be respectively the introduction and results of the tests performed in order to verify the accuracy of the analysis tools developed in the sixth chapter. Finally, the tenth chapter shall present a confrontation of the developed tools with an actual shorefront at Vestpynten (Svalbard).

2. Identification of erosion mechanisms

A coast is a specific environment at the cross point of three systems - the land, the sea and the atmosphere. The reshaping process is a result of the mechanisms of those systems combined, which makes it very dynamic. Primarily, the coast is an exchange area between land and sea. Sediments or rocks moved by rivers and glaciers are accumulated on the shore and carried into the sea. In some areas, at the opposite, sea currents and waves accumulate sedimentary materials on the shore that adds to the landmass. The focus here is on the processes moving the soil materials on the shore into the sea.

The geomorphologic shape of the shore depends on the soil material at hand in the area, as well as climatic and sea conditions. There are two main types of shore land materials : sediments and rocks. Sediment coasts usually forms gentle slopes with a small bluff, while rock coasts presents a cliff up to several tens of meters, whit or without a beach at the foot.

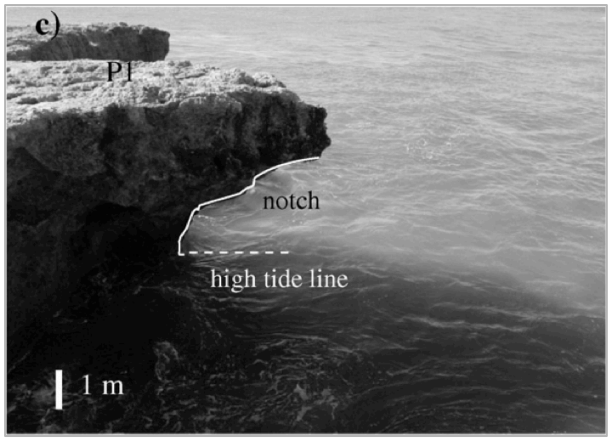

fig. 1 : rock platform with notch, Algarve coast (Portugal), courtesy Moura et al. (2006) via ScienceDirect

Those two morphologies reflect the erosion process behind. While most sediment obey to slope stability mechanisms and are in constant equilibrium between the sea actions and their own cohesion, rock cliffs are sculpted by block failures of various scales.

2.1. Erosion processes

This paragraph is an attempt to explain the different erosion processes observed in coastal areas. For a better understanding, one may refer to the literature review (Lim et al., 2010), (Davidson-Arnott, 2010).

2.1.1. Rock shore

Rock cliff erosion obeys to a wide range of factors, including waves, wind, chemical attacks, vegetation and human activity. Cracks form and develop in the rock under the action of these elements, until a failure point is reached and a part of the cliff collapse. Although this phenomenon is fairly easy to describe, the fact that it is very local in time and place makes it difficult to model on the scale of the entire shore. Rock cliff has been observed to remain

unchanged over a long period of time, and then retreat rapidly in a short event. This erratic and seemingly unpredictable event is often described by the term “episodicity” (Lim et al., 2010).

Because of this complexity, current modeling methods are based on statistical observations (Teixeira, 2006). However, because of the relatively slow and very irregular erosion process of rocky shores, statistically significant sets of data are very long to obtain and thus still rare.

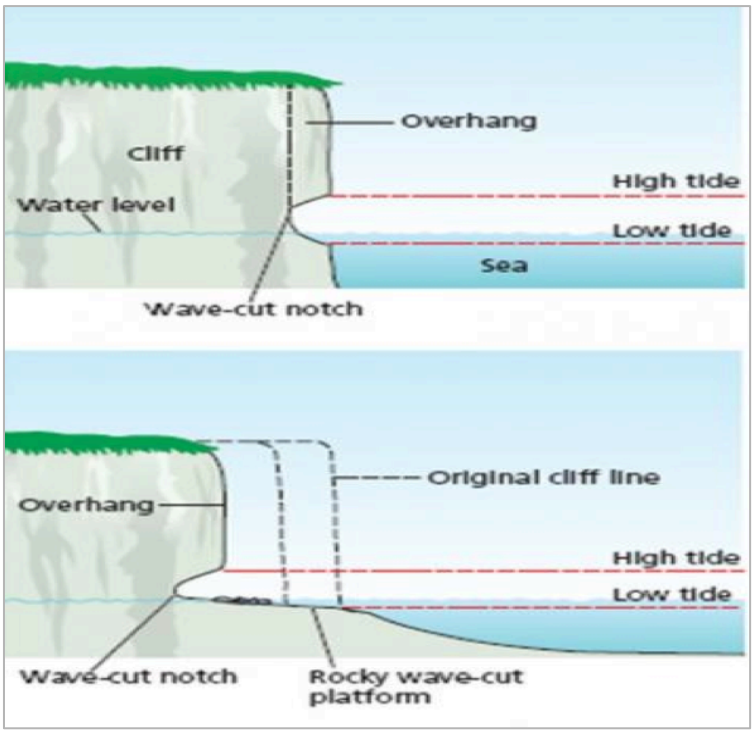

Fig. 2 : cliff erosion by wave carving at the footing, courtesy Geography GCSE

In most cases, rock cliffs are attacked at the foot by the wave actions. Although the wave energy while breaking on a cliff is hard to compute or measure, it can be tremendous, enough to slowly break chunks of rock and drill a notch. Once this wave-cut notch is deep enough, a plastic surface is created under the weight of the overhang, often following local weaknesses in the rock. This process is described in the figure 2.

A very typical erosion mechanism is karstification, a chemical process in carbonate rocks due to water. Rainwater enters the rock via originally present cracks, and initiate a chemical reaction with CO_2 and calcium carbonate ($CaCO_3$), enlarging the crack until it forms wide holes (or caves) in the rock. This phenomenon gives birth to very surprising features such as arches (e. g. on the “côte sauvage” in France).

2.1.2. Sedimentary shore

On sedimentary shore, the shape is the result of a constant struggle between the soil stability, governed by cohesion and friction, and the effects of elements such as wind and waves. Erosion rates are generally higher than for rocky shores because the mechanical properties are lower, but huge differences exist between different configurations, for this process is widely dependent on the shore topography and exposure.

The continuous balance between sediment deposit and removal of material by sea current and waves leads to erosion rates rather constant. However, punctual events such as storms can brutally increase the land retreat.

fig. 3 : silty shore at Camden Bay, courtesy Kanevskiya et al. (2013) via ScienceDirect

The approach developed in this thesis is to consider a typical ground slope stability problem. Although sea actions obviously play a big role in shaping the coast, the shore profile will be taken for known and the analysis will be performed on a steady geometry.

2.2. Specificity of the artic coasts, thermal abrasion

The arctic coasts are characterized by the presence of permafrost, both onshore and offshore, and the presence of sea ice that impeach wave action during 8-9 month per year (Lantuit et al. 2012). The presence of frozen soil can be a factor of stability, as ice content generally improves mechanical properties, but also leads to specific erosion processes.

Thermal abrasion is a process in which the soil integrity is destroyed by frost action. In rocky soils, the water trapped in the cracks expands while freezing, thus enlarging the crack until it causes a block failure. This phenomenon leads to sharp featured cliffs, with or without a beach at the foot composed of the crushed rock blocks. In sedimentary soils, the effect is less spectacular but is equally or more efficient. Studies of landslides in Canada (McRoberts and Morgenstern, 1974) evidenced that the excess of water during thawing disturb the inner equilibrium and decreases the inter-particle friction and cohesion. The natural material tendency to reach a new equilibrium with a gentler slope combined with the washing effect of the waves reshapes the coast. Exceptional storm events have been observed to cause coast retreat of 10 m in the same year in silt/clay soils (Jorgenstern and Brown, 2005).

This thesis shall focus onto the thermal abrasion in sedimentary soils. Although the main topic concern the heat transfers that leads to melting temperature, the mechanisms of soil thawing is explained in the chapter 5.

3. Thermal properties of soil

In order to handle a soil subjected to freezing and thawing, a geotechnical engineer must understand the physical laws behind heat propagation, which are quite different from the usual cohesion and stress capacity issues. Fortunately, the logic behind the different theories is surprisingly similar in many a way. This chapter aims at describing the parameters used in thermodynamic models, by their physical meaning and how to estimate them.

3.1. Heat capacity

The heat capacity ($J.g^{-1}.K^{-1}$) of a soil sample is the amount of energy needed to raise its temperature 1 degree. For practical purposes, one shall often speak of volumetric heat capacity ($J.g^{-1}.K^{-1}.m^{-3}$) or mass heat capacity ($J.g^{-1}.K^{-1}.kg^{-1}$), because their relation to a defined quantity makes it far easier to correlate with other properties or laws.

Heat capacity is an extensive property, meaning that it adds together when two materials are in interaction. This is a very interesting property, because it makes easy to handle heat capacity of complex materials. The most common way in a porous material like soil is to use the mass heat capacity, for it is often easier to know the mass of each component rather than their volume.

$$c_{soil} = (c_s.m_s + c_w.m_w + c_i.m_i + c_a.m_a).\frac{1}{m_{soil}} \qquad (3.1-1)$$

- c_{soil} and m_{soil} are the mass heat capacity ($J.kg^{-1}.K^{-1}$) and total mass of the soil (kg)
- c_s , c_w, c_i and c_a. are the mass heat capacities of the solid particles, the liquid water, the ice and the air ($J.kg^{-1}.K^{-1}$)
- m_s , m_w, m_i and m_a. are the mass of the solid particles, the liquid water, the ice and the air in the sample of mass m_{soil} (kg)

material	Density ($kg.m^{-3}$)	Heat capacity ($kJ.m^{-1}.K^{-1}$)	Source
air	1,25	1	1
water	1000	4,2	2
Ice (0°C)	900	2,09	2
sand and gravel	2200	0,89	3
quartz	2700	0,8	1
granit	2700	0,8	3

tab. 1, thermal properties of soil components, sources : 1 : De Vries (1966) ; 2 : Alter (1969) ; 3 : Johnston (1981)

Usual heat capacities for different materials are displayed in the table 1.

The contribution of air is small to negligible so this formula can be declined with more usual parameters :

$$c_{soil} = \rho_d.(c_s + c_w.w_u + c_i.w_i) \quad (3.1-1)$$

- ρ_d : dry density of the soil ($kg.m^{-3}$)
- w_u : liquid water content ($kg.kg^{-1}$)
- w_i : solid water content ($kg.kg^{-1}$)

3.2. Thermal conductivity

A heat flux going trough a material is a transfer of kinetic energy from the molecules in the warm part to those in the cooler part. Fourier (1822) established a linear relation between the flux density and the thermal gradient :

$$\vec{\varphi} = -k.\overrightarrow{grad}(T) \quad (3.2)$$

- φ : is the heat flux ($W.m^{-2}$)
- T : represents the temperature repartition in the material (K)
- k : is the thermal conductivity ($W.m^{-1}.K^{-1}$)

The minus sign means that the heat flux is directed from the warm material to the cool material.

As thermal conductivity is an intensive property, it is quite uneasy to handle in porous material such as soils, for there is no straight way to combine the different materials. The main problem is that the microscopic structure of the soil is way too complex to be taken in account as an exact fashion resulting in uncertainties on how each component add to the final conductivity. For this reason, different models shall be developed in this paper.

3.2.1. Series and parallel flow

Heat flux in a porous material can be compared to electricity flux in a circuit. Each component has an effect upon the final resistance that depends on the way it is placed in the pattern. Also, there are two extreme way to combine two materials : series and parallel. They give respectively the lower and upper limit.

The assumption that heat flow goes first trough the material 1 (say solid particle) and then trough the second one (say water) leads to the following :

$$k^{-1} = n_1.k_1^{-1} + n_2.k_2^{-1} \quad (3.2.1-1)$$

The assumption that heat flow goes in parallel trough the material 1 and then trough the second one leads to the following :

$$k = n_1.k_1 + n_2.k_2 \quad (3.2.1-2)$$

- k : resulting conductivity ($W.m^{-1}.K^{-1}$)
- k_1 and k_2 : conductivity of materials 1 and 2 ($W.m^{-1}.K^{-1}$)
- n_1 and n_2 : volume fraction of each material (no unit)

In a saturated soil, considering the two only materials to be the solid particle and water, series flow gives :

$$k = \frac{1}{\frac{n}{k_w} + \frac{(1-n)}{k_s}} \qquad (3.2.1 - 3)$$

and parallel flow :

$$k = n.k_w + (1-n).k_s \qquad (3.2.1 - 4)$$

- k ($W.m^{-1}.K^{-1}$) : resulting conductivity
- k_s and k_w ($W.m^{-1}.K^{-1}$) : conductivity of the solid particle and water
- n (no unit) : porosity

Those two models are of a very limited use in practical purposes. However, they are important to understand for they are the basic mechanisms under most of the theoretical models below. They also can be used to quickly get a range of the final calculation.

3.2.2. Johansen model

The method developed by Johansen (1977) is applicable to unsaturated soils. It presents the thermal conductivity of a 3-component (solid – water – air) soil as a combination of two states : dry (air + solid) and saturated (water + solid). To control this combination, he introduced the Kerten's number (K_e) that is a derivation of the saturation number.

Johansen derived the following formulas from Kersten's data. For coarse unfrozen soil :

$$K_e \cong 0{,}7 \log (S_r) + 1{,}0 \text{ , where } S_r < 0{,}05 \qquad (3.2.2 - 1)$$

- S_r : saturation number, the ratio between actual water content and saturated water content

For fine unfrozen soil :

$$K_e \cong \log (S_r) + 1{,}0 \text{ , where } S_r < 0{,}1 \qquad (3.2.2 - 2)$$

For any type of frozen soil :

$$K_e \cong S_r \qquad (3.2.2 - 3)$$

Then the combination between saturated and dry states stands as :

$$k_u = (k_{sat} - k_{dry}) \, . \, K_e + k_{dry} \qquad (3.2.2 - 4)$$

- k_u : thermal conductivity of the material ($W.m^{-1}.K^{-1}$)
- k_{sat} : saturated thermal conductivity ($W.m^{-1}.K^{-1}$)

- k_{dry}: dry thermal conductivity ($W.m^{-1}.K^{-1}$)
- K_r : Kersten number, that can basically be assumed equal to the saturation number S_r for frozen soils.

Based on researches by Smith and Byers (1938), Smith (1942) and his own experiments, Johansen developed a set of semi-empirical formulas. Those state the dry density (or porosity) as the main factor determining thermal conductivity. The solid particle conductivity has little effect, for its span among soil materials is pretty narrow. The soil microstructure influence is translated by the development of two separate equations :

For dry natural soils :

$$k_{dry}\ (W.m^{-1}.K^{-1}) = \frac{0{,}135\ .\ \gamma_d + 64{,}7}{2700 - 0{,}947\ .\ \gamma_d} \pm 20\% \qquad (3.2.2 - 5)$$

For crushed materials :

$$k_{dry}\ (W.m^{-1}.K^{-1}) = 0{,}039.n^{-2{,}2} \pm 25\% \qquad (3.2.2 - 6)$$

- n : material porosity
- γ_d : dry density ($g.cm^{-3}$)

For calculating saturated soil, Johansen recommends the mean value between parallel and series distribution of water, ice and solid particles, which lead to :

$$k_{sat} = k_s^{\,1-n}.\ k_w^{\,w_u}.\ k_i^{\,n-w_u} \qquad (3.2.2 - 7)$$

- k_s : thermal conductivity of the solid material. If the soil is a mixture of different particles natures, it can be estimated as the multiplication of their thermal conductivity at a power corresponding to the fraction (in mass) of the solid content they represent : $k_s = k_1^{\,a}\ .\ k_2^{\,b}\ .\ k_3^{\,c}$ … where a is the fraction of solid mass of thermal conductivity k_1
- k_w : thermal conductivity of water, around 0,57 W/m.K
- k_s : thermal conductivity of ice is 2,21 W/m.K at 0°C and drops fairly with temperature.

3.2.3. Kersten model

Kersten (1949) tested 19 natural soils and crushed rocks, and established a set of empirical formulas based on the data collected. Kersten correlated thermal conductivity with water content and dry density. Material type's and microstructure's influence are expressed by the choosing of different formulas. Two equations are used to describe frozen (-4°C) and unfrozen (+4°C) states.

For unfrozen fine soils :

$$k\ (\mathrm{W.m^{-1}.K^{-1}}) = 0{,}1442.(0{,}9.logw - 0{,}2).10^{0{,}6243.\gamma_d} \qquad (3.2.3 - 1)$$

For frozen fine soils :

$$k\ (\mathrm{W.m^{-1}.K^{-1}}) = 0{,}001442.10^{1{,}373.\gamma_d} + w.0{,}01226.10^{0{,}4994.\gamma_d} \qquad (3.2.3-2)$$

For unfrozen coarse soils :

$$k\ (\mathrm{W.m^{-1}.K^{-1}}) = 0{,}1442.(0{,}7.logw + 0{,}4).10^{0{,}6243.\gamma_d} \qquad (3.2.3-3)$$

For frozen coarse soils :

$$k\ (\mathrm{W.m^{-1}.K^{-1}}) = 0{,}01096.10^{0{,}8116.\gamma_d} + w.0{,}461.10^{0{,}9115.\gamma_d} \qquad (3.2.3-4)$$

- w : gravimetric water content in %
- γ_d : dry density (g.cm^{-3})

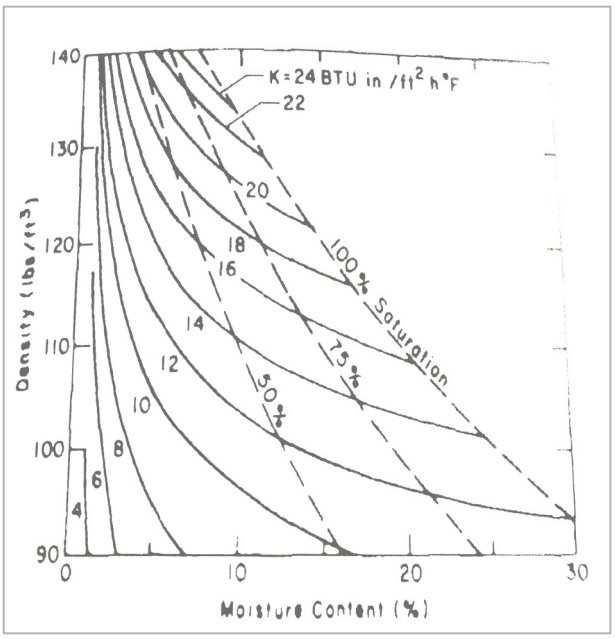

fig. 4 : Thermal conductivity of unfrozen sandy soils as a function of moisture content and dry density, from Kersten (1949)

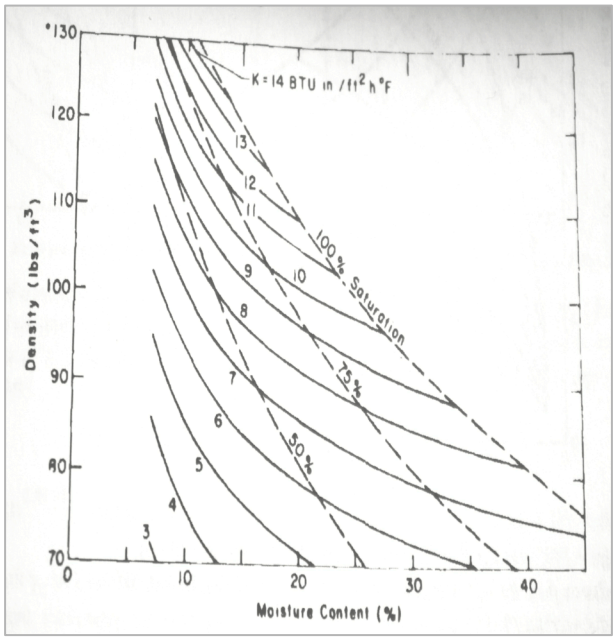

fig. 5 : Thermal conductivity of unfrozen clay and silty soils as a function of moisture content and dry density, from Kersten (1949)

3.2.4. Other models

Many other models have been developed through the 20th century. Most of them are a combination of parallel and series flows, through materials arranged in different geometric patterns.

Smtih's method for dry soils

Smith (1942) considers the heat flow trough a dry soil going by two parallel paths. One is a continuous air column, while the second is solid particles alternated with air layers. Combining the series and parallel flow equations (3.2.1), it leads to the following formula :

$$k = k_a.(n - P_a) + x_a.\frac{(1+\alpha')}{\left(\frac{1}{k_s}\right)+\frac{\alpha'}{1+\alpha'}\left(\frac{1}{k_a}-\frac{1}{k_s}\right)} \qquad (3.2.4-1)$$

- k : thermal conductivity (W.m^{-1}.K^{-1})
- k_a : air thermal conductivity (W.m^{-1}.K^{-1})

- k_s : solid particle thermal conductivity ($W.m^{-1}.K^{-1}$)
- x_a : solid particle volume per total volume (m^3/m^3)
- P_a : air series volume per total volume (m^3/m^3), calculated a $P_a = \alpha'.x_a$
- α' : thermal structure factor, experimentally determined

Soil structure	α'
Medium granular	0,065
Medium platy	0,052
Coarse platy	0,041
Medium blocky	0,045
Coarse blocky	0,036

tab. 2 : α' factors (after Smith 1942)

NB : the thermal diffusivity of a saturated soil can be calculated by this method by changing air by water. The saturated frozen thermal diffusivity can be obtained by filling with ice instead of water.

Modified resistor equation

The modified resistor equation developed by Woodside and Messmer (1961) consider a cube with three parallel paths. The first is pure fluid, the second pure solid particles and the third is fluid and solid in series.

Using the usual laws for series and parallel heat flow (ref), this gives the following :

$$k = \frac{a.k_s.k_f}{(1-d).k_s+d.k_f} + b.k_s + c.k_f \qquad (3.2.4-2)$$

- a : normalized width of the series, fluid and solid, paths (no unit)
- b : normalized width of the pure solid path (no unit)
- c : normalized width of the pure fluid path (no unit)
- d : normalized height of the fluid in the mixed path (no unit)
- k : final thermal conductivity ($W.m^{-1}.K^{-1}$)
- k_s : solid particle thermal conductivity ($W.m^{-1}.K^{-1}$)
- k_f : fluid thermal conductivity ($W.m^{-1}.K^{-1}$)

To fit their experimental results, Woodside and Messmer made two assumptions :

b = 0 and c = n – 0,03

NB : b = 0 means that this method corresponds exactly to the Smith's method

Those assumptions leads to the final semi-empirical equation :

$$k = (n-0{,}03).k_f + (1-n+0{,}03).\left[\frac{1-n}{1-n+0{,}03}.\frac{1}{k_s} + \frac{0{,}03}{1-n+0{,}03}.\frac{1}{k_f}\right]^{-1} \qquad (3.2.4-3)$$

- k : final thermal conductivity ($W.m^{-1}.K^{-1}$)
- k_s : solid particle thermal conductivity ($W.m^{-1}.K^{-1}$)
- k_f : fluid thermal conductivity ($W.m^{-1}.K^{-1}$)
- n : porosity (no unit)

McGaw's conductance equation

McGaw (1969) rewrote the Smith's equation with different geometric parameters :

$$k = (n - n_c).k_f + (1 - n + n_c).\frac{k_s.k_f}{(1-n).k_f + n_c.k_s} \qquad (3.2.4 - 4)$$

- k : thermal conductivity ($W.m^{-1}.K^{-1}$)
- k_f : fluid thermal conductivity ($W.m^{-1}.K^{-1}$)
- k_s : solid particle thermal conductivity ($W.m^{-1}.K^{-1}$)
- n : porosity (no unit)
- n_c : volume of fluid in the ''series'' path (no unit)

McGaw attempted to take into account the refraction of the heat flow lines as they leave or enter the solid grains. This is materialized by an inter-facial efficiency coefficient ε applied to the ''series'' path :

$$\varepsilon = 1 - \frac{\Delta T_i}{\Delta T} \qquad (0 < \varepsilon < 1) \qquad (3.2.4 - 5)$$

- ε : interfacial efficiency coefficient (no unit)
- ΔTi : mean temperature differential across one solid ''grain'' (K)
- ΔT : mean temperature differential between two centers of solid ''grain'' (K)

Which gives :

$$k = (n - n_c).k_f + (1 - n + n_c)^2.\frac{\varepsilon.k_s.k_f}{(1-n).k_f + n_c.k_s} \qquad (3.2.4 - 6)$$

Experiments conducted by Woodside and Messmer showed that the n_c value is around 0,03. The ε proved to be harder to estimate accurately, although McGaw counsel to use the unity.

Finally, McGaw developed his equation for unsaturated soil, by introducing the saturation number. For doing so, he added a third path of pure air and defined the fluid in equation (3.2.4 - 6) as water :

$$k = (n.S_r - n_c).k_w + (1 - n + n_c).\frac{\varepsilon.k_s.k_w}{(1-n).k_f + n_c.k_s} + (n - n.S_r).k_s \qquad (3.2.4 - 7)$$

- k : thermal conductivity ($W.m^{-1}.K^{-1}$)
- k_f : fluid thermal conductivity ($W.m^{-1}.K^{-1}$)
- k_s : solid particle thermal conductivity ($W.m^{-1}.K^{-1}$)
- n : porosity (no unit)
- n_c : volume of fluid in the ''series'' path (no unit)
- S_r : saturation number (no unit) : $S_r = \frac{volume\ of\ water}{volume\ of\ pores}$
- ε : interfacial efficiency coefficient (no unit)

Mickley's method

Mickley (1951) considers a non-saturated soil whose components are arranged in a rather complex fashion. The whole material is taken as a cube, divided in four columns : one of air, one of solid particles, and two identical columns of solid particles striped with air layers. Using the series and parallel flow formulas :

$$k_{dry} = k_a.a^2 + k_s.(1-a)^2 + \frac{k_a.k_S(2a-2a^2)}{k_s.a+k_a.(1-a)} \qquad (3.2.4-8)$$

- k : thermal conductivity of the material ($W.m^{-1}.K^{-1}$)
- k_a : thermal conductivity of air ($W.m^{-1}.K^{-1}$), usually around 0,025 $W.m^{-1}.K^{-1}$
- k_s : thermal conductivity of solid particles ($W.m^{-1}.K^{-1}$)
- a : normalized widht of the air column (no unit)

NB : *this can be used to calculate the conductivity of saturated soil as well, by switching air volume and conductivity with water.*

Then, he added the water in the form of a uniform layer of thickness b on every four of the contact surfaces between the columns.

$$k = k_a.c^2 + k_s.(1-a)^2 + k_w.(a-c)^2 + \frac{2.k_a.k_w.c.(a-c)}{k_w.c+k_a.(1-c)}$$

$$+ \frac{2.k_a.k_w.k_s.c.(1-a)}{k_w.k_s.c+k_s.k_a.(1-c)+k_a.k_w.(1-a)} + \frac{2.k_s.k_w.(1-a).(a-c)}{k_s.a+k_w.(1-a)} \qquad (3.2.4-9)$$

- k_w : thermal conductivity of water ($W.m^{-1}.K^{-1}$), usually around 0,57 $W.m^{-1}.K^{-1}$
- b : normalized thickness of the water layer (no unit)
- c : new normalized width of the air column, c = a – b (no unit)

a, b and c are linked to porosity (n) and saturation number (S_r) via the following relations :

$3a^2 - 2a^3 = n$

$3c^2 - 2c^3 = (1-S_r).n$

NB : This model can be extended to 3D by having the same pattern in each 3 directions. This would mean that the columns would be only (1-a) high, but this detail can be neglected.

Gemant's method

Gemant (1952) consider saturated soil to have only point-to-point contacts between particles, thus the heat conduction at the interface only goes trough the water. He modeled each particle by a cube with three smooth surfaces and three surfaces extended by a square-based pyramid. Then, a water ring is added around the pyramids, providing the contact with the other particles.

Using then the simple laws of series conduction and a set of experimental data, he came to the following formulas :

$$a = 0{,}078.s^{0{,}5}$$

$$h = 0{,}16.10^{-3}.s.w - h_0$$

$$z = \left(\frac{1-a}{a}\right)^{2/3}.\left(\frac{h}{2}\right)^{1/3}$$

$$b^2 = \left(\frac{a}{1-a}\right)^{2/3}.\left(\frac{h}{2}\right)^{2/3}$$

$$\frac{1}{k} = \frac{\left(\frac{1-a}{a}\right)^{4/3}.\arctan\left(\frac{k_S-k_W}{k_W}\right)^{1/2}}{\left(\frac{h}{2}\right)^{1/3}.[k_W.(k_S-k_W)]^{3/2}} + \frac{1-z}{k_S.a}.f\left\{\frac{b^2}{a}\right\} \qquad (3.2.4-10)$$

- a : normalized width of the particle cube, without the pyramids (no unit)
- b : normalized width of the water ring around the pyramid point (no unit)
- h : 'effective water', normalized volume of the water ring (m^3/m^3)
- h_0 : water film at the surface of the particles, that must be subtracted to get the 'effective water' volume (m^3/m^3). It depends on the temperature.
- z : maximal thickness of the water ring, normalized (no unit)
- k : thermal conductivity of the material ($W.m^{-1}.K^{-1}$)
- k_w : thermal conductivity of water ($W.m^{-1}.K^{-1}$), usually around 0,57 $W.m^{-1}.K^{-1}$
- k_s : thermal conductivity of solid particles ($W.m^{-1}.K^{-1}$)
- f is a function experimentally determined by Gemant (1952)

NB : the conductivity of air is neglected.

Method of Kunii and Smith

Kunii and Smith (1960) modeled the particles in saturated soil as a pile of spheres. Like in the Germant's method, water assumes the inter-particle conduction. After some arbitrary simplifications, they came to :

$$k = k_a.\left(n + \frac{1-n}{\Phi + \frac{2k_a}{3k_s}}\right) \qquad (3.2.4-11)$$

- k : thermal conductivity of the material ($W.m^{-1}.K^{-1}$)
- k_a : thermal conductivity of air ($W.m^{-1}.K^{-1}$), usually around 0,025 $W.m^{-1}.K^{-1}$
- k_s : thermal conductivity of solid particles ($W.m^{-1}.K^{-1}$)
- n : porosity (no unit)
- Φ : effective length of series air as a ratio of the particle diameter

Kunii and Smith related Φ to porosity and the packing pattern of the spheres. After several experiments, they proposed the following formulas for Φ :

$$\Phi = \Phi_2 + (n - 0{,}259)\frac{(\Phi_1 - \Phi_2)}{0{,}217} \qquad (3.2.4 - 12)$$

- Φ_1 : Φ corresponding to a cubic packing
- Φ_1 : Φ corresponding to a rhombohedral packing

3.2.5. Comparison of thermal conductivity models

It can be difficult to choose within such a maze of methods. Even as most of them are derived from the same theoretical laws, differences come from the geometric and empirical assumptions made by the different searchers. Because of that, most models have a limited useful area.

Comparison of variation with porosity

Porosity is a main factor in every single method listed above, though sometimes indirectly through the dry density. Farouki (1981) made a very complete comparison of those methods against varying dry density. A different approach will be developed in this thesis, varying directly the porosity.

The figure 6 displays porosity variation for a saturated soil, the figure 7 the same for dry soils. Of course, Gemant's method cannot be used in dry soils, because all heat transfer between particles is assume to go trough the water. Kersten's empirical equations are also not to use, because the logarithmic function included does not have any significance for water content below 0,1.

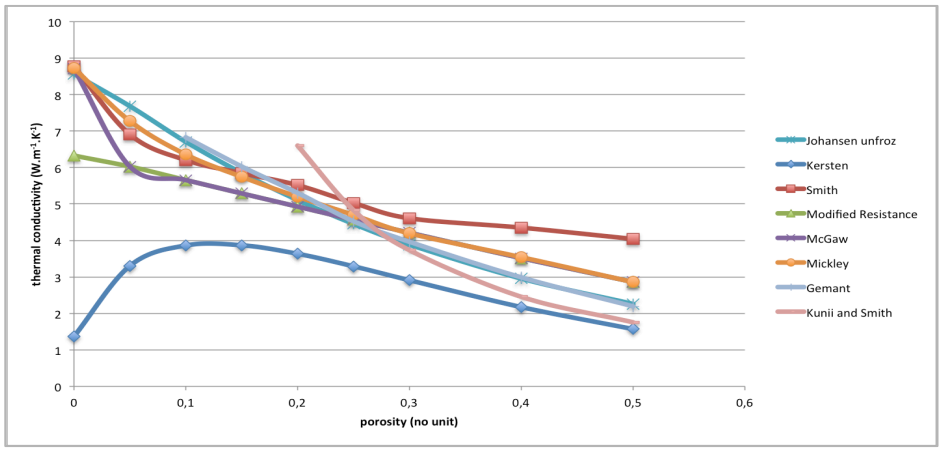

fig. 6 : thermal conductivity as a function of the porosity, for the different models, in saturated soils

The diagrams plainly show that very theoretical equations such as the Modified Resistance method and its derivate Mickley's method and McGaw's method are by far more stable in a wide range of porosity. It is even more dramatic with dry soils. However, they strongly diverge when it comes to dry soils : either they have a full-solid path (Mickley's) that obliterate the effect of other paths, or they do not (Modified Resistance and McGaw's) and the serie air does

not allow for conductivity to increase when the porosity approaches zero (although any theoretical model should by definition converge toward k_s when the porosity hit zero).

A bit higher than the other methods, Smith's equation offer a rather supple estimation. However, the α' coefficient estimation makes it rather hard to use upon incomplete data.

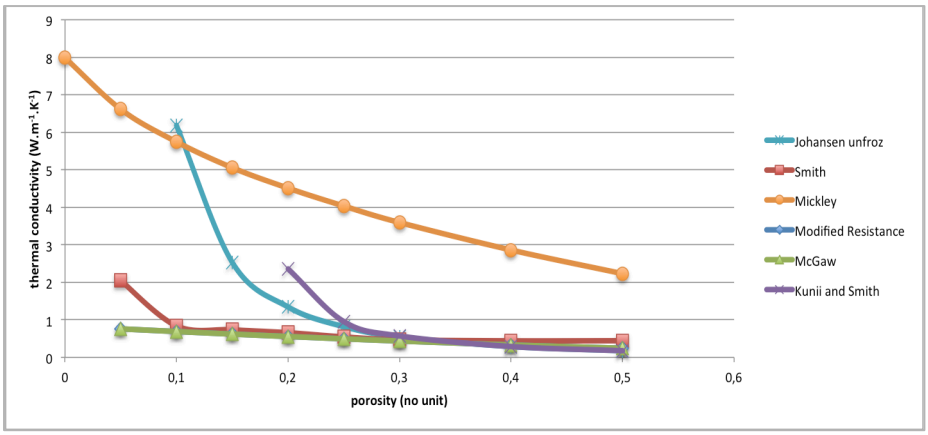

fig. 7 : thermal conductivity as a function of the porosity, for the different models in dry soils

Gemant's method matches rather well the Modified Resistance method, although with a quite different theoretical approach. The importance of the porosity is a bit higher, which is normal since the role of porous water is the critical factor.

Kunii and Smith's method is pretty close to the other theoretical methods, although the approach is completely different also. However, the function Φ cannot allow a porosity below 0,2, due to the (n - 0,259) factor in its calculation (a negative Φ does not make sense).

The completely empirical Kersten's equations seem to react rather badly to high porous changes. This can be explained by the splitting between two set of equations. The equation used in the figure 6 is applicable to sands. The fact that is it rather complicated to imagine a sandy soil with a porosity below 0,1 may explain the significant loss of accuracy in the low-porosity range. However, it is the logarithmic function of the water content that is ultimately responsible for this deviation. While is works rather well for high porosity soils, the logarithmic function react dramatically with low water content associated with low porosity.

Using a semi-empirical model, Johansen's method combines the advantages of both. The saturated soil theoretical calculation is a rather good approximation of the Modified Resistance method (in fact, it merely suppress the pure-air path, that is anyway reduced to zero in saturated soil). But when it comes to dry soil, the empirical formula supply the lack of realistic theoretical model able to take over the dramatic drop in conduction due to the absence of water. However, the results suggest he could have used Smith's method, which remind of the

theoretical saturated soil method of Johansen with its two paths (but is still different, using a combination of series and parallel paths instead of merely averaging the two).

Comparison of variation with saturation number

The water content has indeed a very strong importance for thermal conduction estimations. Because the contact between the soil particles is by nature imperfect, it falls to the fluid to fill the gaps. Without those fluids, most of the models in the paragraph above will not even allow any heat transfer.

However, some of these methods are especially designed for bi-components medias, that is to say, either saturated or dry soils. When it comes to non-saturated soils, the choice is thus more limited.

The figure 8 displays the variation of thermal conductivity for a medium-porous (n = 0,2) pure quartz soils.

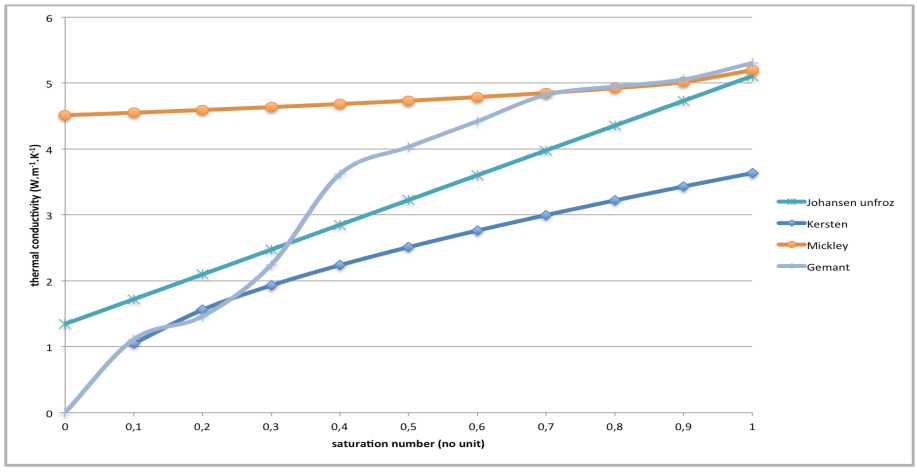

fig. 8 : thermal conductivity as a function of the saturation number, for the different models, with a porosity fixed at 0,2

Of the three theoretical methods issued from the Modified Resistor equations, only Mickley's method considers a variation in water content, via the parameter b (see 3.2.4, Mickley's method). It proves to be not much affected by a water content variation, varying slightly more than 10%. This comes from the geometry of the model. While Smith and Johansen consider only pure-fluid and mixed paths, Mickley add a pure solid parallel path. With a porosity equal to n = 0,2, this path (which is not affected by water content) takes about 40% of the element volume, making alone the near-integrality of the total heat transfer capacity. Due to the lowest thermal conductivity of water and air, the saturation variation only has a margin effect.

Gemant's method is the only theoretical method that is able to translate the dramatic thermal conduction loss that goes with the gradual loss of water ($0,3 < Sr < 0,5$). This is due to the absence of full-solid parallel path that is present in Modified Resistance's type methods,

meaning that the whole heat flux has to go trough the water. However, when the water content decreases, the water "ring" around the pyramid becomes harder to estimate. In particular, when $w < 0,04$ (kg/kg) there is no proper way to quantify the water film h_0 that cover the whole particle.

The semi-empirical Johansen's method describes a linear approximation of Gemant's results. Of course, with a Kersten's number set as $K_e = S_r$, a segment was to be expected. Therefor, since the saturated results for Johansen and Gemant's equation match, this is not surprising.

Kersten's empirical formula seems to follow Johansen's results but is still rather low probably for the same reason as in the porosity-related comparison.

Comparison of frozen ground variation with porosity

For theoretical models, the frozen soil calculation is pretty close to that of unfrozen soil, the only difference being the thermal properties of the "fluid", that is replaced by ice. Thus, the results are not very different.

The diagram 9 shows the variation of thermal conductivity with the porosity for the different methods.

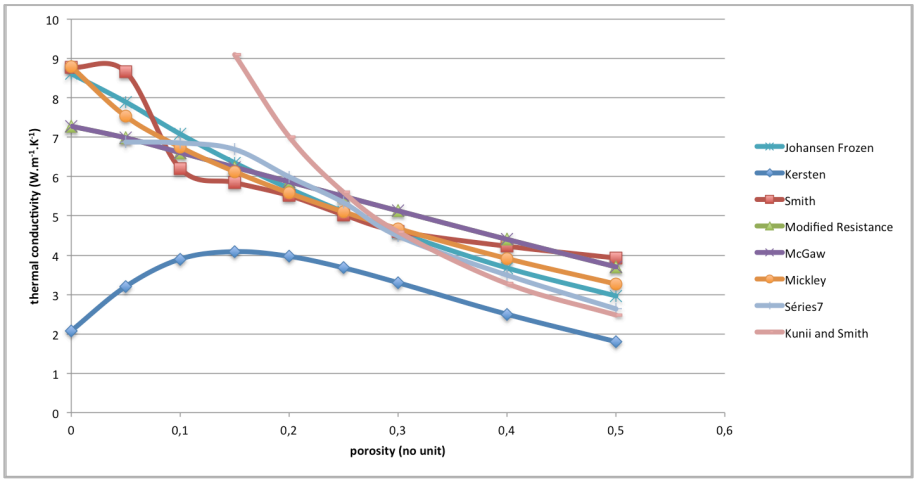

fig. 9 : thermal conductivity as a function of the porosity, for the different models, in a frozen saturated soil

As before, the Modified Resistance method and its cousins McGaw's and Mickley's are rather close to each other. They vary smoothly even close to the null porosity.

Smith's equation although from a different approach, reaches about the same results. However, it struggle to represent low-porosity soils due to the high sensitivity of its α' coefficient.

Gemant's method endures about the same problem. When the porosity drops close to zero, the water content is not sufficient to accurately quantify the water "ring", thus theoretically

dropping the heat conduction to zero (remember the inter-particle contact is taken by porous water only).

The same problem is even more significant in Kunii and Smith's method. This time, it is the ϕ function that is not calibrated to handle low porosity, thus resulting in non-convergent results.

Johansen's method, by its simplicity, avoids the problem of convergence while hitting low-porosity soils. However, it stays as a good approximation of more complicated methods such as the Modified Resistance.

Kersten's equation seems underrating, for the same reasons as in unfrozen soils.

Conclusion

Most of the methods exposed above have a deviation below 25%. Researches by Farouki (1981) show that for most practical applications, such a deviation is not a big concern. Variations in local soil properties due to lack of homogeneity can have a rather big impact, for example a large boulder that will create a very conductive parallel path. It may therefor be pointless to attempt a more precise prediction.

Most of the methods are well designed for unfrozen, saturated soils. However, Gemant's, McGaw and Kunii and Smith's have divergent effects due to the geometrical models chosen, and Kersten has a divergent path due to its logarithmic expression. Simpler models such as Johansen's or the Modified Resistance, that only consider two components, are not affected by huge deviations in low-porosity soils. Surprisingly, Smith's method, that has been developed for dry soils, proves also to be rather robust thanks to its two-components model, although it is a bit overestimated, in particular in high porosity soils.

When it comes to dry soils, theoretical methods such as the Modified Resistance and McGaw (which are, in this case, exactly the same) are again more robust in low porosity soils. Too robust, in fact, for empirical results conducted by Johansen (1977) and Smith (1942) show that microstructural behavior in dry soils have a huge impact, thus dramatically increasing the conductivity in low-porosity soils. This increase is very difficult to represent in theoretical models, because of the lack of a full-solid parallel path (except Mickley's method). However, Kunii and Smith's method manages this by implementing the Φ function that account for the structural change. Unfortunately, that is this same Φ function that does not allow the model the represent low-porosity soils. Finally, the Johansen's empirical equations are regarded as the most precise description of natural material (Farouki, 1981).

Few of the methods above have the ability to handle three components, which is required for unsaturated soils. Of the Modified Resistance method cousins, only Mickley's method offers a proper estimation. However, as seen in the paragraph above, it does not allow for fine estimation of near-dry soils, as the total conductivity is completely ruled by the full-solid path. The approach by Gemant allow for this non-linear effect of water to express, if the user is careful with the h_0 expression (the undulating representation is a result of a very coarse estimation of this factor). The semi-empirical method of Johansen is a simple but effective representation, while Kersten's formula stays underestimated.

Within all those methods, the mineral composition seems to have very little impact. According to Farouki (1981), quartz-poor materials can be subjected to deviation from 20 to 30 percent, while quartz-rich materials let very little room for other materials conductivity to show up.

This wide choice in methods finally leads to a rather easy and satisfying choice of thermal conductivity even with a poor set of data. The critical factor to measure is by far the porosity (or dry density, which is closely linked). However, dramatic changes of the saturation number may set it as an even more critical parameter, in particular in the case of the creation of segregated water (meaning that S_r in a certain way exceeds 1, or more technically correct that the porosity highly increases). Saturation number can although be harder to measure and even more to use in this late case because of the huge variation.

3.3. Thermal diffusivity

The thermal diffusivity describes the capacity of a material to transmit a temperature signal. It is defined as :

$$\alpha = \frac{k}{\rho.c} \tag{3.3}$$

- α : thermal diffusivity ($m^2.s^{-1}$)
- k : thermal conductivity ($W.m^{-1}.K^{-1}$)
- ρ : density ($kg.m^{-3}$)
- c : mass heat capacity ($J.kg^{-1}.K^{-1}$)

3.4. Water content

Soils are porous medias, and often partially or completely filled with water. Especially in coastal environment, it is natural to assume that this water will have an important role. Trough the different methods seen in this chapter, water content will have a strong influence upon both heat capacity and thermal conductivity.

In addition to this significant impact, water will also freeze and melt. This mechanism will act in parallel (see 4.5).

Porous water content can be easily measured in soil samples. The simplest method is to completely dry the sample in an oven and compare its weight with before the drying.

Variation of porous water content obeys to two factors. The first is the soil porosity. Water content cannot of course exceed the material porosity. Porosity variation occurs trough mechanical stresses in the soil. The second factor is the saturation number. This one is directly linked to the water fluxes in the soil. Water has a tendency to go down until it reaches the water table (the sea here), but is slowed by the permeability. Above-water table water can come either from a higher water table further in the land or from the climate (ice/snow melting or rain).

4. Thermal behavior of soil

Soil is a complex mixture of mineral particles, water and air. Each of these has its own behavior. Solid particles react fairly to strain by changing their microstructure, but are not much influenced by the temperature. Water on the contrary does not strain (at least, from a geotechnical point of view) but flows, and react heavily to temperature change trough its phase changes.

Despise this complexity, heat flux trough the soil can be modeled in a quite accurate manner. The key is to isolate the most dominant behaviors and link them to simple thermodynamics laws.

4.1. Seasonally and perennially frozen ground

In cold regions, it is often practical to isolate the seasonally frozen layer, called "active layer", for it is siege to the most important changes due to temperatures. It is fairly easy to separate it from the other layer, using a plot of extreme annual temperatures related to depth (figure 10).

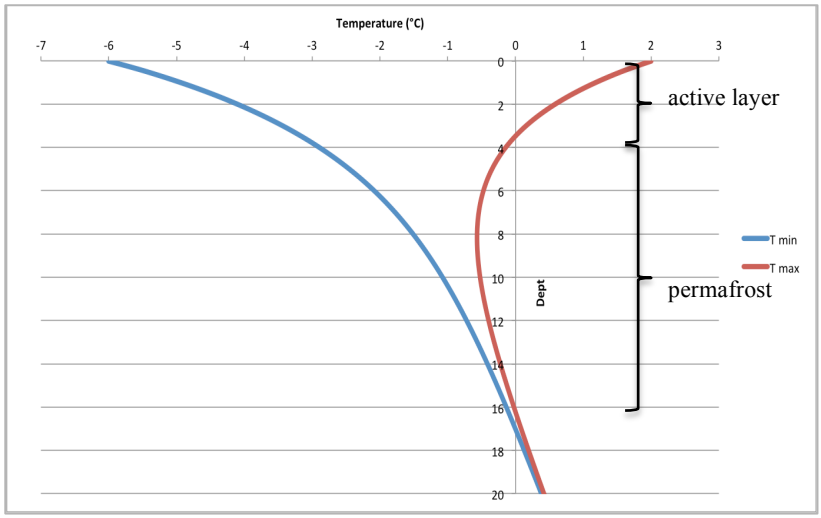

fig. 10 : example of temperature profile in permafrost

4.1.1. Active layer

The upper layer of the ground in which the temperature goes above and below zero during the year is called the "active" layer. As its name let imagine, the active layer is the most critical part of the soil, for it is the area that is subjected to freezing and melting.

The thickness of the active layer varies between 15 cm in very cold areas and 1 m or more in sweeter climates (Andersland and Ladanyi, 2004). In arctic or cold areas, its low limit is generally the permafrost, although it can be otherwise in some cases (water bodies, ancient permafrost, human structures …). The thickness depends on many factors, the most important

being the climate mean temperature and amplitude (high frequency variations have little effect or not at all, except those who hit the extreme temperatures), including effects of the surface coverage (vegetation, ice, snow). The soil thermal conductivity and heat capacity have a very significant effect, while slopes and mechanical stresses (except those who lead to slope collapse, which of course completely disrupt the system) have a more secondary impact.

The annual freezing of the active layer causes heave in porous soils. Water contained in the soil will increase by about 9%. In addition, the formation of segregated ice (ice lenses) boosted by the water suction (Konrad and Morgenstern, 1981) can multiply the porosity up to several times its initial value in particular when the water table is close. Although freezing often considerably increases the mechanical capacities of the soil, the differential heave due to heterogeneity in the temperature repartition can be rather impressive (remember that local variations of ±25% in thermal conductivity are not uncommon, added to local disturbances like water pockets or buried boulders).

Thawing causes a big loss of stress capacities of the upper layer. Not only is the unfrozen ground generally weaker that its frozen counterpart, but thawing decreases the cohesion sometimes up to nothing. After the water content has dramatically increased during freezing due to water suction, the water content in thawing soil is several times higher than its optimum. In simpler words and in the worst cases, thawing changes the soil into mud. The cohesion loss in itself is not often dangerous for structures, but can lead to slope instability (see 5.2).

Meanwhile, the consolidation process of the thawed soil leads to huge settlement. The material, weakened by its abnormal water content, will expel water (thus settling in the process) until the equilibrium is reached. Thaw settlements up to 55% have been observed (Pullman, Jorgenson and Shur, 2007). Such settlements are obviously extremely dangerous for structures with shallow foundations.

4.1.2. Permafrost

Permafrost, or perennially frozen ground, is defined as a soil having temperatures below 0°C during at least two consecutive winters and the summer between (Andersland and Ladanyi, 2004). The presence of permafrost is mostly controlled by the climate, above all the mean annual temperature. However, it is not uncommon to have residual permafrost heir to very ancient cold climates. That is particularly common in Northern Europe.

The thickness of the permafrost is related to the mean annual temperature and the geothermal gradient, as seen in figure 10. Classical thicknesses vary between a few centimeters in southern regions to more than a hundred meters in arctic areas.

4.2. Fourier's Law

Conduction is the main mode of heat transfer trough the ground. It is the transfer of kinetic energy, at a molecular level, from the most agitated (warm) matter to the least agitated (cold) one. Conduction exists whatever the type of material, provided that the two pieces of matter are in contact (which is the most noticeable difference with radiation, that does not need contact).

The rate at which heat is transferred to a cooler material follows a linear law, evidenced by Fourier (1822) :

$$q = -k.\frac{dT}{dx} \tag{3.4}$$

- q : heat flow per area (W/m^2)
- k : thermal conductivity ($W.m^{-1}.K^{-1}$)
- dT/dx : thermal gradient (K/m) in the direction of the heat flow

Conduction is the dominant heat flux propagation mechanism inside a solid material. Although the presence of air restrains the contact areas between each element (technically, conduction occurs in air also, but is negligible as air conductivity is very low), even very porous soils have a behavior very similar to continuous medias when seen from a general scale. Conduction mechanisms at particle scale are detailed in 3.2.

4.3. Convection

Convection is not a heat transfer mechanism between two pieces of matter, but rather a movement of the matter itself. Within a fluid, du to its intrinsic properties or to external stresses, particles of different temperatures move. By doing so, although the individual particle temperature never changes, they change the heat repartition within the fluid.

When combined to a conduction process, it greatly increases its efficiency. This is because the convection movement has a tendency to regulate the fluid temperature at the contact surface.

There are two types of convection : natural convection and forced convection.

4.3.1. Natural convection

Natural convection is due to the difference of density within the fluid that comes with the temperature gradient. Warm fluid, lighter, will go up while cold fluid, heavier, will go down until the complete system is at the same temperature.

Natural convection is described by the Rayleigh number :

$$R_a = \frac{g.\beta}{\nu.\alpha}(T_s - T_\infty).x^3 \qquad (4.3.1-1)$$

- R_a : Rayleigh number (no unit)
- g : gravity acceleration ($m.s^{-2}$)
- β : thermal dilatation coefficient, volume ratio (K^{-1})
- ν : cinematic viscosity ($m^2.s^{-1}$)
- α : thermal diffusivity ($m^2.s^{-1}$)
- T_s : surface temperature (K)
- T_∞ : temperature at a distance sufficient for the surface not to have any influence (K)
- x : specific distance, correlated to the geometry of the surface (m)

A Rayleigh number above 2000 will typically trigger the movement of natural convection. Then, the heat transfer can be calculated as :

$$\varphi = h.S.(T_s - T_\infty) \qquad (4.3.1-2)$$

- S : contact area (m^2)
- φ : heat flux ($W.m^{-2}$)
- h : heat transfer coefficient ($W.m^{-2}.K^{-1}$) that depends on the properties of both fluid and surface material

4.3.2. Forced convection

Forced convection is a molecule movement created by an external stress. It can be natural, the most common being wind and current (that can be in fact natural convection at a higher scale, but are considered forced at local scale because a part of the fluid system is beyond the boundaries of the used model). It can also be man-made, with turbines or pumps.

In soils, forced convection is generally due to the wind, and limited to a depth equal to the surface roughness (Kane et all., 2000). Such a phenomenon will not be studied in detail in this paper, for surface conditions are reduced to a thermal condition, but it would be very important to account for in a study based on climate conditions as it is a necessary link between air temperature and surface temperature, especially in arctic areas with powerful winds.

Soil water flow can also have a forced convection effect. But this is a margin phenomenon, as forced convection suppose a rather high velocity (Kane et all., 2000) that is seldom observed in a soil, or is restrained to the surface.

4.4. Radiation

Radiation is the third heat transfer mechanism. As opposed to the other two, it does not involve contact between the two exchanging pieces of matter. The main example of radiation heat

transfer is the sunlight that goes trough 150 million km of near vacuum to warm any exposed surface on the earth.

Any existing molecule (beyond 0K, that is to say any known piece of matter) will emit electro-magnetic radiations. Those radiations are due to the own random movement of the molecule that is commonly called heat. Thus, the wavelength of the radiation is intimately linked to the temperature : the higher the temperature, the higher the frequency (and shorter the wavelength).

When the electromagnetic wave hit another molecule, it will transmit a fraction of its energy under the form of heat. Although the characteristics of the wave depend only on the source, the fraction of energy that is converted into heat depends only on the target (however, properties are not the same for every wavelength).

NB : heat is not the only cause of radiation. Electromagnetic waves are created by all kinds of atomic movements, including fusion, fission, reactions or orbital changes of electrons. This is a very interesting topic that this paper unfortunately have no time to cover.

4.5. Water enthalpy

In addition to its effect upon thermal diffusivity, porous water influence the heat flux trough phase change when the temperatures goes around 0°C.

Whenever a solid material hit its melting temperature, it requires additional thermal energy to change phase. This energy, characteristic of the material, is called enthalpy of fusion, or heat of fusion. The materials temperature will not increase until it is all melted, as all heat energy it receives will serve to melt the remaining solid matter.

Of course, the same amount of energy is released during solidification. Similar mechanisms also exist for vaporization/condensation, via the enthalpy of vaporization.

Enthalpy of fusion only depends on the material. Actually, pressure has a limited impact that can be neglected for all practical purposes. Dissolved matters or particle in suspension (typically salt) have a kind of indirect influence trough the change in density, but only the quantity of water molecule ultimately has any effect.

Water enthalpy of fusion is 333,55 $kJ.kg^{-1}$. With a density of 1 (fresh water), that is 333,55 $MJ.m^3$.

4.6. Mechanical behavior of porous soil

As stresses are applied to the soil, it will react with deformation. The strain, and possibly the structural changes, will impact the thermal properties.

The dominant factor will be the change in the microstructure. Two opposite paths will occur. First, the reduction of porosity will have a tendency to increase both thermal conductivity and heat capacity. But then, the loss in porosity may mean a loss of porous water, and the thermal conductivity and heat capacity it add. However, in definitive a more compact soil will have increased thermal diffusivity, conductivity and heat capacity.

4.7. Water flux

From a thermal point of view, the water flux in soil can be seen as convection. Water of different temperature will move trough the soil, carrying its own heat and transmitting wherever it goes.

As soil is a porous material, water will move more or less freely within. This liberty of water movement is ruled by the permeability.

Permeability depends on the soil material and structure. The particle size is of a prime importance : the more coarse (and badly graduated) the material, the more permeable. Thus, sand and gravel are considered highly permeable, while clay can be almost impervious. Bedrock can also be permeable thanks to its cracks.

4.8. Effect of surface geometry

The effects of geometry are subtle, and complicated to check with theoretical calculations, because they involve heat flux in two dimensions. However, this paper shall try to understand them.

The direct effect of the surface geometry is to control the distance of every soil element to the surface. This is definitely important, because the distance to the surface (which may be very different to the depth if the soil is not horizontal) rule the heat flux received by this soil element, thus its changes in temperature.

A simple way to account for the surface pattern would be to “bend” the isotherms. However, it is rather obvious that the closest surface will not be the only one ruling the temperature in a soil element, especially when the slope is steep. Thus, this paper will try to develop a very simple theoretical model, and use FEM calculations to calibrate it.

4.9. Geothermal gradient

The soil temperature is naturally increasing with depth, with an average of 1°C every 30 m. This come from that the Earth core is at extremely high temperature, around 7000 K, due to its history and radioactive decease of heavy atoms. The heat escapes through the soil.

This heat flow is not equally distributed over the Earth surface. It depends on the nature of the deep soil and the proximity of tectonic ridges. The continental crust thickness for example implies that heat flux is by far lower than trough the slimmer ocean shelf. Mean heat flow for continental shelf is 65 $mW.m^{-2}$.

In order to simplify, and considering the low impact of slight changes in thermal conductivity while going through different materials this heat flux shall be assimilated as a thermal gradient. It shall range from 0,05 to 0,01 K/m, that correspond respectively to 250 and 50 mW/m^2 trough soil with 5 W/m.K conductivity.

The figure 11 displays extreme temperatures for different geothermal gradients (in K/m) in a pure quartz sand with a low porosity and medium frozen water content. The effect of this geothermal gradient is that the curve is tilting to the right when the depth increases.

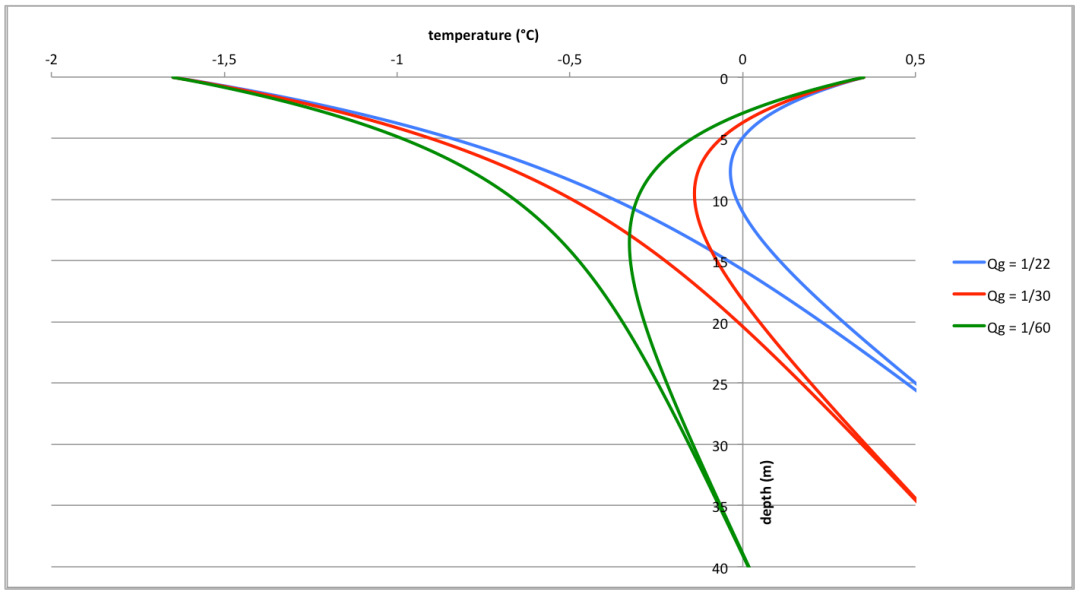

fig. 11 : temperature profile in the same material for different geothermal gradient

5. Mechanics of thawing soil

After freezing in winter, the soil is saturated in ice water. In spring, the melting of this water lead to a settlement that in some cases can be dramatic.

Soil thawing settlement often corresponds to the opposite of frost heave. However, the settlement is not the only concern. When frost heave increases the soil strength, thawing weaken the soil and destroys its cohesion. This is generally not dangerous for structures with a good foundation system, but in the case of erosion this is a very important factor.

5.1. Thaw settlement

Thaw settlement will be caused by both water phase change and excess water flow. The phase change is rather small in most soils, as it is nothing but the volume difference between ice and liquid water (that is 9%). Drainage of the melted water can lead to additional settlement.

5.1.1. Settlement from water phase change

In a saturated soil, the volume change due to the phase change of porous water alone is associated with the volume phase change of the water :

$$\frac{\Delta V}{V_0} = -0{,}09.n \qquad (5.5.1)$$

- ΔV : soil volume variation (m^3)
- V_0 : soil initial volume (m^3)
- n : porosity (no unit)

0,09 represent the volume difference between ice and liquid water, for the same mass.

5.1.2. Settlement from water flow

Excess water in the soil is closely linked to the behavior of the soil during the previous winter, and particularly the formation of segregated ice. While the soil is freezing, part of the porous water is liquid and part is solid. In fine-grained soils (especially silts and clays), the ice formation has a tendency to grow apart from the pores, creating pure ice formations called ice lenses. This process empties the pores, leading to more liquid water pouring from the neighbor soil. This phenomenon, called water suction, is amplified by the proximity of the water table that cut the energy required to lift the water up to the freezing soil.

The process of ice segregation can lead to dramatic changes in porosity. A simple thaw settlement measurement involves placing a bloc of frozen soil in a container and allowing it to

freely thaw. The amounts of water that will leak from the soil typically represent the thaw settlement.

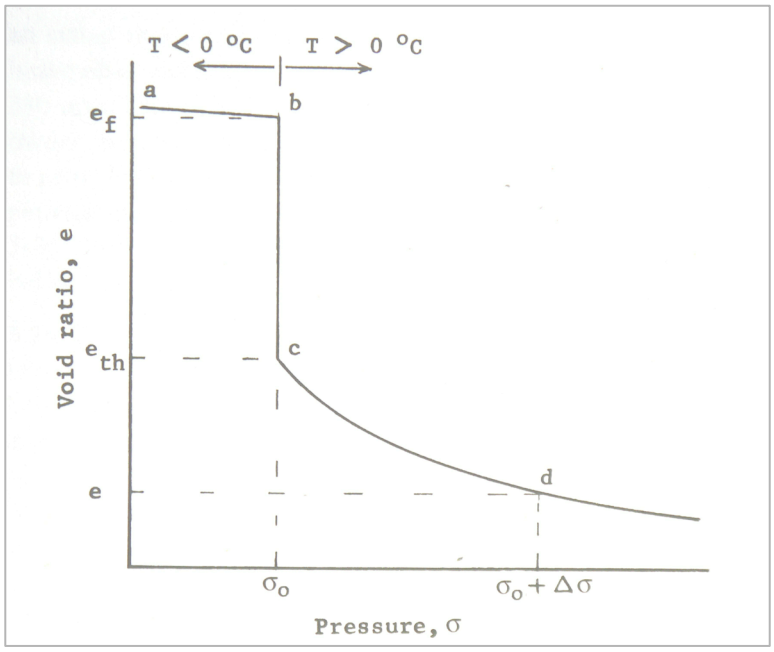

fig. 12 : typical void ratio versus pressure curve for frozen soil subject to thawing, courtesy Andersland and Ladanyi (2004)

A typical thaw test result is shown in figure 12. The small decrease in void ratio from a to b represents the behavior of the frozen material. The thawing (b to c) is done once the σ_0 pressure reached (generally the sample initial overburden pressure. Then, the material resumes to the normal behavior (c to d) of its unfrozen phase.

The thaw settlement is expressed as :

$$\frac{\Delta H}{H} = \frac{e_f - e_{th}}{1 - e_{th}} = A_0 \qquad (5.1.2 - 1)$$

- ΔH : change in layer thickness (m)
- H : initial thickness (m)
- e_f : frozen material void ratio ($m^3.m^{-3}$)
- e_{th} : thawed material void ratio ($m^3.m^{-3}$)

A_0 (no unit) is called the thaw-strain parameter and define a volume decrease due to thaw only (will ΔH is also result of pressure increase).

The void ratio can be replaced by the porosity easily enough :

$$e = \frac{n}{1 - n} \qquad (5.1.2 - 2)$$

$$\Rightarrow \qquad A_0 = \frac{n_f - n_{th}}{1 - n_{th}} \qquad (5.1.2 - 3)$$

- n_f : porosity of frozen soil ($m^3.m^{-3}$)
- n_{th} : porosity of thawed soil ($m^3.m^{-3}$)

Crory (1973) designed an alternative relationship using the dry densities :

$$A_0 = 1 - \frac{\rho_{d,f}}{\rho_{d,th}} \qquad (5.1.2-4)$$

- ρ_f : frozen material density (kg.m^{-3})
- ρ_{th} : thawed material density (kg.m^{-3})

This relation allows for a very quick estimation of a potential settlement, as dry densities are rather easy to measure in a lab.

Another approach presented by Crory (1973) uses the moisture content. The complete equation also account for the volume loss by phase change of water :

$$A_0 = \frac{\Delta w + 0{,}09.i_r.w_0}{\frac{\rho_w}{\rho_s}.S_r + (1+0{,}09.i_r).w_0} \qquad (5.1.2-5)$$

- w_0 : initial material moisture content (kg.kg^{-1})
- Δw : moisture content loss (kg.kg^{-1})
- S_r : initial saturation number (m^3.m^{-3})
- i_r : initial iciness ratio (kg.kg^{-1}) = $\frac{w_i}{w}$
- ρ_w : water density (kg.m^{-3})
- ρ_s : mineral material density (kg.m^{-3})

5.2. Stability of thawing soil

Many observations in cold areas evidence landslides in spring. The most surprising aspect of these is the very low angle, down to 1° (McRoberts and Morgenstern, 1974). It was found that many of the landslides associated with thawing could be described by a flow behavior.

Flow movement is a term used to describe the motion of a material that behaves like a viscous fluid. In the case of soil, it results in the absence or lack of evidence of shear stresses on the sliding plane. Huge displacements are distributed into the moving mass, and the pre-failure surface is often destroyed. Flow movement is disturbed by slope changes and obstacles such as boulders or vegetation.

Varnes (1958), describes flow landslides as follow :

> "In flows, the movement within the displaced mass is such that the form taken by the moving material or the apparent distribution of velocities and displacements resembles those of viscous fluids. Slip surfaces within the moving mass are usually not visible or are short-lived, and the boundary between moving and stationary material may be sharp or it may be a zone of plastic flow."

5.2.1. Effects of frost/thaw cycles on the microstructure

Uniaxial tests on frozen clays and sand by Bourbonais and Ladanyi (1985) show that with decreasing temperature and increasing porosity, the bonds between solid grains are gradually destroyed and replaced by an ice matrix. This replacement is due to the expansion of the ice (frost heave) as seen in scheme 13. While temperatures are negative, this new structure is strong, as ice bonds are way stronger than water bonds. However, if undrained (that is to say, quick) thawing occurs the water bonds have no time to restore as solid particles are too dispersed.

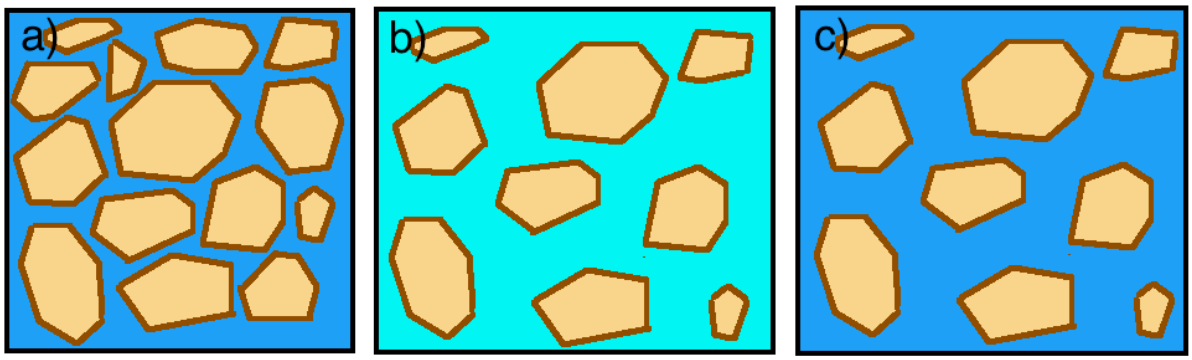

fig. 13 : frost cycle on microstructure : initial material a), frozen and expanding microstructure b), expanded microstructure saturated and unstable c)

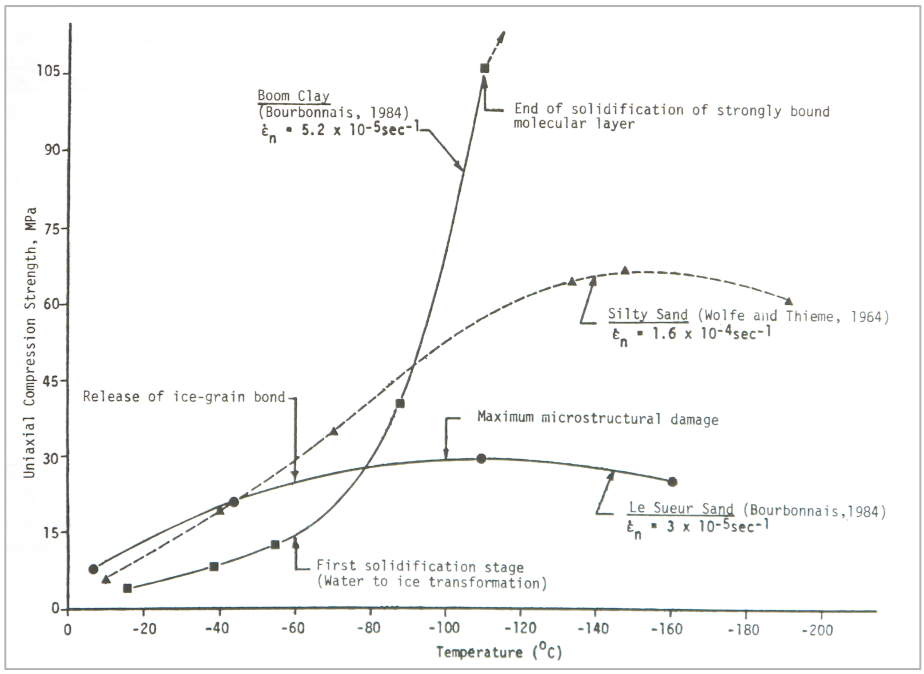

fig. 14 : influence of temperature and soil type on uniaxial compression strength for three typical frozen soils, Bourbonnais (1984)

The same reasoning can be hold for friction soils. Even if the frost heave is not as huge as in clays and ice lenses do not form, it decreases the compaction of the soil. Thus, the friction angle is widely affected.

5.2.2. Stability of low angle planar flows

The main problem in calculation of flow landslides is the low angle. In geotechnical engineering, it is usual to consider the stability of long, shallow slopes in an infinite analysis, thus calculating the safety factor as :

$$F_S = \frac{\gamma'}{\gamma} . \frac{\tan(\Phi')}{\tan(\theta)} \qquad (5.2.2 - 1)$$

- γ'/γ : ratio of effective to total unit weight, usually 0,5 (no unit)
- Φ' : friction angle (°)
- θ : slope angle (°)

However, observations along the Mackenzie River show that clays with friction angle up to 23° are common. According to the formula (5.2.2 - 1), such materials should be stable for slopes below 12,5°. But many slopes in the studied area failed at angles between 3° and 9°.

The formula (5.2.2 - 1) has been developed using the hydrostatic pore pressure condition. In attempt to explain the low failure angle, McRoberts assumed the existence of an excess pore pressure. This excess pore pressure was first evidenced by Morgenstern and Nixon (1971), by coupling the Terzaghi traditional consolidation theory with a thaw boundary defined by the Neuman solution :

$$d = \alpha . \sqrt{t} \qquad (5.2.2 - 2)$$

- d : depth of thawing (cm)
- t : time (s)
- α : a constant ($cm.s^{-1/2}$) depending the thermal properties of the soil, Nixon and McRoberts (1973)

The term α can be used to define the thaw consolidation ratio R :

$$R = \frac{\alpha}{2.\sqrt{c_v}} \qquad (5.2.2 - 3)$$

- c_v : coefficient of consolidation ($cm^2.s^{-1}$)

This number express the ratio between the rate at which water is produced from thaw and the rate at which is can be evacuated. McRoberts found that for an infinite soil mass thaw-consolidating under self-weight conditions, the excess pore pressure u is :

$$u = \frac{\gamma'.d}{\left(1+\frac{1}{2.R^2}\right)} \qquad (5.2.2 - 4)$$

- γ' : effective weight ($kg.m^{-3}$)
- d : depth of thawing (m)

Considering a slope of angle θ, McRoberts assumes that a measure of the pore pressure parallel to the sliding plane is :

$$u = \frac{\gamma'.d.\cos(\theta)}{\left(1+\frac{1}{2.R^2}\right)} \qquad (5.2.2-5)$$

- θ : slope angle (°)

After a static balance analysis, the safety factor becomes :

$$F_S = \frac{\gamma'}{\gamma}.\left(1-\frac{1}{1+\frac{1}{2.R^2}}\right).\frac{\tan(\Phi')}{\tan(\theta)} \qquad (5.2.2-6)$$

This formulation shows that the slope angle below which the slope is unstable can be decreased to a fraction of its initial value. Especially if the consolidation rate c_v is low, meaning the water evacuate slowly, the thaw consolidation ratio R will increase and the safety factor will drop.

According to McRoberts's observations, consolidations rates ranging from 0,1 $cm^2.s^{-1}$ in sandy soils to 10^{-5} $cm^2.s^{-1}$ or less in fine-grained clays, while α can be expected between 0,01 and 0,1 $cm^2.s^{-1/2}$. In practical, R ratio can go up to 2 (McRoberts and Morgenstern, 1974), which mean a safety factor decrease to 10% of its initial value.

Indeed, cohesion soils such as clays are particularly vulnerable. Because of their low permeability and their tendency to form ice lenses, they evacuate water slowly. In addition, the residual friction angle is lower than in friction soils such as sands.

6. Mathematical tools for thermal simulation

In order to perform a good thermal analysis, any user shall properly select the kind of results he is expecting, what he needs to know. Is him interested in a yearlong analysis displaying temperature every day ? Or are maximal and minimal temperatures enough ? In this paper, the temperature profile, which displays extreme temperatures at every depths will be the main analysis tool. One example is shown in figure 10 in chapter 4.

6.1. Temperature profile, "simple" model

The so-called "trumpet" curve is a plot of maximal and minimal temperatures at every depths below a single point at the surface. This kind of temperature profile is a powerful tool, both for its simplicity and for the crucial elements it permits to quickly grasp.

Ground temperatures can by calculated with climate, thermal conduction and geothermal conditions. This method (Andersland and Ladanyi, 2004) considers only heat flux by conduction. The ground surface temperature, related to the climate and surface conditions (vegetation, snow, topography…) can be approximated as a sinusoidal function :

$$T_{S,t} = T_m + A_S . sin \frac{2\pi . t}{p} \qquad (6.1-1)$$

- $T_{S,t}$: surface temperature at every time (°C)
- T_m : mean surface temperature (°C)
- A_S : amplitude of the surface temperature plot (°C)
- t : time (s)
- p : period of a cycle, so 1 year = 365x24x3600 = 31 536 000 s

Applying the Fourier's law to a semi-infinite and homogeneous soil with a upper limit defined by this temperature lead to the following equation :

$$T_{z,t} = T_m + A_S . e^{\left(-z\sqrt{\frac{\pi}{\alpha . p}}\right)} . sin\left(\frac{2\pi . t}{p} - z . \sqrt{\frac{\pi}{\alpha . p}}\right) \qquad (6.1-2)$$

- $T_{z,t}$: surface temperature at every time (°C)
- z : depth (m)
- α : thermal diffusivity ($m^2.s^{-1}$)

From this equation, it is fairly easy to extract the extreme annual temperatures :

$$T_{z,extreme} = T_m \pm A_S . e^{\left(-z\sqrt{\frac{\pi}{\alpha . p}}\right)} \qquad (6.1-3)$$

Such a relation will define the "trumpet-shaped" curve. This is a rather simple theoretical model, but is a fair approximation, particularly in dry coarse soils or rocks. Saturated and/or

fine soils will show divergent behavior. Those can be caused by porous water latent heat, difference between frozen and unfrozen thermal properties, heterogeneities in soil or non-sinusoidal surface temperatures (in particular asymmetrical patterns due to snow cover). In order to include these effects, numerical calculations such as Finite Element Method will be a very powerful tool.

6.2. impact of annual diffusivity change, "bi-diffusivity" model

The effect of a change in thermal diffusivity while the porous water in the soil freezes or melts can be estimated by plotting two different diffusivities into the equation (6.1 – 3). Thus, it becomes :

$$T_{z,min} = T_m - A_S . e^{\left(-z\sqrt{\frac{\pi}{\alpha_f \cdot p}}\right)} \quad ; \quad T_{z,max} = T_m + A_S . e^{\left(-z\sqrt{\frac{\pi}{\alpha_u \cdot p}}\right)} \qquad (6.2)$$

- α_f and α_u are frozen and unfrozen thermal diffusivities ($m^2.s^{-1}$)

However, simulations in 9.3.1 will later show that this equation has some flaws, and corrected models will be proposed.

6.3. Impact of surface geometry, "corner" model

The soil geometry is obviously a determining factor for the temperature distribution. Even using the semi-infinite model developed in 6.1, the slope will determine the distance of an element to the surface. But a more precise analysis must expect the variation of the surface shape to have more effect than merely shaping the isotherms to be parallel to the surface (like in the semi-infinite model above).

As far as I know, there is no analytical model available to calculate the effect of a change in slope upon the temperature profile. This paper will then aim at propose its own method, called "corner" model, developed on the basis of the analytical model proposed by Andersland and Ladanyi with the necessary modifications. Numerical analysis by TempW will help calibrate the model, as experimental measurements are not available.

In a rectangular model, heat flux goes only downward. Now, if one shifts the rectangle so that the model is an infinite and constant slope, he gets the very same result in a shifted coordinate system. So the problem is not the slope, it is variations in slope, the corners.

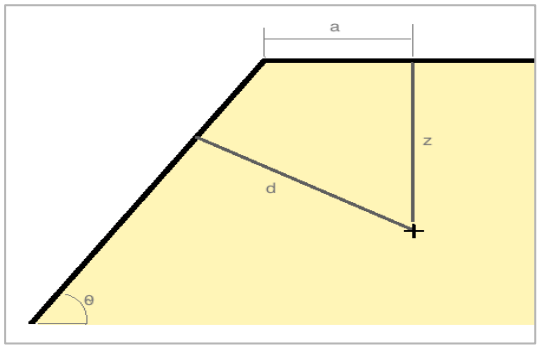

fig. 15 : geometrical parameters for the "corner" model

Each side of the corner, at infinite distance, the

effect of the opposite profile is not significant. One can safely assume that, going farther to the corner, each profile resume to its “normal” pattern.

Considering the additive property of heat flow, and the linear expression of the thermal conduction, his paper will make the hypothesis :

the temperature in a soil element under a corner, is increased by the temperature that would result by the infinite slope, pondered by a factor η :

$$\eta = \left(1 - e^{-\frac{z}{d}}\right) \quad (6.3-1)$$

- z : depth (m)
- d : ‘’shifted’’ depth (m)

The ‘’shifted depth’’ d is calculated as :

$$d = [z + a.\tan(\theta)].\cos(\theta) \quad (6.3-2)$$

- z : depth (m)
- a : horizontal distance to the corner (m)
- θ : slope angle (rad)

Those

$$T_{z,t} = \left[\left(T_{m,S1} + A_{S1}.e^{\left(-z\sqrt{\frac{\pi}{\alpha.p}}\right)}\right) + \eta.\left(T_{m,S2} + A_{S2}.e^{\left[-d.\sqrt{\frac{\pi}{\alpha.p}}\right]}\right)\right] \quad (6.3-3)$$

- $T_{m,S1}$: mean temperature of the horizontal surface (°C)
- $T_{m,S2}$: mean temperature of the sloping surface (°C)
- η : slope factor (no unit)
- A_{S1} and A_{S2} : temperature amplitudes at the horizontal and sloping surfaces (°C)
- z : depth (m)
- d : ‘’shifted’’ depth (m)
- α : thermal diffusivity ($m^2.s^{-1}$)
- p : time period of the sinusoidal surface temperatures (s)

This formula can be generalized to every slope change by just shifting the whole model by a in second angle β that correspond to the first slope. First, one must change the formula for d and η :

$$d = \left[\frac{z}{\cos(\beta)} + a.\tan(\theta - \beta)\right].\cos(\theta - \beta) \quad (6.3-4)$$

$$\eta = \left(1 - e^{-\frac{z}{d.\cos(\beta)}}\right) \quad (6.3-5)$$

- z : depth (m)
- a : distance to a line perpendicular to the slope β crossing the corner point (m)
- β : first slope angle (rad)
- θ : second slope angle (rad)

So the formula becomes :

$$T_{z,t} = \left[\left(T_{m,S1} + A_{S1}.e^{\left(-\frac{z}{\cos(\beta)}\sqrt{\frac{\pi}{\alpha.p}}\right)}\right) + \eta.\left(T_{m,S2} + A_{S2}.e^{\left[-d.\sqrt{\frac{\pi}{\alpha.p}}\right]}\right)\right] \qquad (6.3-6)$$

As far as I know, no such hypothesis as been made in the literature. Therefor, this model shall be tested against FEM calculations by TempW, and also confronted to the experimental case at Vestpynten.

6.4. Impact of a layered structure

It is rather obvious that a brutal change in thermal diffusivity will appear on the temperature profile. Although the analytical model in 6.1 supposes that the soil is homogeneous, it is rather simple to adapt it in order for it to allow a layered structure.

The method developed in this paper first considers that the temperature in a layer only depends on its internal thermal properties, and the temperature conditions at the upper limit. The model in 6.1 perfectly follows those hypotheses.

Now the method considers that soil layers interact only via the limit between them. In addition, it supposes the continuity of the temperature. Based on those hypotheses, the temperature at the bottom of the upper layer can be used as the upper limit condition for the layer below.

The modified equations are :

$$T_{z,t} = T_m + A_S.e^{\left(-z\sqrt{\frac{\pi}{\alpha.p}}\right)} \qquad \text{for } z \leq e \qquad (6.4-1)$$

$$T_{z,t} = T_m + A_S.e^{\left[e.\sqrt{\alpha_2}+(z-e).\sqrt{\alpha_1}\right].\sqrt{\frac{\pi}{\alpha_1.\alpha_2.p}}} \qquad \text{for } z > e \qquad (6.4-2)$$

- T_m : mean surface temperature (°C)
- A_S : amplitude of the surface temperature plot (°C)
- α_1 : thermal diffusivity ($m^2.s^{-1}$)
- α_2 : thermal diffusivity ($m^2.s^{-1}$)
- z : depth (m)
- e : thickness of the first layer (m)
- t : time (s)
- p : period of a cycle, so 1 year = 365x24x3600 = 31 536 000 s

This is simpler to do in incremental calculation, via a spreadsheet calculation software such as Excel. The trick is to calculate the temperature extremes in incremental layers of soil, of a thickness that will rule the precision (but does not must to be constant). Thus, the amplitude calculated in the last increment of the upper layer can be used to start a new calculation in the second layer. This method will be used in the chapter 8.2 and 9.2.

6.5. TempW

TempW is a software developed by GEO-SLOPE for civil engineering purposes. It can be used to calculate thermal changes in the ground, due to environmental changes or constructions.

TempW uses a finite element calculation method. In a few words, that means it divides the soil in a mesh of many small elements. Each of these elements is a simple polygon (mostly triangles and quadrilaterals) with nods at the edge and sometimes within. These elements interacts with each other through the nods they share and simple laws. Finally, users can act upon the entire model trough boundary conditions, meaning they can force a flux or a state in edge areas, and then watch the effect in the entire structure.

6.5.1. Meshing

Meshing in TempW is semi-automatic, meaning that the computer will generate the mesh using basic parameters chosen by users. The automatic generation will guaranty the compatibility and will tend to be the most uniform.

There are two types of elements in TempW : quadrilaterals and triangles. Triangles are the most simple element possible. Quadrilaterals are a little more complicated, for they have one more angle and so at least one more nod. However, they are the easiest element to fit most geometric forms (except discs or ovals, that are better represented with triangular meshes).

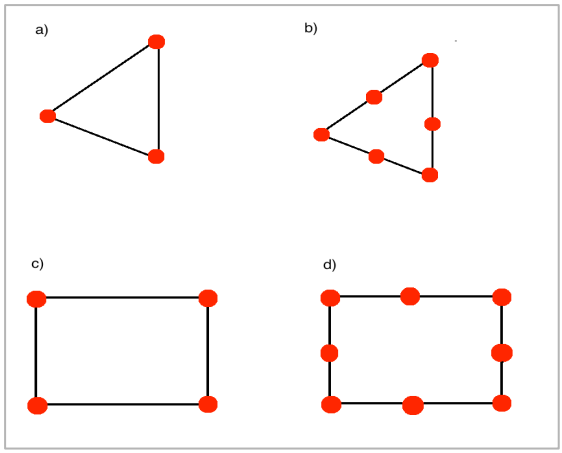

fig. 16 : example of finite elements : triangular 3 and 6 nodes a) and b), and quadrangular 4 and 8 nodes c) and d)

6.5.2. Material model

TempW has two main material models : simplified thermal and full thermal. The two are based upon the Fourier law, but full thermal allows more supple definition of the properties.

Simplified thermal model

In the simplified thermal material, three parameters are entered : conductivity, volumetric heat capacity and water content. The material has a double behavior : frozen state and unfrozen state. Both thermal conductivity and heat capacity can be distinguished in the two states, but within a state it is fixed. This is a rather good approximation for coarse or unsaturated soils, as well as rock and crushed rocks that have not a huge difference between frozen and unfrozen state.

Full thermal model

In the full thermal model, we find exactly the same parameters. But both the heat capacity and the conductivity can be defined with a complete, user-defined law. Basically, it is a generalization of the first. This can be useful for fine description of soils very susceptible to thermal conductivity changes. This can also, with extreme caution, be used to mimic the thermal effects of frost heave and creation of ice lenses.

Water content

In both models the user it able to define a fixed water content. This water has not effect upon the conductivity and heat capacity (within the software), it is therefore important to carefully account for this water before setting his hands on the software, and integrate the effect of water when entering those two parameters in the model.

The water content will enable TempW to calculate the energy needed during phase change (see 6.5.3, Water Enthalpy).

6.5.3. Physical laws

A finite element mesh is no more than a mathematical object. In order to be able to represent the behavior of real soils, it must be completed with a set of physical laws. Those laws are nothing but relations describing the variation of a set of parameter within an element in function of the state of the surrounding elements. Thus flux equations, being related to mechanics (Hook's law for example), water flow (Darcy's law) or thermodynamic (here is Fourier's law), are particularly well suited for this method.

The equation controlling the system is defined as :

$$\frac{\delta}{\delta x}\left(k_x.\frac{\delta T}{\delta x}\right)+\frac{\delta}{\delta y}\left(k_y.\frac{\delta T}{\delta y}\right)+Q=\left(c+L.w.\frac{\delta W_u}{\delta T}\right).\frac{\delta T}{\delta t} \qquad (6.5.3-1)$$

- T : temperature (°C)
- k_x and k_y : horizontal and vertical thermal conductivity ($W.m^{-1}.K^{-1}$)

- Q : applied flux at boundary ($W.m^{-3}$)
- c : heat capacity ($J.m^{-3}.K^{-1}$)
- L : latent heat of water ($J.m^{-3}$)
- w : moisture content (m^3/m^3)
- W_u : ratio between unfrozen water and total moisture content (no unit)

The left part of the equation defines the heat flux, and the right part is called the heat storage capacity.

Heat flux

The main heat transfer way within the soil is conductivity, that is to say the heat goes from one element to another via their contacts, embodied by the nodes they share. The theoretical models for calculation are based upon the Fourier's law :

$$Q = -k.grad(T) \qquad (6.5.3-2)$$

This law is explained in 4.2.

Heat storage capacity

Heat storage is defined in TempW by the parameter λ :

$$\lambda = \left(c + L.w.\frac{\delta W_u}{\delta T}\right) \qquad (6.5.3-3)$$

The volumetric heat capacity is a material property, indicated by the user in the material model. The term $w.\delta W_u$ correspond to the amount of water that changes in phase. This phenomenon implies creation/loss of heat energy that is added to the heat capacity. The physical process is explained in paragraph 4.5.

7. Preliminary study, hands on TempW

Before performing a complete study it is important to calibrate a methodology. Results and conclusions of this chapter shall be used later for more advanced simulations. Optimization of the calculation process is an important concern, as some simulations developed in chapter 8 contain more than 200.000 iterations, each handling a 1000x1000 matrix. Such calculations can take tens of minutes depending on the computer power available.

For the purpose of this preliminary study, a simple rectangular model shall suffice, and is also very convenient for checking with hand calculations (see chapter 6). The boundary conditions are the following :

- top : T = surface temperature, $T_{S,t}$
- sides : heat flux = 0
- bottom : T = mean surface temperature T_m

As this simple simulation will later prove to be very easy to compare with analytical calculations, it will be used later for calibration of the calculation methodology.

7.1. Convergent calculation method

The ground that interests us is submitted to a cyclic change of temperature, whose period corresponds to a year. However, the temperatures at a time are related to the nature of the soil as well as the climate. For this reason, it would be hard to start a simulation straight away from correct temperatures. A simple method to avoid this problem is to run a transient simulation from a soil at an arbitrary temperature. After some years, the temperature pattern in the soil will become stable, and therefore approach the steady state we are looking for. Figure 17 shows a typical behavior of a ground reaching its steady temperature from an arbitrary uniform temperature.

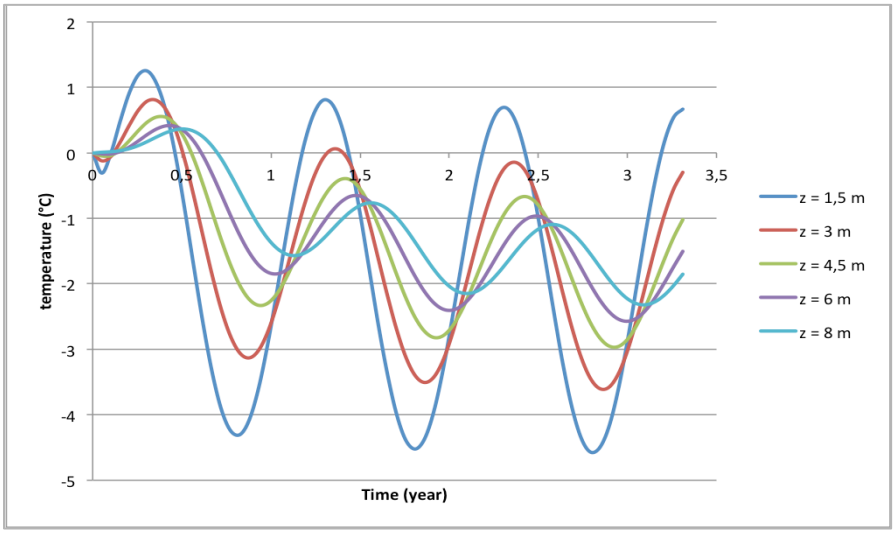

fig. 17 : typical convergence figure of the daily temperatures at different depths

This transient state will be of no use in the simulation, for it is a virtual step whose only purpose is to converge to the actual yearly cycle. However, it is important to know how many years it takes to converge, in order to later avoid picking results in this phase.

The figure 17 displays the temperature at 5 different nodes trough 3 years. At t = 0, the whole soil is at 0 degrees, and then it is submitted to a sinusoidal temperature change at the surface. The node 1, close to the surface, follow almost instantaneously the climate pattern, but the node 5, that is 8m into the ground, takes almost 4 years to become stable. Based on this figure, we could say this model takes 4 years to converge, and results become significant only starting from the 5th.

7.1.1. Influence of climate

The climate obviously is a prim-importance factor in the convergence being quick or slow. A soil will follow quick enough a pattern that is close to its initial temperature. A sinusoidal surface temperature pattern has tree factors that could be influencing the convergence speed : the frequency, the mean temperature and the amplitude. Since only a yearly period interest us, this paper shall not discuss about the frequency and its effects.

First, the mean temperature, or more precisely the distance between the mean temperature and the initial temperature of the ground, is very significant. In order to show the importance of the mean surface temperature, 3 simulations have been done with mean temperatures of 0, -2 and -4°C, keeping the initial ground temperature to zero.

This curves in figure 18 shows the behavior of a single node, opposed to its modeled steady state. This steady state is none but the mean of the 3 last years of simulation, repeated again and again. The difference between those 2 curves will then be calculated. The figures 21, 22 and 23 show the convergence of 5 nodes, in the 3 climates described.

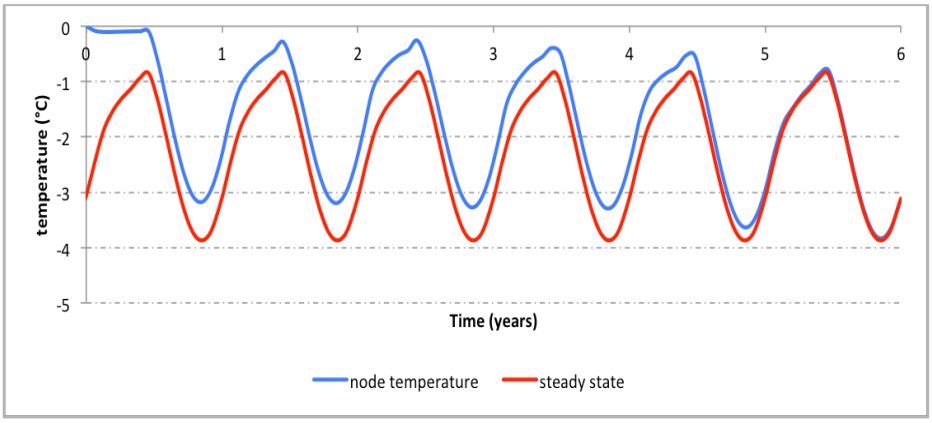

fig. 18 : convergence of the temperature at fixed depth, compared with the steady state

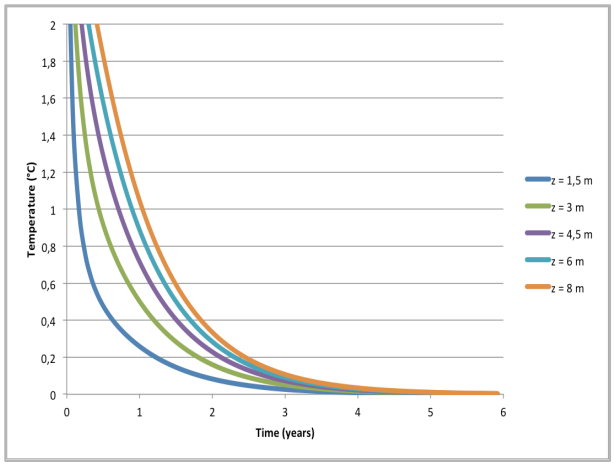

fig. 19 : difference of the temperature of different nodes with their steady state counterpart, for a climate amplitude of 4 and mean temperature 2°C below starting temperature

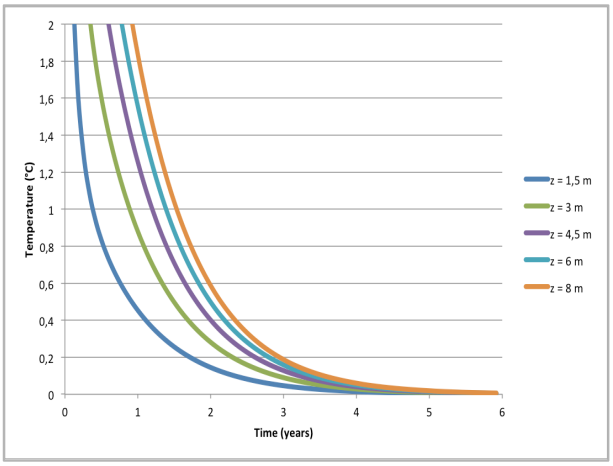

fig. 20 : difference of the temperature of different nodes with their steady state counterpart, for a climate amplitude of 4 and mean temperature 4°C below starting temperature

fig. 21 : difference of the temperature of different nodes with their steady state counterpart, for a climate amplitude of 8 and mean temperature 2°C below starting temperature

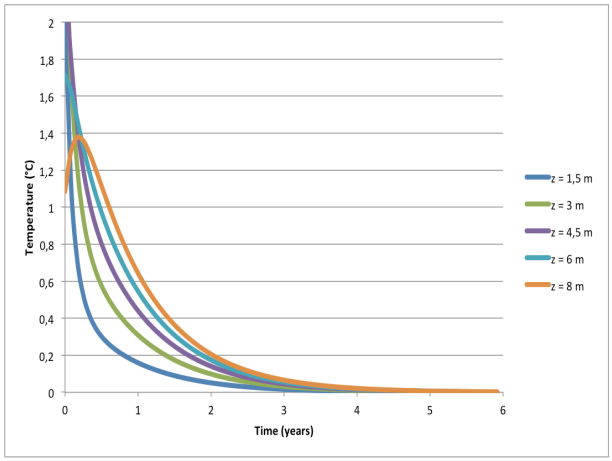

If a complete set of initial ground temperature cannot be obtained, it seems that setting it to the mean surface temperature considerably reduces the time of convergence. In the 3rd climate (fig. 21), a steady state is reached in 3 years, against 5 for the 2nd (fig. 20).

7.1.2. Influence of material

Thermal properties of the material will have also an influence over the convergence time.

Thermal conductivity is the opposite to the resistance to a heat flux. Therefore, it could be easily foreseen that a biggest conductivity will cause a quickest convergence. The two simulations above show that.

The influence of heat capacity is slightly more complicated. Heat capacity is the thermal equivalent for inertia. At first view, one shall say that a greater inertia means a longer time to move and reach the steady state. But a very great inertia will also mean that the steady state is almost constant, and so reached immediately because the temperature does not move at all.

The figures 22 to 24 show the convergence of three “designed” materials. One is typical for a compact dry sand, the other for a clay and the last is more like a granite. They have been designed such as the material 1 (“sand”) share the same thermal conductivity as material 2 (“clay”), and the same heat capacity as material 3 (“granite”). It can therefor be used as a control material for study of the influence of both parameters.

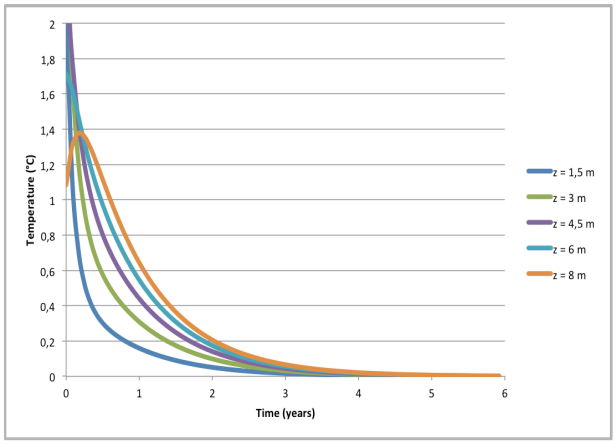

fig. 22 : difference of the temperature of different nodes with their steady state counterpart in material 1 (sand)

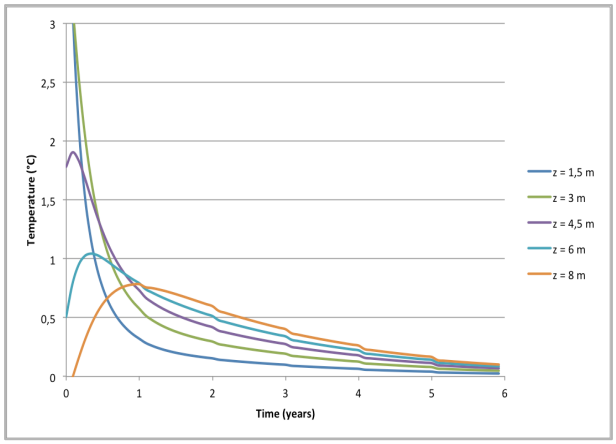

fig. 23 : difference of the temperature of different nodes with their steady state counterpart in material 2 (clay)

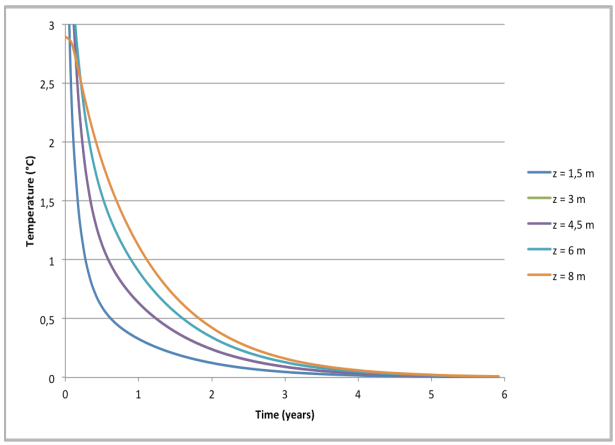

fig. 24 : difference of the temperature of different nodes with their steady state counterpart in material 3 (granite)

The conclusion of this study is that thermal conductivity and heat capacity has the exact same influence over the convergence of the simulation. Precisely, it is the thermal diffusivity (aka the ratio of the two) that changes the convergence time. However, heat capacity variation typically ranges between soils from a factor 0,25, against a factor 10 for thermal conductivity. Thus, while heat capacity has a very limited influence, thermal conductivity has a huge impact.

7.2. Estimation of a reasonable model depth

The depth of the models that shall be used in this research has to be sufficient for boundary limits to be realistic. It is thereby important to fix that depth as soon as possible. In order to do that, one shall estimate at which depth the surface temperatures ceases to have any influence.

The figure 25 shows the depth of influence varying with the material. The used materials are the same as used previously in 7.1. Water content is set to zero.

fig. 25 : temperature amplitude versus depth for different materials

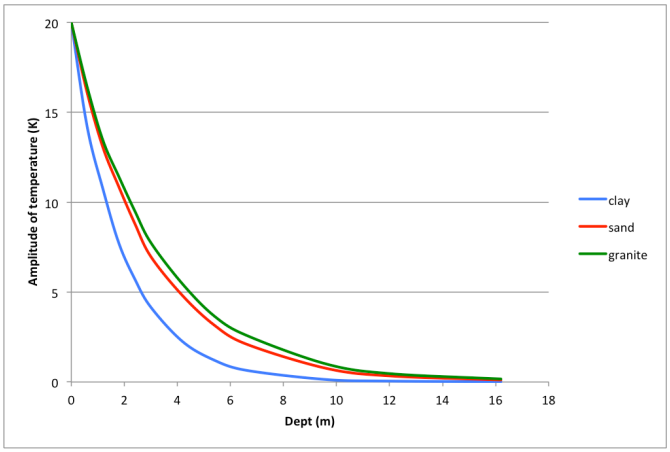

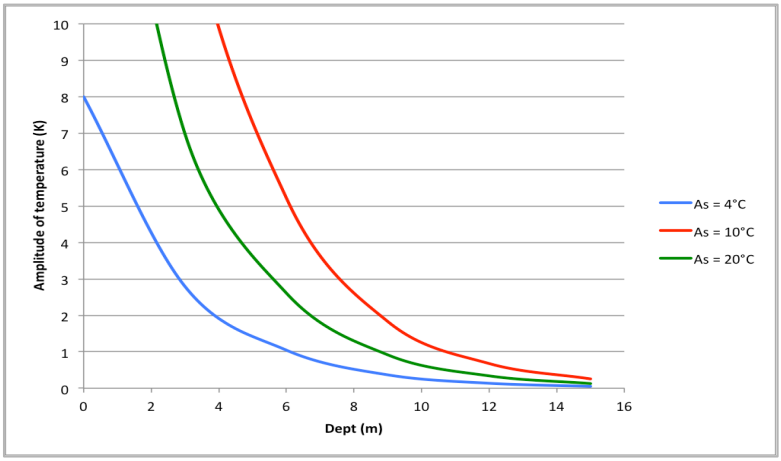

fig. 26 : temperature amplitude versus depth for different surface conditions (As = temperature amplitude)

The gap between the blue curve and the red shows the great influence of the conductivity. That is simple to explain : the lower the resistance, the deeper the heat flux shall go before it fades. The red curve is also slightly below the green. That is so because, as the heat capacity is higher in the sand, the system has more inertia.

The climate of course has an impact over the influence depth. In such a simple model, the amplitude of temperature at a certain depth is directly proportional to the amplitude at the surface. However, the mean temperature has no effect of the kind.

The influence of water upon the critical depth shall not be described here. However, the energy consumption during the state changes act as a kind of inertia, for it impeach the temperature in the concerned element to move until the change is completed. Thereby, the adding of water in the soil numerical model can only reduce the critical depth.

7.3. Time increment

In a transient simulation, the time increment is a kind of third (or fourth, if the simulation is in 3D) dimension of a mesh. The same way one divides the material in pieces called elements, one divides the time in increments. The smaller the increment, the better the precision and the higher the number of calculations required.

It is then important to define a good time increment. Not too big, in order to stay accurate, but not too small also in order too keep the calculation time low.

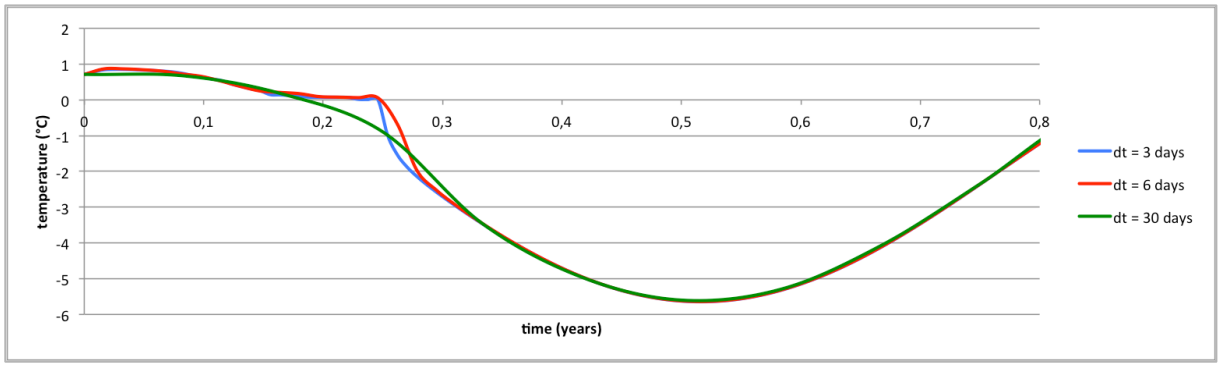

fig. 27 : comparison of near-surface (40 cm) temperatures for different time increments

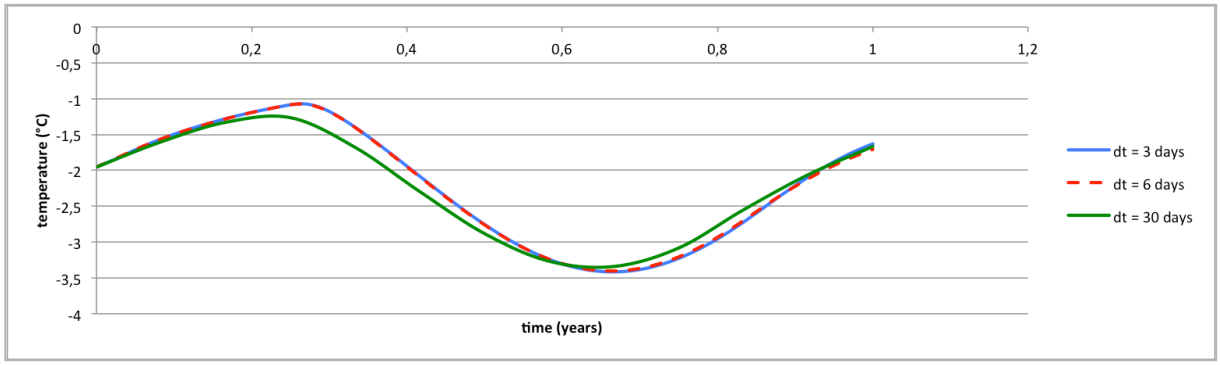

fig. 28 : comparison of temperatures for different time increments at 5 m depth

It appears that simple sinusoidal variations are quite well represented with wide increments. However, when the temperature is close to zero, part of the ground freeze/unfreeze, thermal properties change and the pattern becomes slightly more complicated. As it is plain in the figure 27, this phenomenon is quite badly represented with such a wide time increment.

A time increment of 6 days seems enough to represent this phenomenon quite well. It is however interesting to note that it appears to add a lot of inertia in the thawing zone. This difference fades with depth, as one goes deep into the permafrost. But it is appears plainly that a 30 days time increment is too wide, for even at 6m depth the pattern shall not be strictly sinusoidal even if it stay completely frozen, because of the influence of the temperature in the

layer above. The figure 28 shows the same comparison at a depth of 6m, that is to say within the permafrost.

7.4. Influence of mesh

The mesh is a very important factor in Finite Element calculations. Although the semi-automatic meshing care for most of the job, it is important to determine the differences of behavior between a fine and a coarse mesh, or between triangular and quadrangular elements.

7.4.1. Element size

The size of elements basically rules the precision. When a very coarse mesh will be enough to accurately show a simple sinusoidal variation within a soil that keeps the same properties along the year, it will struggle with complicated patterns that are found near thawing temperatures. The figures 29 and 30 show the difference between a coarse mesh and a fine mesh. The first one will tend to be more sinusoidal.

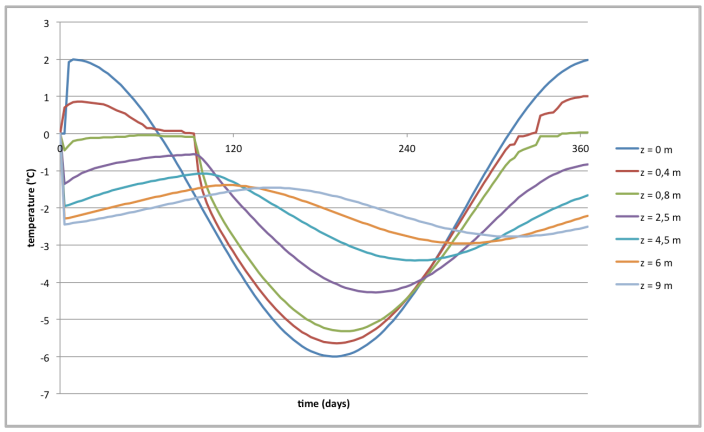

fig. 29 : temperature variation at various depths in a fine mesh (≈ 0,4 m wide elements)

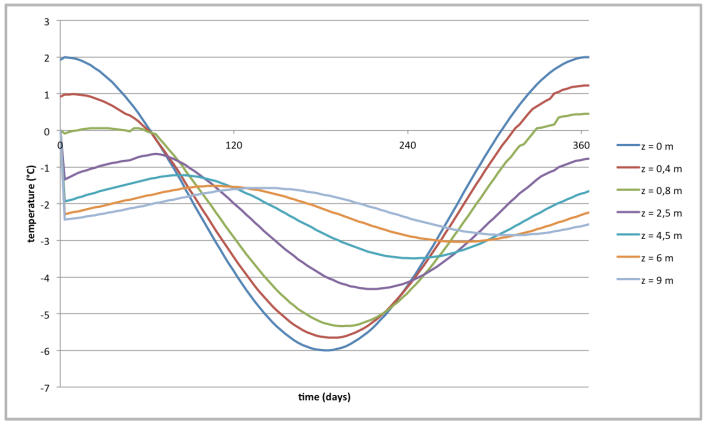

fig. 30 : temperature variation at various depths in a coarse mesh (≈ 1 m wide elements)

The figures 31 and 32 show the difference at two depths between three meshes. It is important to note that the initial temperatures have been calculated using a mesh close to the coarse one (a little more fine). However, it seems a little bit too coarse, for it has a tendency to follow the sinusoidal shape of the very coarse mesh.

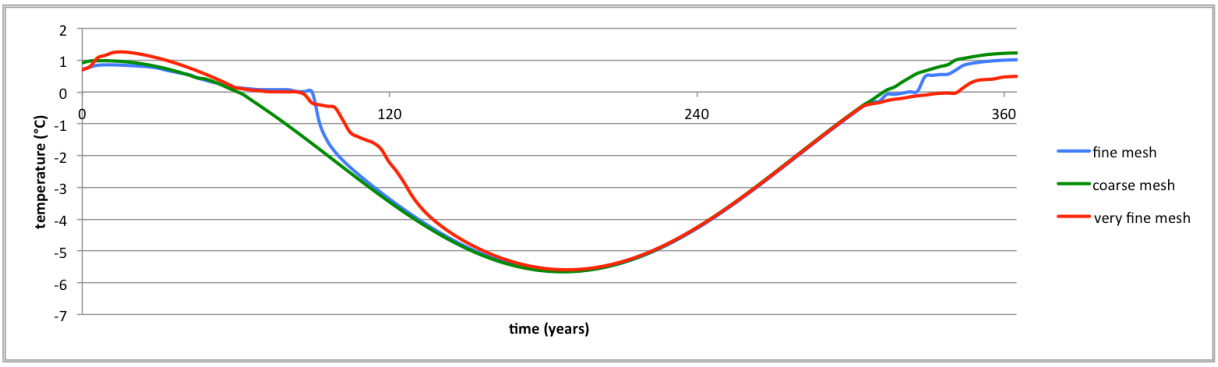

fig. 31 : comparison of near-surface temperatures for different meshes

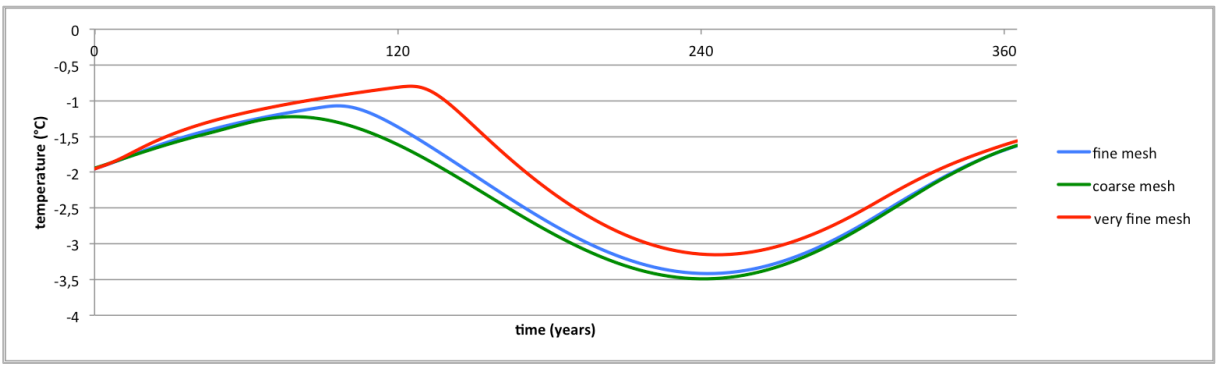

fig. 32 : comparison of temperatures for different meshes at 6 m depth

One shall note the "winter" temperature, far bellow zero, keeps its sinusoidal shape whatever the mesh. That shows that meshing is an important concern only when there are complex pattern involved by properties changes. Starting from a certain depth, as one goes deep into the permafrost and the temperature does not approaches zero anymore, one shall observe the same even in "summer".

7.4.2. Element type

The type of element is of course a question one shall ask himself. By default, TempW uses quadrangular, 4 nodes elements, so it is the element type that has been used until now. However, one shall ask if a triangular element would not be more accurate.

As it appears in the figure 35, the triangular mesh has a tendency to behave like a finer mesh of quadrangles. That is so, because for the same amount of nodes the triangular mesh has more elements. The figure 35 shows a comparison at 3m depth between a fine quadrangular, a coarse triangular and a coarse quadrangular mesh.

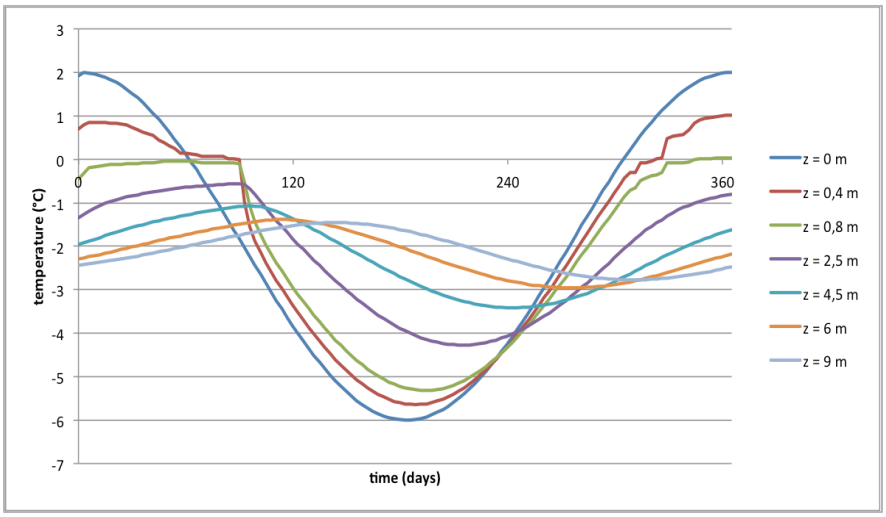

fig. 33 : temperature variation at various depths in a mesh of quadrangular, 4 nodes elements

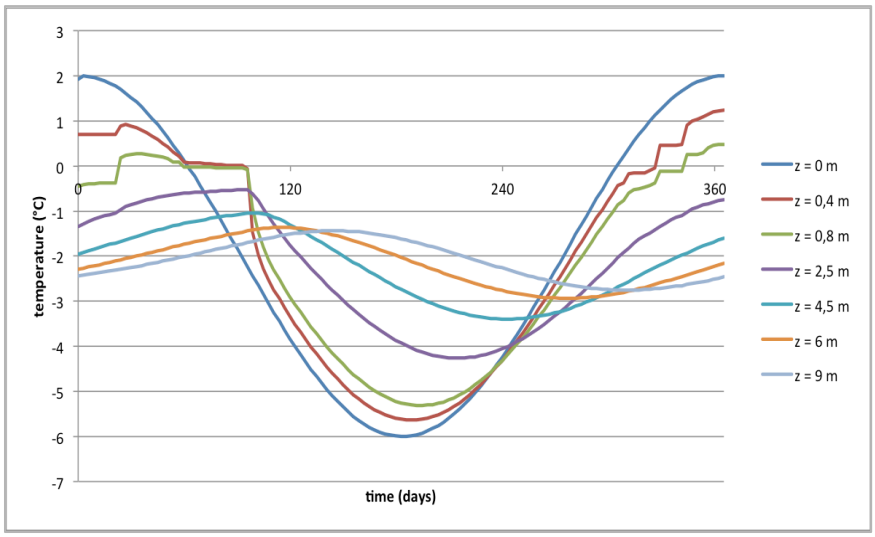

fig. 34 : temperature variation at various depths in a mesh of triangular, 3 nodes elements

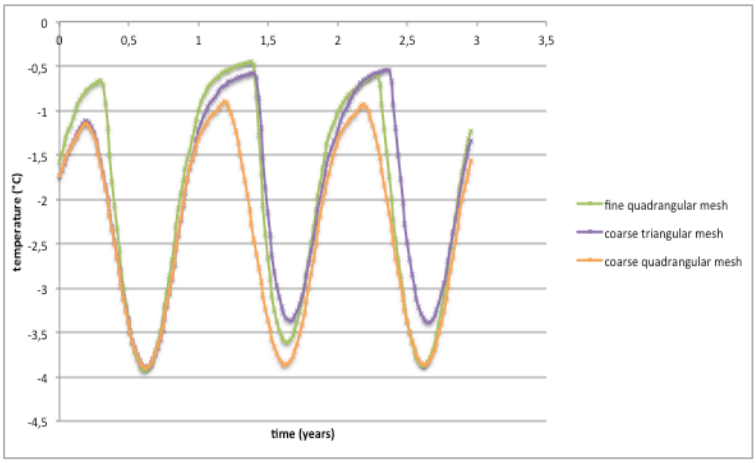

fig. 35 : comparison of temperatures for different meshes at 3 m depth

Finally, TempW proposes the use of second order elements, that is to say quadrangle with 8 nodes and triangles with 6 nodes. However, in this case, this still requires a quite fine mesh in order to stay accurate, and so add a lot of calculation for no real gain.

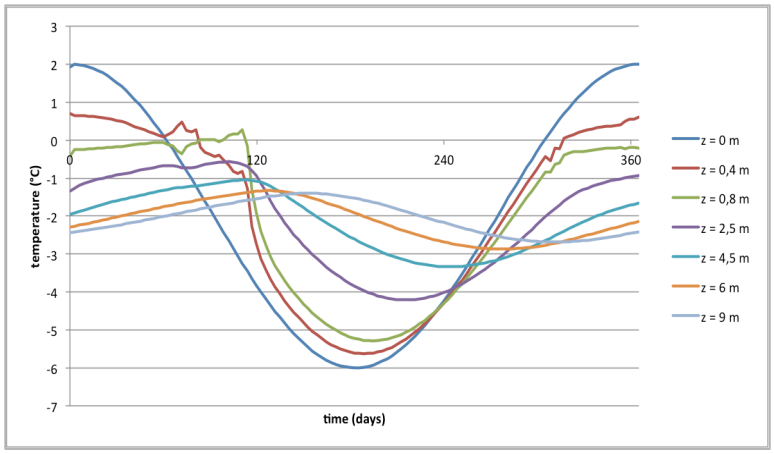

fig. 36 : example of thermal curves at different depths with 6 node triangular elements

In conclusion, precision of the thermal calculation is ruled almost entirely by the number of elements. The number of nodes has no visible impact. Thus, optimization of the meshing shall be obtained by reducing it to the minimum. Three node triangular elements are therefor the best suited for further simulation.

7.5. Boundary conditions

The boundary conditions are a crucial factor in every Finite Element calculation. In this analysis, they will permit to apply on the numerical model the conditions experienced by the actual site.

The top boundary condition is critical. It will represent the effect of the climate on the ground. There are two options : either it can apply the heat flux at the top, that is to say the actual heat transfer from the air to the soil, or it can force the surface temperature to coincide with the temperature resulting from the climate effect. The second choice seems better suited for further calculations, as it is simpler to handle. Moreover, it will be very easy to calibrate thanks to the surface measurements at Vestpynten.

As it has been discussed in 7.2, in an ideal simulation the bottom boundary condition has no influence at all. For this, it is equivalent to apply a temperature boundary condition equal to the mean surface temperature, or a flux boundary condition equal to zero. However, in some cases where there is ancient permafrost near the surface, with a constant temperature different from the mean surface temperature, it is helpful to use a temperature boundary condition in order to represent it.

The side boundary condition shall be a zero flux boundary condition, because of the assumption that the model is wide enough for getting no influence from the sides.

A special temperature boundary condition shall be used to represent the water temperature of the sea in chapter 10.

7.6. Conclusion of the preliminary search

This preliminary study will be especially useful for the design of further experiments. It shall aim at estimating control parameter such as geometry, mesh, time increment or the choice of boundary conditions.

7.6.1. Results

Tanks to the study of convergence, we know that a steady state is reached in a matter of 3 to 10 years. This can be improved by choosing appropriate initial temperatures. This study also permits to validate the geometry and boundary conditions. A surface of 20x20 m seems wide enough for our purposes. At 20 m depth, a fixed temperature is accurate. A mesh of triangular elements with 3 nodes seems the most appropriate, providing the geometry stays simple.

7.6.2. Establishment of simulation protocol

The depth of the model shall be at least 20 m, except if consistent measurements show a steady temperature at another depth.

The meshing shall use three node elements, with a default width of 0,8 m. For optimization of the calculation time, a size ratio of 0,5 shall be used in areas of secondary importance. A size ratio of 2 shall be used also in special areas with measurements sensors close to the boundary conditions.

The top boundary condition shall be a sinusoidal temperature. This temperature shall be calculated through climate and surface conditions analysis, or simply measured at a few spots on the ground, a few centimeters below the surface. The side boundary conditions shall be the flux equal zero on both sides. Bottom boundary condition shall be a steady temperature. By default, this shall be the mean surface temperature, but the existence of an old permafrost heir to ancient climates can be accounted by changing this temperature (see chapter 10).

The convergence of the transient simulation toward a steady cyclic state is a great concern. A 10 year simulation shall be taken as a default convergence time. However, such a long simulation does not permit the use of a fine time increment, because that will multiply the time of calculation (already consistent). A smart technique will consist of calculating initial temperatures trough a rough (coarse mesh and time increment, arbitrary initial temperature)

simulation, and picking the resulting temperatures as an initial temperature for a finer simulation, that will converge in one single year.

This shall work very well for simple studies. However, if water (or more precisely, freezing or melting of porous water) is involved, it shall be used carefully, that is to say with a medium time increment of 20 day, and an extended time of convergence of two years in the second (fine) simulation.

8. Simulation with TempW

In order to understand the parameters that have an influence over the thermal behavior of the coast profile, Finite Element Method calculations are a powerful tool. This chapter will explain how to calculate the influence of a wide range of parameters including thermal diffusivity, surface geometry, layers composition, climate and water content.

8.1. Climate and thermal diffusivity

According to the analytical model, the first parameters of any importance are the climate and thermal diffusivity. They are very well described by the analytical model, and so very easy to manipulate.

8.1.1. Sinusoidal climate

With the simple model defined in 6.1, it is rather easy to plot a model describing the conjugated effect of a sinusoidal climate and thermal diffusivity.

The tests 1 to 6 have been performed, and compared with theoretical calculations.

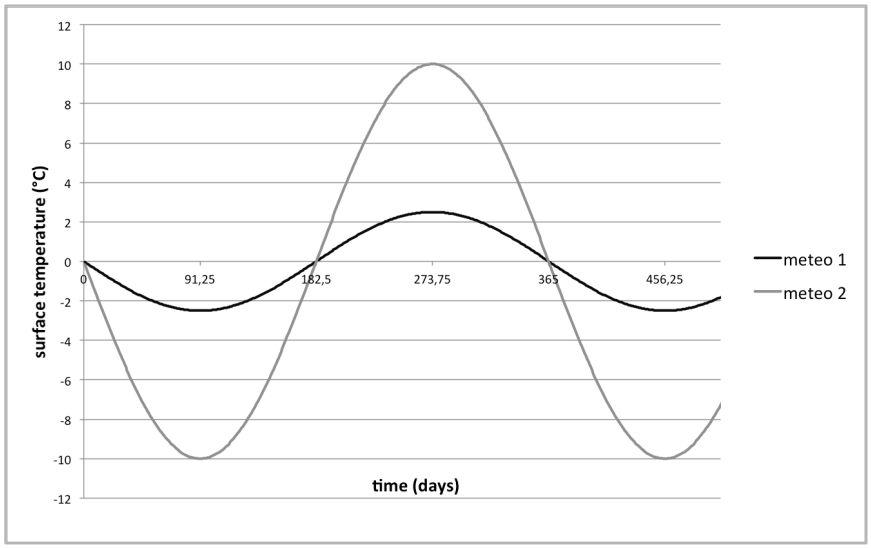

fig. 37 : boundary conditions used in tests 1 to 6

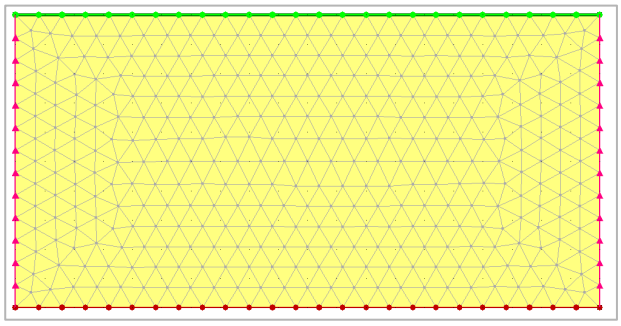

fig. 38 : mesh used for tests 1 to 9 and 16 to 24

Test n°	1	2	3	4	5	6
Climate amplitude As (°C)	2,5	10	2,5	10	2,5	10
Diffusivity α (10^{-7} $m^2.s^{-1}$)	1,3	1,3	6,0	6,0	13	13

tab. 3 : control parameters for tests 1 to 6

8.1.2. Non-sinusoidal climate

A special interest will be awarded to non-sinusoidal surface temperatures. As a sinusoidal climate is often a good approximation, it may significantly diverge from the actual behavior in several cases. Snow cover notably can significantly affect the surface temperature, shaping the annual temperature very differently from the sinusoid. According to the theoretical model in chapter 6, there shall not be any difference in the extreme temperatures profile. However, the change in shape should be visible in the annual temperature profile at every depth.

Two opposite temperature curve shape will be compared : the "normal" sinusoid, and the square (or crenels). It is assumed that every cyclic temperature pattern is a combination of the two.

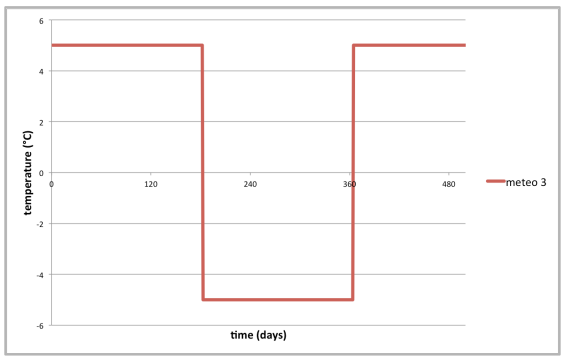

fig 39 : surface boundary condition for tests 7, 8 and 9

Test n°	7	8	9
Climate amplitude As (°C)	2,5	10	2,5
Diffusivity α (10^{-7} $m^2.s^{-1}$)	1,3	1,3	6,0

tab. 4 : control parameters used for tests 7, 8 and 9

8.2. Effect of layers

The impact of different configurations of layers is also very well described by the "multilayer" model in the chapter 6. The tests 10 to 15 shall verify the accuracy of this model. They will oppose again TempW simulations to analytical calculations, and try to propose explanations and corrections accounting for the appearing differences.

The structure used for the tests is represented in the figure 40. Each layer is 4m thick, with a different diffusivity. The surface boundary condition used correspond to "meteo 2" (see figure 37). The table 5 shows the diffusivities of the different layers.

Test n°	**10**	**11**	**12**	**13**	**14**	**15**
Diffusivity α_1 (10^{-7} $m^2.s^{-1}$)	1,3	1,3	6,0	6,0	13	13
Diffusivity α_2 (10^{-7} $m^2.s^{-1}$)	6,0	13	1,3	13	1,3	6,0
Diffusivity α_3 (10^{-7} $m^2.s^{-1}$)	13	6,0	13	1,3	6,0	1,3

tab. 5 : control parameters used in tests 10 to 15

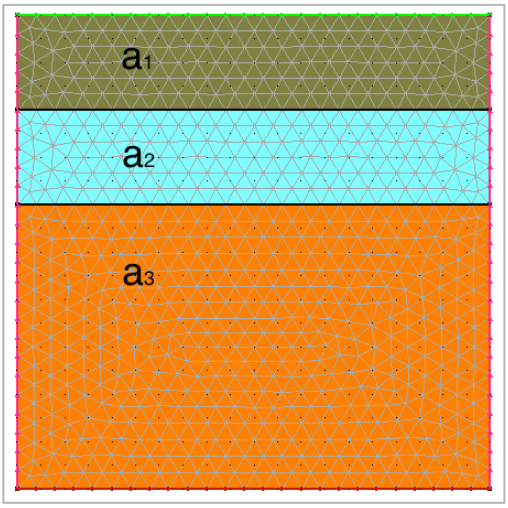

fig. 40 : mesh used for tests 10 to 15

8.3. Effect of water content

Water content is the first parameter that will need FEM to account for. Water has a double effect upon thermal behavior of the soil. First, it plays a big role in thermal diffusivity, and then it creates inertia via its enthalpy of fusion.

8.3.1. Water effect on thermal diffusivity

The heat capacity of water is 4,2 $kJ.kg^{-1}.K^{-1}$. That is more than four times higher than most mineral materials, so even if the mass of water is rather small compared to that of the mineral material, its effect is significant. But even more significant can be its contribution to conductivity, by filling the gaps between solid particles. However, those effects are easily calculated, using the "bi-diffusivity" method in chapter 6.

The most noticeable fact about the contribution of water to thermal diffusivity is its important variation between the frozen and the unfrozen state. Indeed, ice heat capacity is twice lower (2,09 $kJ.kg^{-1}.K^{-1}$) while its thermal conductivity, depending on its temperature, can be up to

2,21 $W.m^2.K^{-1}$ (4 times that of water). Moreover, water suction during freezing and huge increases in porosity can completely destroy the structure of the material, thus dramatically changing the thermal properties.

In order to represent this phenomenon, the material models in TempW can change of thermal diffusivity when freezing/thawing. The effects are very easy to spot. Frozen diffusivity has little to no effect upon maximal temperature, and unfrozen diffusivity has little to no effect upon minimal temperature. Thus, the difference between frozen and unfrozen diffusivity results in a dissymmetry of the temperature profile, that can also be back calculated using hand calculations.

The analytical solution is obtained by applying formula (6.1 – 3) to both unfrozen and frozen material. The maximal solution of the unfrozen and the minimal solution of the frozen material are then put together.

The thermal diffusivity change in freezing/thawing can be easily plotted in TempW. The climate and thermal properties used in the simulations are displayed in table 6. The surface boundary condition again is corresponding to "meteo 2" (see figure 37).

Test n°	**16**	**17**	**18**
Diffusivity $\alpha_{unfrozen}$ (10^{-7} $m^2.s^{-1}$)	1,3	1,3	6,0
Diffusivity α_{frozen} (10^{-7} $m^2.s^{-1}$)	6,0	13	13

tab. 6 : control parameters used in tests 16 to 18

8.3.2. Water enthalpy

The material model in TempW asks for porous water content. This content will remain the same in each element during the whole calculation. However, TempW will plot another parameter W_u (iciness ratio, see 6.5.3) that is the ratio between frozen and liquid water content.

When a given element hit 0°C, its iciness ratio will change, using the heat flux to melt/freeze the water content. During this whole process, all heat energy transmitted to the element goes to this phase change. Therefor, the temperature remain zero until W_u hit 0 or 1.

Water enthalpy has a very visible effect upon the annual temperature variation of the ground. It is characterized by a radical flattening of the curve wherever it hits 0°C. If not for this effect, according to 6.1, temperature over time plots would follow a sinusoidal pattern.

However, the effect upon the extreme temperature profiles is rather less obvious. Acting like an inertia force, water enthalpy should keep temperatures closer to zero. But it widely depends on the inertia of the system itself, that is to say its thermal diffusivity. If the response of the soil to climate stimuli is quick, the only contributors to extreme temperature will be the deep of winter and the pit of summer, when water is long frozen/melted, thus reducing the effect of enthalpy to nothing. In "slower" soil systems, the minimal temperatures of winter will arrive as the water is not entirely frozen. Thus enthalpy plays its inertia role entirely (same for summer).

As the water enthalpy is not taken in account by the theoretical models defined in chapter 6, a more careful analysis shall be performed. The climate and thermal properties used in the simulations are displayed in table 7. Surface temperature amplitude is set as 10°C.

Test n°	**19**	**20**	**21**	**22**	**23**	**24**
Mean surface temp (°C)	0	0	0	5	5	5
Water content ($m^3.m^{-3}$)	0,2	0,6	0,6	0,2	0,6	0,6
Heat capacity ($MJ.m^{-3}.K^{-1}$)	2	2	4	2	2	4
Resulting diffusivity α (10^{-7} $m^2.s^{-1}$)	*13*	*6,0*	*13*	*1,3*	*6,0*	*1,3*

tab. 7 : control parameters used in tests 19 to 24

8.4. Effect of surface geometry

FEM calculation is flexible in terms of geometry, thus permitting to reproduce the behavior of complicated slopes rather easily. This will permit to check the validity of the "corner" model developed in (6.3). The table 8 displays the different angles used in the calculation as well as the climate and thermal properties.

Test n°	**25**	**26**	**27**	**28**	**29**	**30**
Slope angle (°)	30	30	45	45	90	90
Diffusivity α (10^{-7} $m^2.s^{-1}$)	1,3	13	1,3	13	1,3	13

tab. 8 : control parameters used in tests 25 to 30

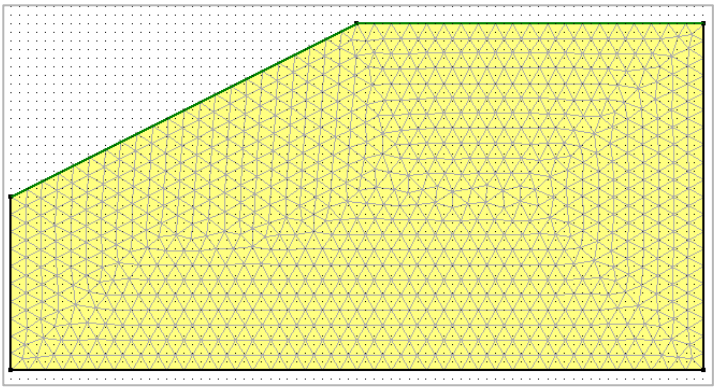

fig. 41 : mesh used for tests 25 to 30

8.5. Full-scale analysis

Now that the main factors influencing the temperature in the soil have been identified and their effect quantified, it is time to combine them into a full-scale model.

This study proposes to simulate the behavior of a typical shore profile, and see what happens. In order to be able to compare with the previous analysis, it will however be kept rather simple.

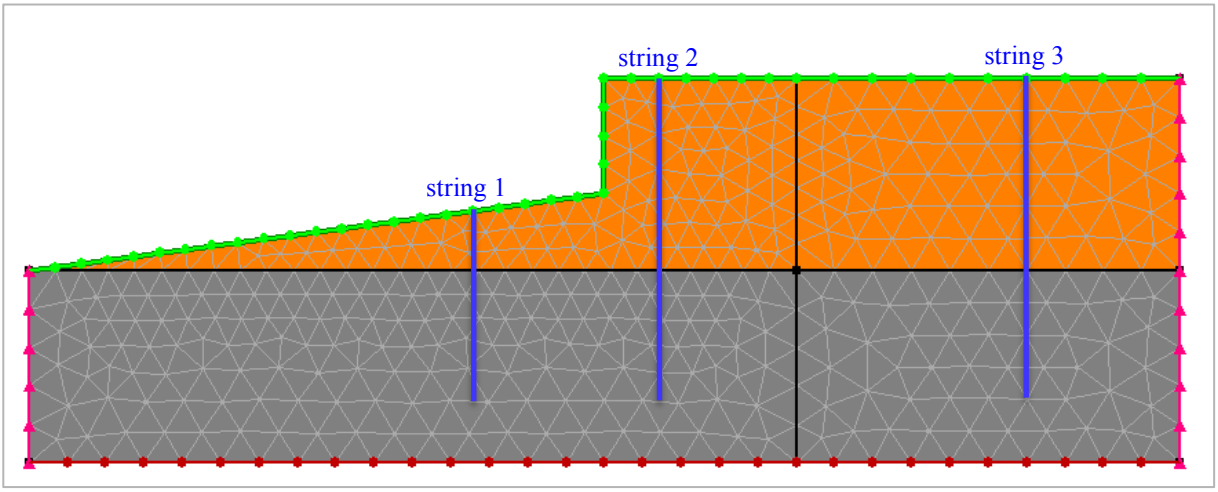

fig. 42 : geometry used for the full scale simulations

The numerical model is composed of two main features : a cliff, vertical, 3 m high prolonged in semi-infinite landside, and a beach with a gentle slope (20% ≈ 11°). A bedrock is installed at 5 m below the surface. The soil material (gravel) has different frozen and unfrozen thermal diffusivity while the bedrock keeps the same all year long. Three different measurements will be performed : the first far away from the shore, the second on the cliff top and the third on the beach. Those features are presented in figure 42.

On the first measure, the soil shall act as a rectangular soil model with a strong dissymmetry due to the change of diffusivity (see 8.3.1). The maximum temperature profile should present a

brutal change at the interface between gravel and bedrock (see 8.2), while the minimum temperature profile should not.

On the second measurement, those same features should be combined with a reshaping of both temperature profiles due to the presence of the cliff (see 8.4).

On the third measurement, the temperature profile should only be affected by the beach slope, i. e. slightly elongated due to the difference between depth and distance to the surface. The fact that the bedrock is close will also be observable trough the temperature profile.

9. Results

The simulations in TempW aims at verifying the adequacy between the models exposed in the chapter 6 and the Finite Element calculation. Individual particularities developed in the chapter 8 will be measured and compared with the respective theoretical analysis.

Once every aspect that makes a complicated site is carefully mastered, the full-scale analysis shall be performed. Its purpose is to test the trends observed in a simple model representing a classic shore and see how they resist the confrontation with each other.

9.1. Climate and thermal diffusivity

9.1.1. Sinusoidal climate

The results showed by figures 43 to 48 tend to confirm that the analytical model is very good followed for a semi-infinite, homogeneous soil. For such a simple model, TempW is not a very useful tool, but this shows that it is indeed very compatible with the analyses developed in chapter 6.

Indeed, the amplitude of the surface temperature profile is directly proportional to that of every temperature amplitude in the soil. This suggests that the climate is the first-importance factor, particularly the extreme temperatures.

The thermal diffusivity affects the depth of influence of the surface temperature. The influence follows a negative exponential law, less reactive than a linear. Thus, a small error around the thermal diffusivity, such as ±25%, is not significant.

9.1.2. Non-sinusoidal climate

The effect of a square-shaped signal is obtained in the theoretical analysis by replacing the sin term by a $\frac{\sin}{|sin|}$.

But it seems rather obvious that a real soil will degrade the squared signal when it goes trough the depth of the soil. The instant switching from –A to A supposes that at the time of the changing, $\frac{dT}{dt} = +\infty$, meaning the material has infinite diffusivity.

This is very well showed by the figures 50, 52 and 54. They suggest that when the diffusivity tends toward the infinite, the square pattern is more and more conserved. Of course, an infinite diffusivity would mean that the temperature is equal everywhere, thus following exactly that of the surface (which is imposed by the boundary condition).

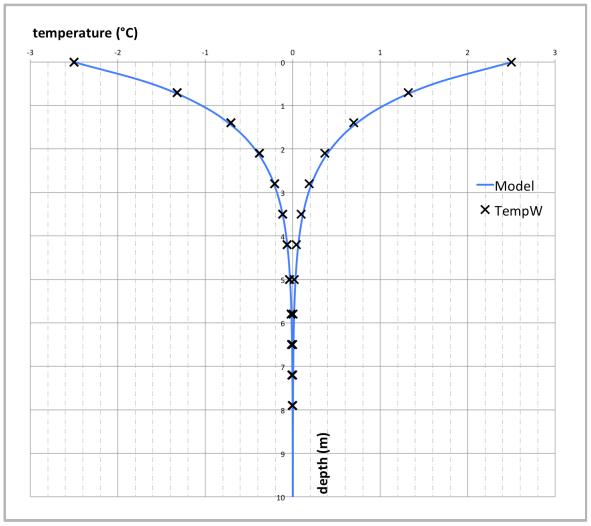

fig. 43 : temperature profile for test 1 : meteo 1 and α = 1,3.10^{-7}

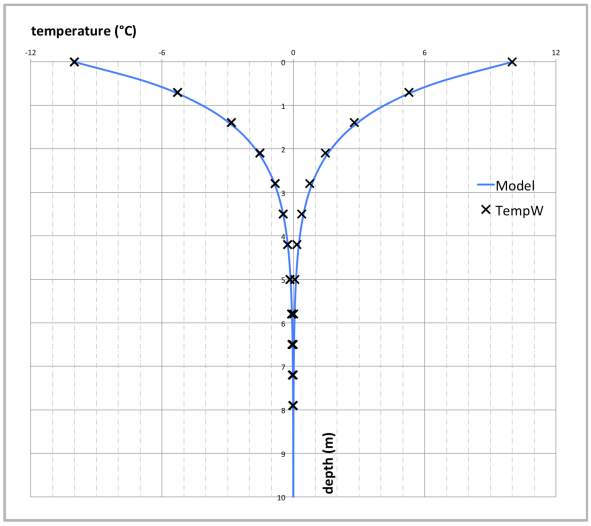

fig. 44 : temperature profile for test 2 : meteo 2 and α = 1,3.10^{-7}

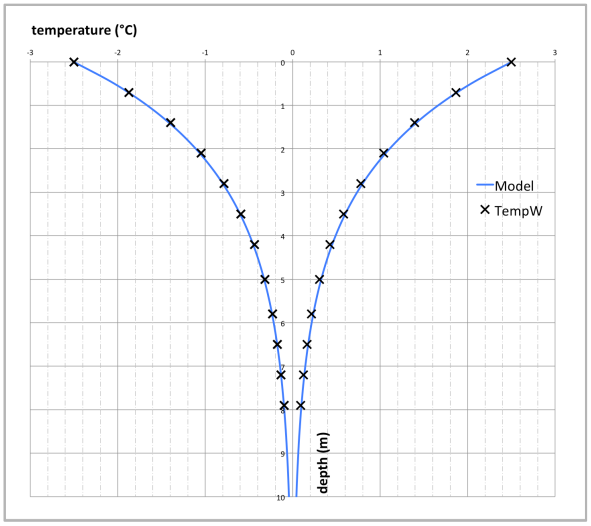

fig. 45 : temperature profile for test 3 : meteo 1 and α = 6,0.10^{-7}

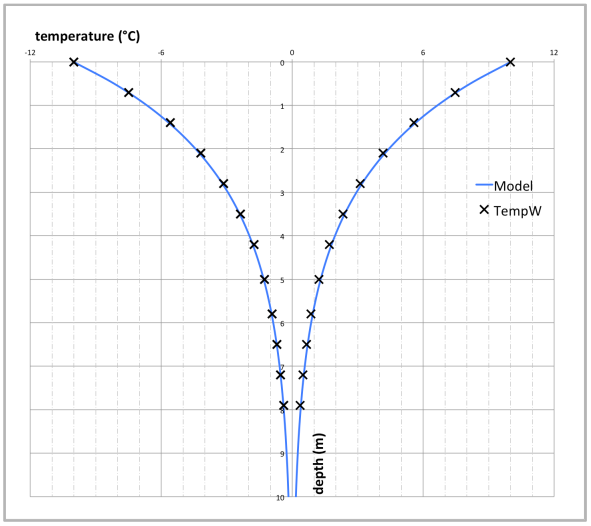

fig. 46 : temperature profile for test 4 : meteo 2 and α = 6,0.10^{-7}

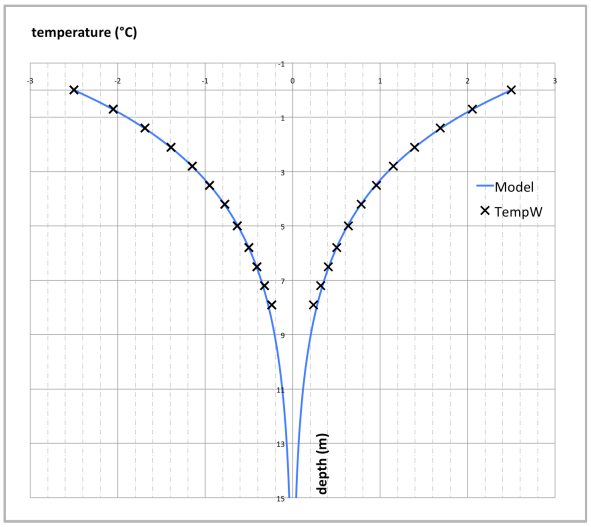

fig. 47 : temperature profile for test 5 : meteo 1 and α = 1,3.10^{-6}

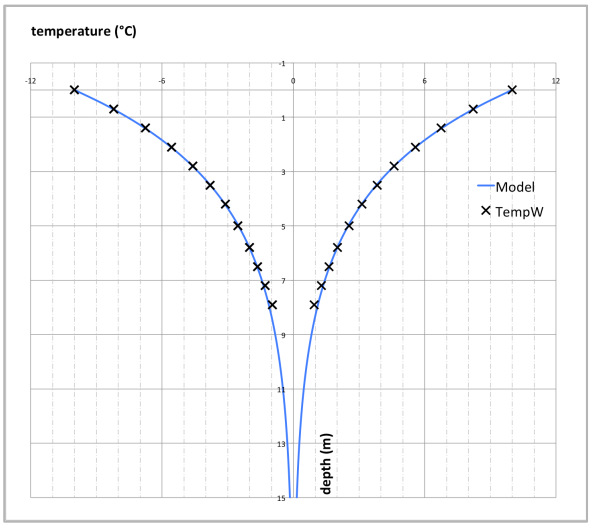

fig. 48 : temperature profile for test 6 : meteo 2 and α = 1,3.10^{-6}

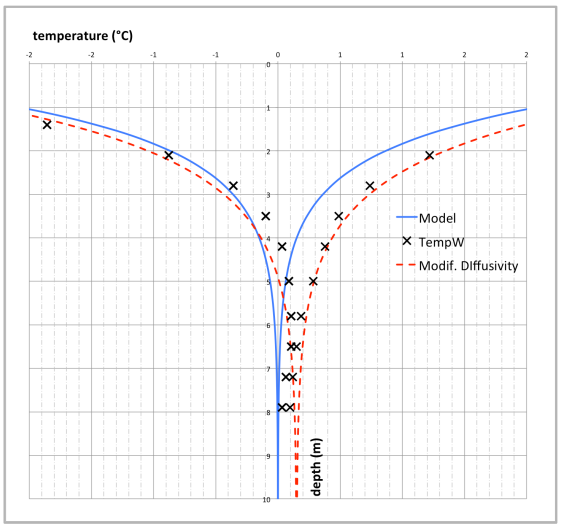

fig. 49 : temperature profile for test 7 : meteo 3 and α = 1,3.10^{-7}

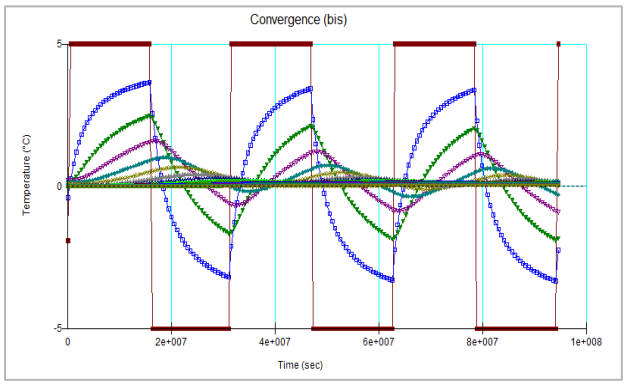

fig. 50 : temperatures at different depths for test 7

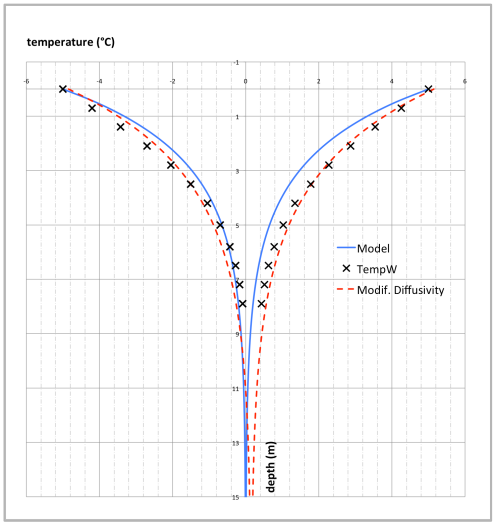

fig. 51 : temperature profile for test 8 : meteo 3 and α = 6,0.10^{-7}

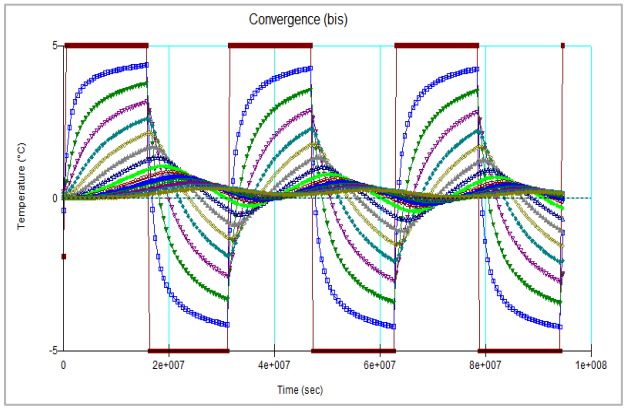

fig. 52 : temperatures at different depths for test 8

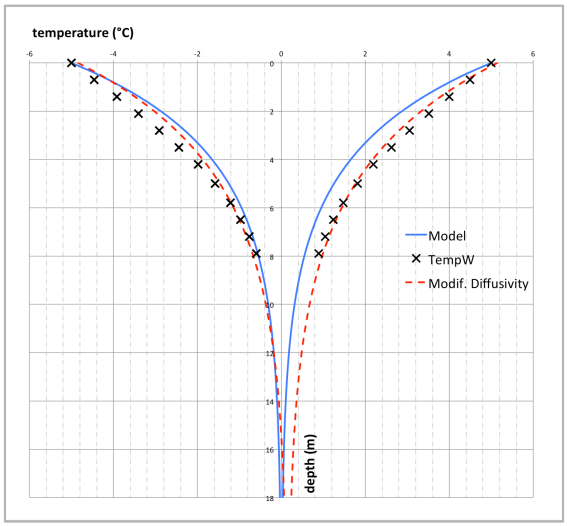

fig. 53 : temperature profile for test 9 : meteo 3 and α = 1,3.10^{-6}

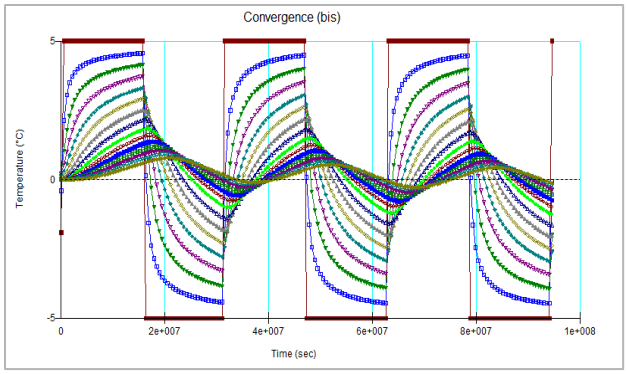

fig. 54 : temperatures at different depths for test 9

What is more surprising is how this distortion of the signal affects the shape of the temperature profile. First, it slightly increases the amplitude at every depth. Further studies translated by the dotted lines suggest that the square shape is roughly equivalent to a 50% increase of thermal diffusivity. Although that could seem much, one shall keep in mind that such a variation is barely noticeable.

Second, the small shifting of the temperature profile to the right is more difficult to explain. In the model, the surface temperature is perfectly symmetric around the zero axis, soil properties are not affected by the temperature and the bottom boundary condition keep the symmetry.

NB : contrarily as what one could suppose, the heat capacity in itself does not have any effect. The equation (6.5.3 – 1) shows that, at equal thermal diffusivity, the soil has exact same behavior even for very different heat capacity whatever the temperature pattern at the surface. Diffusivity alone rules the behavior in soils with zero water content implemented.

9.2. Effect of layers

A multi-layered structure is well described by the "multilayer" model (6.4). In fact, the reasoning below multi-layer theoretical calculation is exactly the same as in TempW : the upper layer act as a boundary condition for the lower layer.

It is of no surprise then to have results very similar to the analytical prediction. The comparison with the "multiplayer" model is displayed in figures 55 to 60. However, the figures 32 and 33 clearly show the importance of the meshing when there are brutal changes in diffusivity. The limit between the layers in TempW has to be on a node otherwise the pseudo-boundary condition of the second layer is not accurate.

The important results are within the top layer, which reduce the interest of really caring about the lowest layers. Thus, the "multilayer" model offers a good enough estimation.

9.3. Effect of water content

The effect of water is more complex to anticipate, because of its highly non-linear action around the freezing temperature. However, a short study in two steps shall give some clues about how to handle water content in the soil.

9.3.1. Frozen and unfrozen thermal diffusivity

Under the assumption that the model is reactive enough for the temperature profile to be ruled only by the extreme temperatures (meaning the diffusivity is high, see 9.1.2), the analytical model is rather simple. However, the simulations presented in 8.3.1 show a big flaw : it

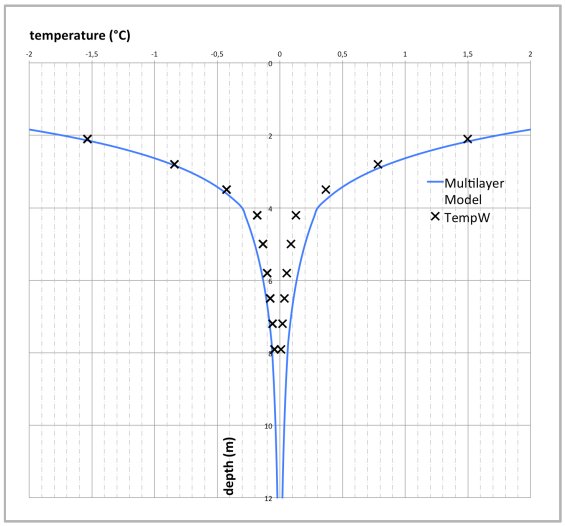

fig. 55 : temperature profile for test 10 : $\alpha_1 = 1{,}3.10^{-7}$, $\alpha_2 = 6{,}0.10^{-7}$ and $\alpha_3 = 1{,}3.10^{-6}$

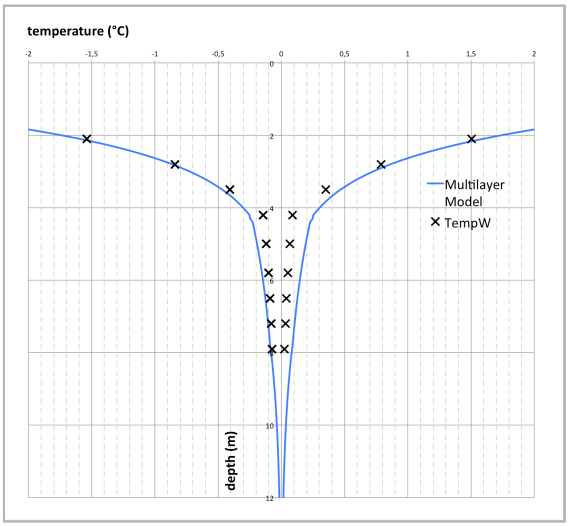

fig. 56 : temperature profile for test 11 : $\alpha_1 = 1{,}3.10^{-7}$, $\alpha_2 = 1{,}3.10^{-6}$ and $\alpha_3 = 6{,}0.10^{-6}$

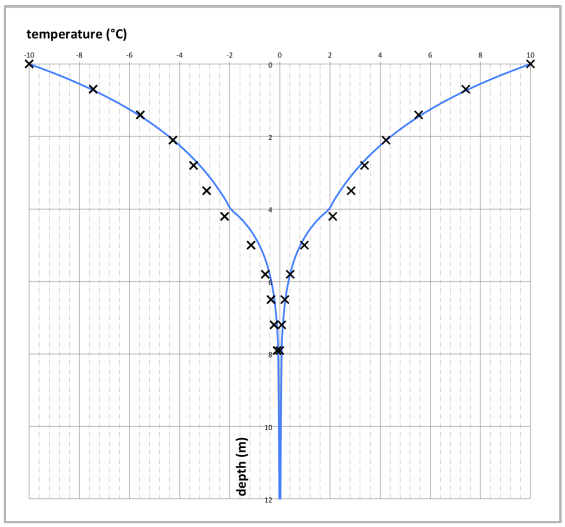

fig. 57 : temperature profile for test 12 : $\alpha_1 = 6{,}0.10^{-7}$, $\alpha_2 = 1{,}3.10^{-7}$ and $\alpha_3 = 1{,}3.10^{-6}$

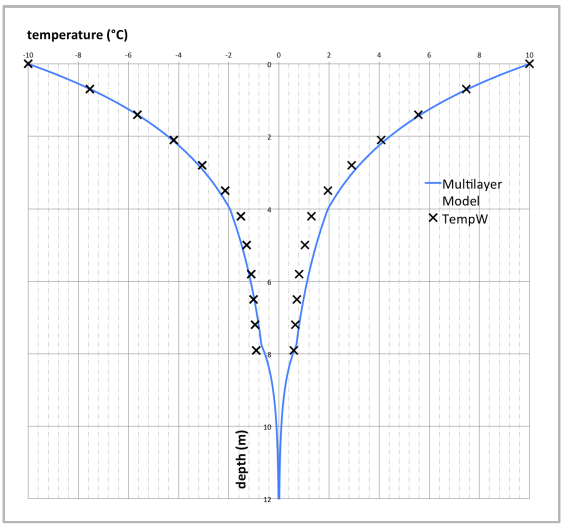

fig. 58 : temperature profile for test 13 : $\alpha_1 = 6{,}0.10^{-7}$, $\alpha_2 = 1{,}3.10^{-6}$ and $\alpha_3 = 1{,}3.10^{-7}$

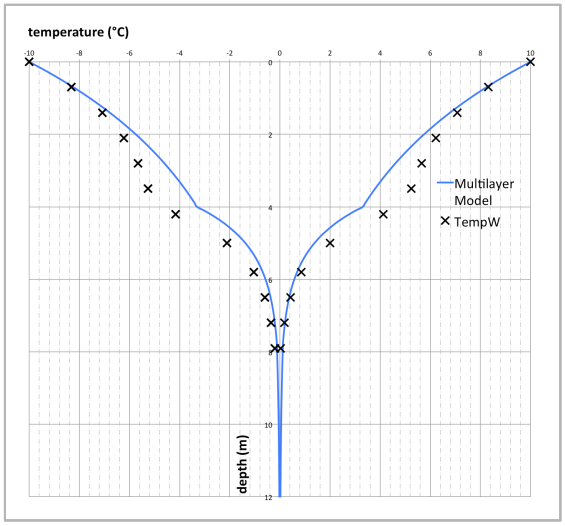

fig. 59 : temperature profile for test 14 : $\alpha_1 = 1{,}3.10^{-6}$, $\alpha_2 = 1{,}3.10^{-7}$ and $\alpha_3 = 6{,}0.10^{-7}$

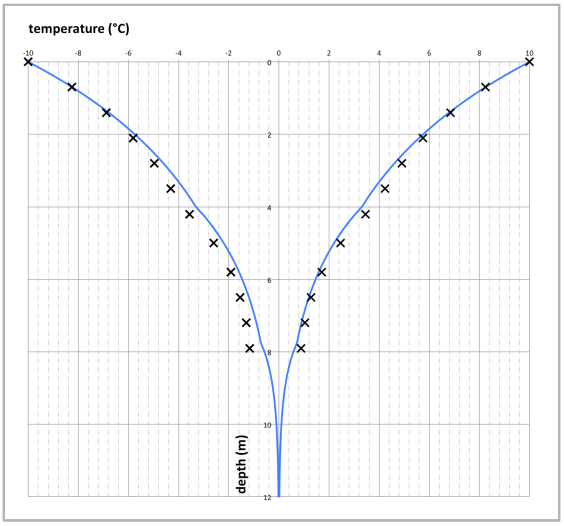

fig. 60 : temperature profile for test 15 : $\alpha_1 = 1{,}3.10^{-6}$, $\alpha_2 = 6{,}0.10^{-7}$ and $\alpha_3 = 1{,}3.10^{-7}$

neglects the fact that the mean temperature into the ground is displaced into negative temperatures. This proves to have a big impact upon the temperature profile in the soil below, as seen in figures 61, 63 and 65.

In order to overcome this issue, an incremental model has been developed. The trick is to divide the soil in layers and solve the equation 6.1.3 – 3) for each according to the method presented in 8.2. Thus, the numerical temperature profile is correctly displaced as the mean temperature decreases with depth. The blue profile in figures 62, 64 and 66 presents temperature profiles calculated with this method. But the secondary effect is that the mean annual temperature converges toward a negative temperature. Thus, a virtual gradient has been added in order to correct this effect and force the mean temperature to return to zero after a certain depth. This gradient can be observed in the dotted red curves in figures 62, 64 and 66.

9.3.2. Enthalpy of fusion

The effect of water phase change is supposed to add inertia to the system and thus reduce temperature amplitude symmetrically around zero. But tests 19, 20 and 21, represented in figures 67, 68 and 69 are heavily dissymmetric. Further calculations will point out the reason : the elements of the numerical calculations start with a water content 100% frozen. Thus, the water enthalpy strongly weight in favor of negative temperatures, displacing the temperature profile to the left.

Although very inaccurate, those calculations permit an interesting insight of the effect of water enthalpy and possible analytical modeling. An attempt has been represented by the red dotted curves in figures 67 to 72. To get those curves, water enthalpy has been considered equivalent to a virtual heat capacity, using the “bi-diffusivity” model. Thus, a new thermal diffusivity is implemented, only in summer because of the dissymmetry observed on the numerical temperature profile, into the model developed in 9.3.1.

Although the new model with modified thermal diffusivity seems to match pretty well the finite element calculations in figures 67, 68 and 69, it is rather inaccurate when the mean surface temperature starts getting away from zero. In fact, further simulations shows that in tests 22, 23 and 24 the soil always stays always unfrozen. Thus, a thermal diffusivity change between winter and summer does not appear. However, a virtual thermal gradient is still necessary to force deep temperatures to converge back toward zero. In figures 70, 71 and 72, the tests 22 to 24 are presented, with the initial analytical model (horizontal, mono-diffusivity) and the new one.

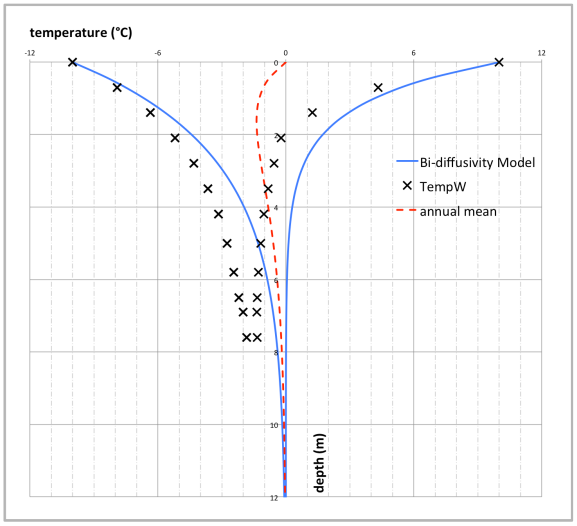

fig. 61 : temperature profile for test 16 : $\alpha_u = 1{,}3.10^{-7}$ and $\alpha_f = 6{,}0.10^{-7}$

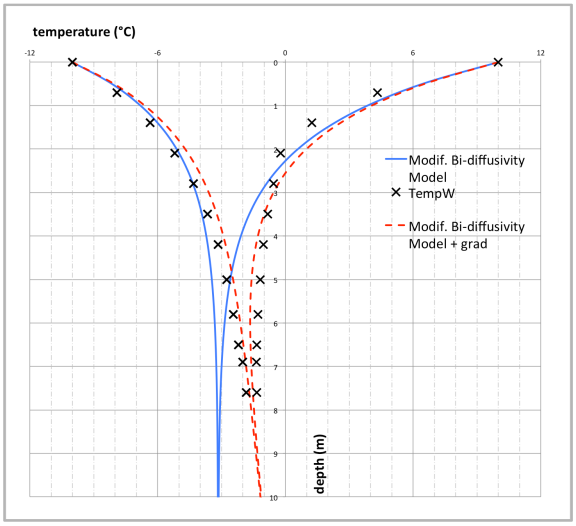

fig. 62 : bi-diffusivity model with factor accounting for mean temp. and correction gradient, test 16

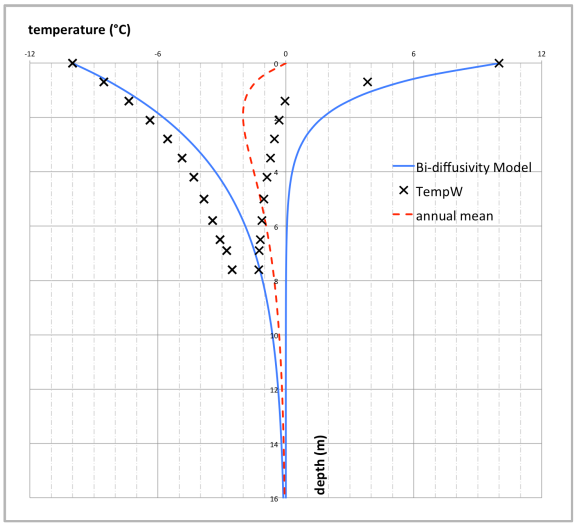

fig. 63 : temperature profile for test 17 : $\alpha_u = 1{,}3.10^{-7}$ and $\alpha_f = 1{,}3.10^{-6}$

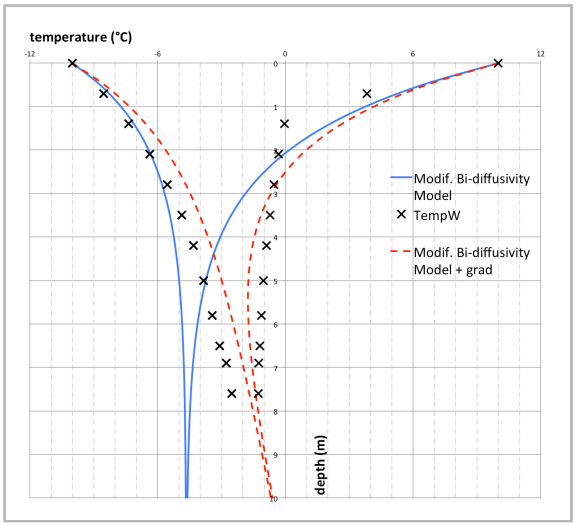

fig. 64 : bi-diffusivity model with factor accounting for mean temp. and correction gradient, test 17

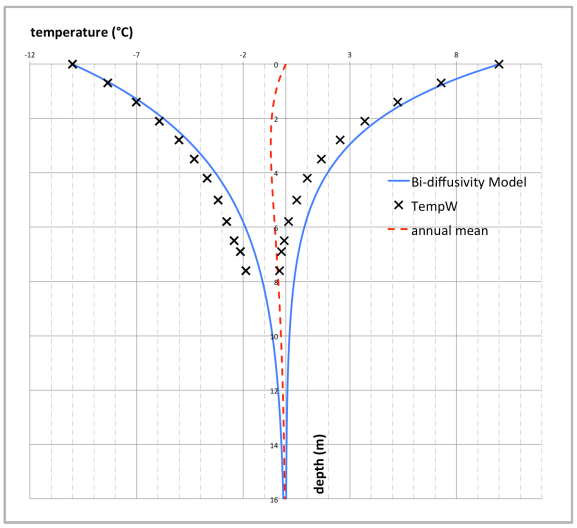

fig. 65 : temperature profile for test 18 : $\alpha_u = 6{,}0.10^{-7}$ and $\alpha_f = 6{,}0.10^{-6}$

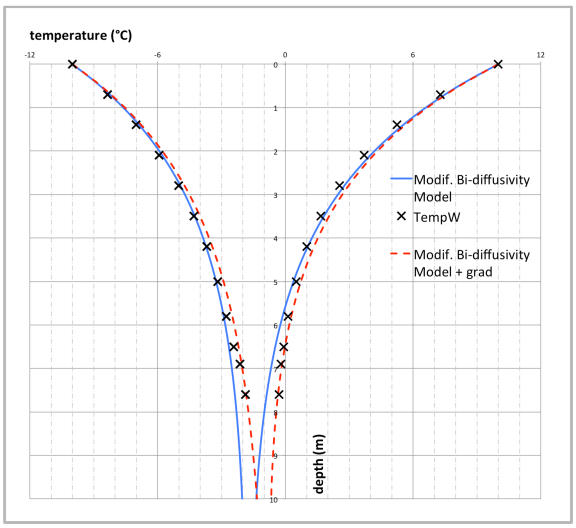

fig. 66 : bi-diffusivity model with factor accounting for mean temp. and correction gradient, test 18

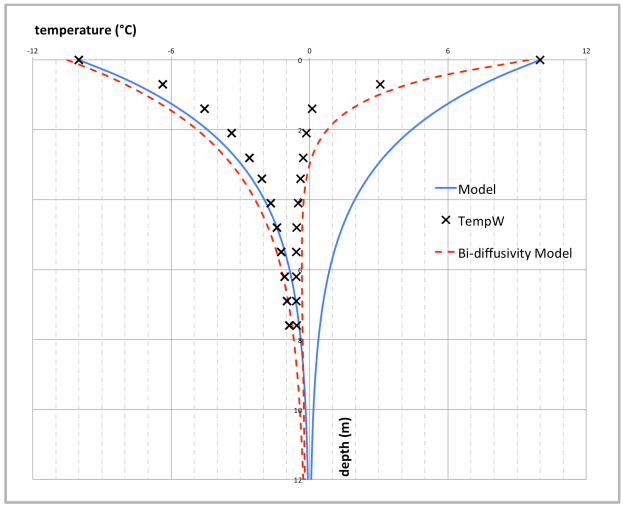

fig. 67 : temperature profile for test 19 : w = 0,2 and c = 2,0 MJ.m^{-3}

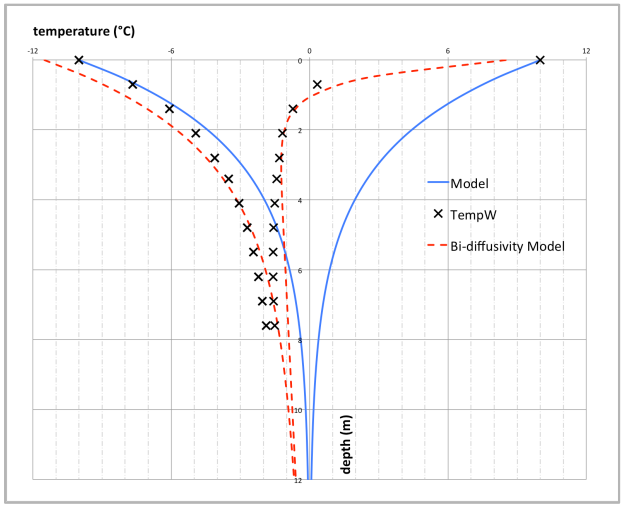

fig. 68 : temperature profile for test 20 : w = 0,6 and c = 2,0 MJ.m^{-3}

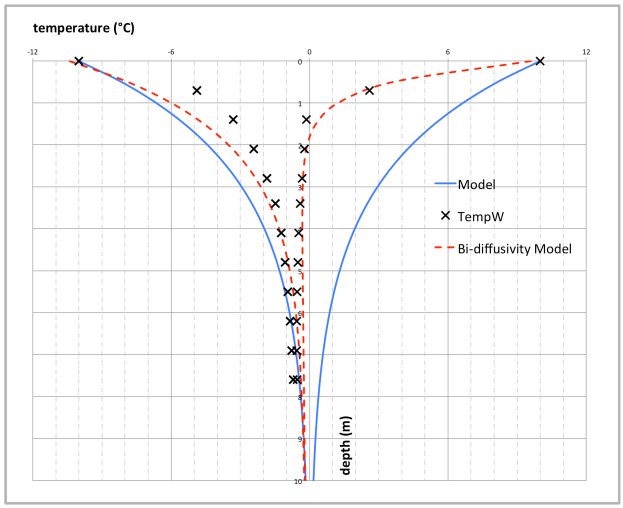

fig. 70 : temperature profile for test 21 : w = 0,6 and c = 4,0 MJ.m^{-3}

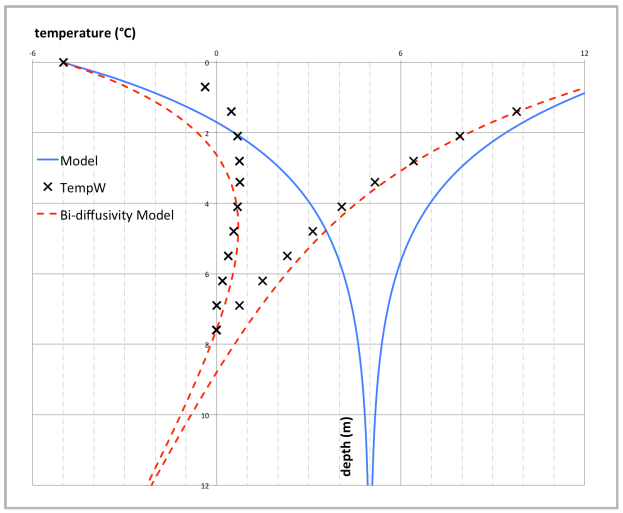

fig. 69 : temperature profile for test 22 : w = 0,2, c = 2,0 MJ.m^{-3} and mean surface temperature increased

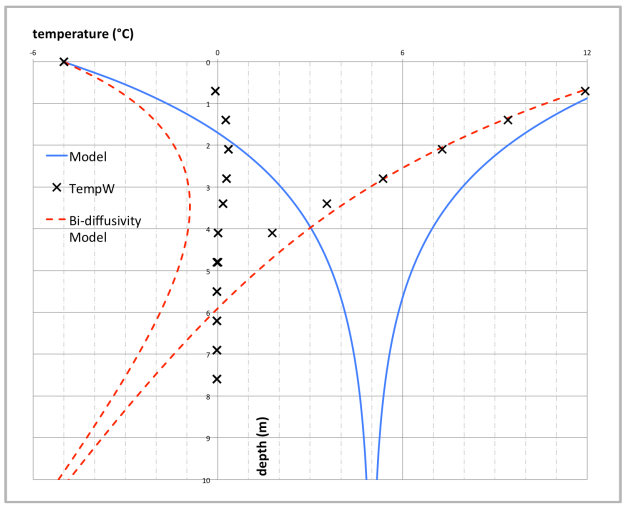

fig. 71 : temperature profile for test 23 : w = 0,6, c = 2,0 MJ.m^{-3} and mean surface temperature increased

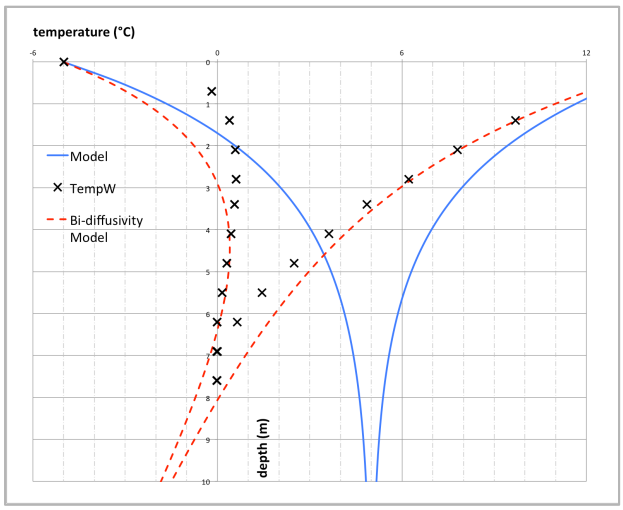

fig. 72 : temperature profile for test 24 : w = 0,6, c = 4,0 MJ.m^{-3} and mean surface temperature increased

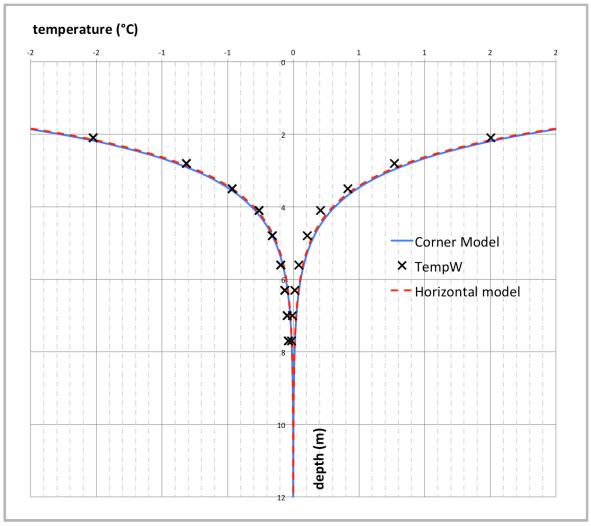

fig. 73 : temperature profile for test 25 : θ = 30° and α = 1,3.10^{-7} m^2.s^{-1}

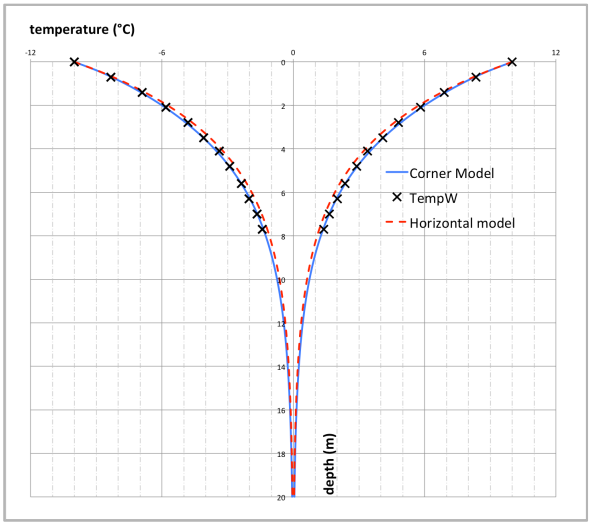

fig. 74 : temperature profile for test 26 : θ = 30° and α = 1,3.10^{-6} m^2.s^{-1}

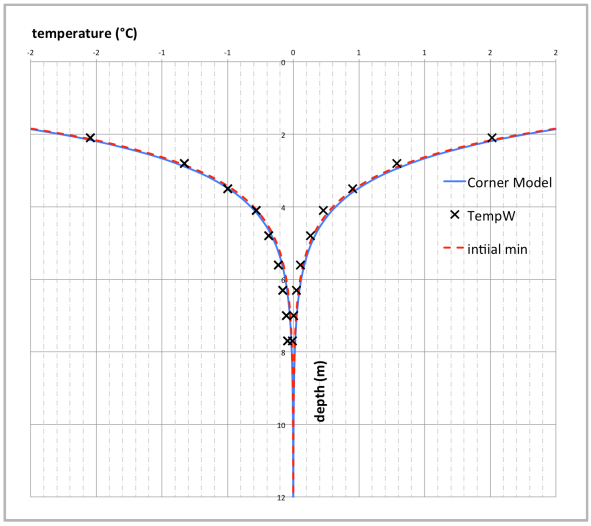

fig. 75 : temperature profile for test 27 : θ = 45° and α = 1,3.10^{-7} m^2.s^{-1}

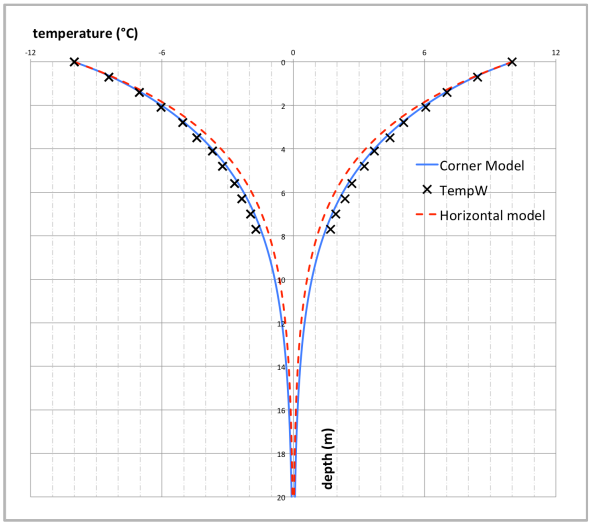

fig. 76 : temperature profile for test 28 : θ = 45° and α = 1,3.10^{-6} m^2.s^{-1}

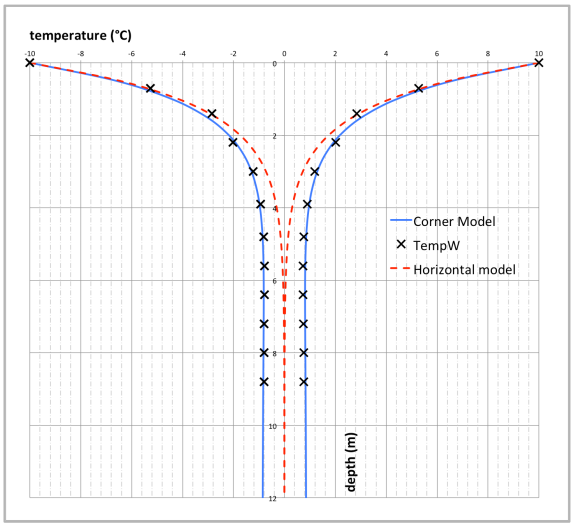

fig. 77 : temperature profile for test 29 : θ = 90° and α = 1,3.10^{-7} m^2.s^{-1}

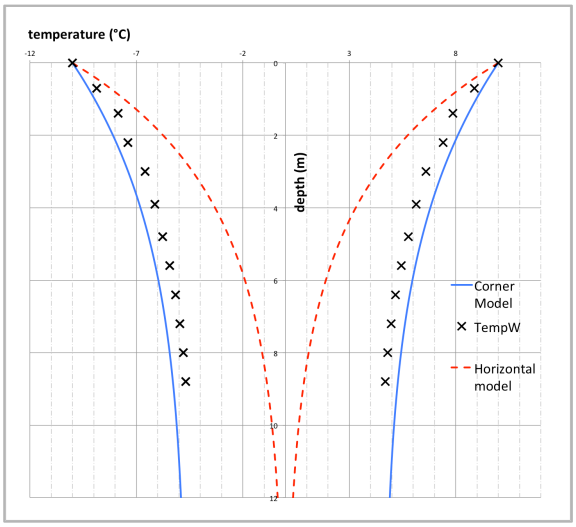

fig. 78 : temperature profile for test 30 : θ = 90° and α = 1,3.10^{-6} m^2.s^{-1}

9.4. Effect of surface geometry

The figures 73 to 78 show the temperature profiles of three different slope changes, 30°, 45° and 90° (the latest simply being a vertical cliff), for two different soils, one having a thermal diffusivity 10 times larger than the first. They stick very well to the "corner" model curves, calculated using the analytical method in 6.3. The dotted lines represents what the temperature profile would look like in a perfectly horizontal soil.

The results suggest that the model is not perfectly followed by TempW. The slope has much less effect that what the analytical calculations would predict. However, for steeper slopes, the results begin to diverge from the horizontal model curve toward the modified model, until they superpose for a vertical cliff. For this reason, the study suggests that the horizontal analytical model should be kept for slope variations below 45°.

The results suggest that the slope should have a much more important impact into the slope factor η. Experimentally, this could be done by adding an exponent :

$$\eta = \left(1 - e^{-\frac{z}{d}}\right)^{[1+a.\cos(\theta)]} \tag{9.4}$$

- z : depth (m)
- d : ''shifted'' depth (m), see 6.3
- a : horizontal distance to the corner (m)
- θ : slope angle (rad)

NB : we keep the hypothesis that one of the surfaces is horizontal. If not, the whole model must be rotated, the way it has been demonstrated in chapter 6.

9.5. Full-scale analysis

A full-scale analysis is supposed to combine each of the factors studied in the previous paragraphs. Because the models are too complicated for analytical calculations, the results shall be discussed under the light of the preceding calculations and their conclusions.

The figure 80 represents the temperature profile measured by the string 1, on the beach. The blue curve is the model elaborated in 6.3, with a correction coefficient that account for the gentle slope (see 6.3). It seems to match the numerical simulation rather well. However, it does not converge toward zero as quickly when reaching the bottom. In fact, the flaw is on the numerical TempW model, because the bottom boundary condition forces the temperature profile to converge more quickly with depth.

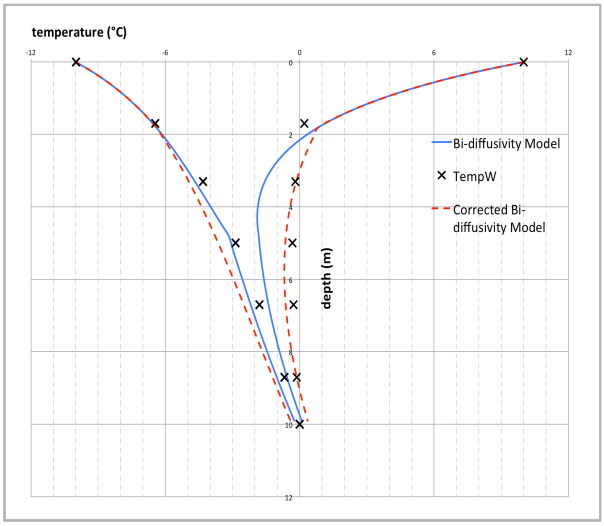

fig. 79 : temperature profile for full scale simulation, string 3 (landside)

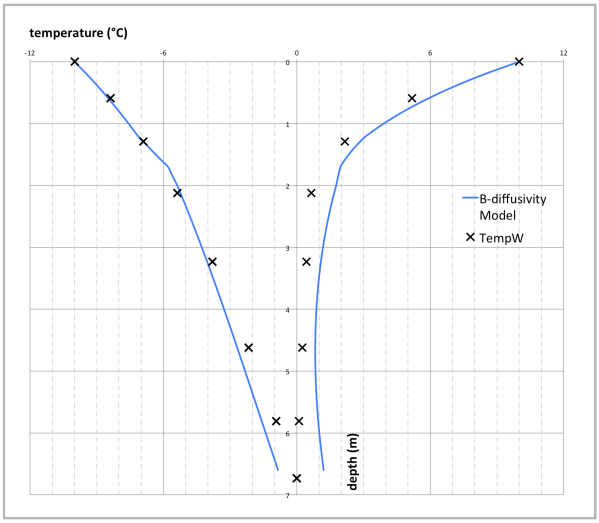

fig. 80 : temperature profile for full scale simulation, string 1 (beach)

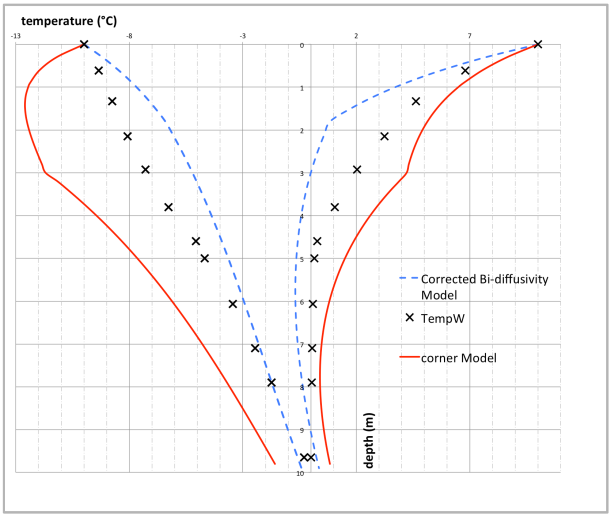

fig. 81 : temperature profile for full scale simulation, string 2 (cliff)

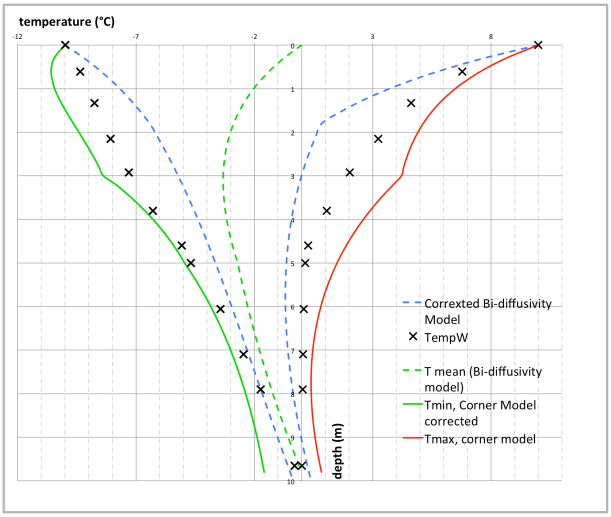

fig. 82 : temperature profile for full scale simulation, string 2 (cliff) showing model correction for "corner" model

The figure 79, showing the temperature profile measured and calculated for the string 3, is rather similar. But as the minimum temperatures calculated by TempW seems to match those by the model, maximum temperatures deviates at 2 m depth. This is certainly due to the temperature never reaching positive at this depth, thus keeping the soil frozen and the thermal diffusivity high even in the gravel. A correction taking account for this has been added under the form of the red dotted curve.

Finally, the figure 81 displays the results of the string 2. This one is the most complicated as it combine the effect of both water and cliff. Thus, a first model in blue (dotted) neglects the effect of the cliff, with the correction for negative maximum temperatures (being, in fact, the same as the red dotted one calculated in figure 79). As to be expected, the profile calculated by

TempW is larger, because of the influence of the temperatures on the vertical surface of the cliff. However, the red curve that presents the “corner” model seems to overestimate this effect.

This simulation seems to point out that the “multilayer” model and the “bi-diffusivity” model are very compatible. Great care shall be taken because of the asymmetry of the temperature profile, in particular for negative maximum temperatures and positive minimum temperatures, which are badly represented by the “bi-diffusivity” model.

At the opposite, the “bi-diffusivity” model combine badly with the “corner” model. The figure 81 seems to point out that the very inaccurate results for minimal temperatures are induced by the displacement of the mean temperature curve. In order to verify this supposition, the figure 82 implements the mean annual temperature in green (dotted). A corrected minimum temperature profile, the green curve, is calculated from the preceding with a correction factor equal to the deviation of the mean temperature to zero :

$$T'_{min,}(z) = T_{min}(z) + \eta . T_{min}(z = 1) + [T_m(z = 0) - T_m(z)] \quad (9.5)$$

- T'_{min} : corrected temperature profile (°C)
- T_{min} : temperature profile according to the “bi-diffusivity” model
- η : modulation factor for the effect of the vertical cliff, according to the “corner” model
- T_m : mean annual temperature according to the “bi-diffusivity” model

The figure 82 seems to validate the hypothesis, as the green dotted curve representing T'_{min} match pretty well the TempW simulations. Thus, it shows that the “corner” model is inaccurate in situations with an asymmetrical temperature profile, as it is often the case in real soils, but a correction is possible and rather easy to make. However, if no extremely precise calculations are needed, it seems preferable to neglect the effect of the cliff, and simply “bend” the isotherms to be parallel to the surface shape.

10. Case study : Vestpynten

In order to see if the analyses above can actually be put to use, they shall be confronted to a real site. Vestpynten is a good place for this purpose. The elements of a complex analysis are put together : multi-layer, complex surface shape, non-sinusoidal climate and presence of porous water.

10.1. presentation of Vestpynten

Vestpynten is a shore west of Longyearbyen (Svalbard), near the airport. The shore is rather typical, with a beach composed of crushed materials and a small bluff 2-3m high. It is covered in snow a significant part of the year, which provides interesting insights of the influence of a snowcap. But the main advantage of this location is the accessibility, by a short track from Longyearbyen.

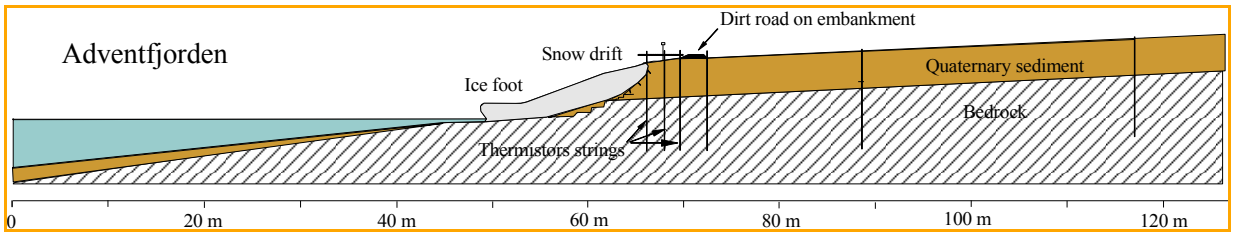

fig. 83 : shore profile at Vestpynten, and location of the thermistor strings, courtesy E. Guegan (2012)

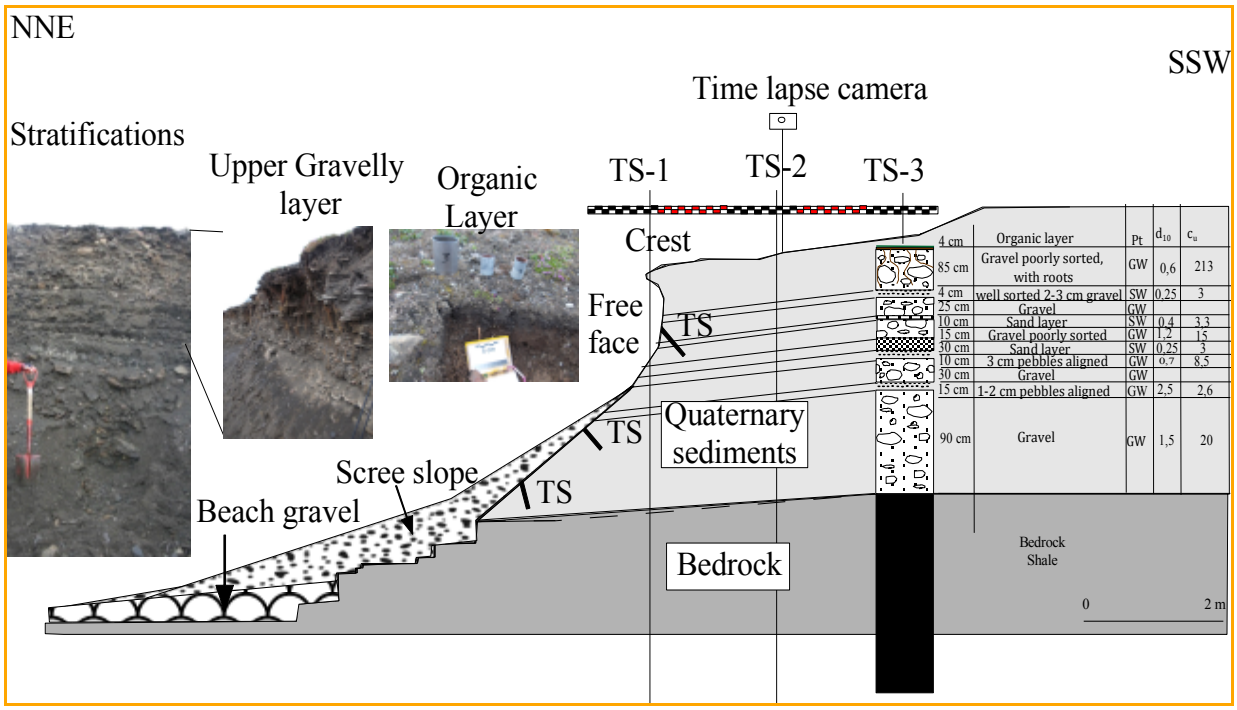

fig. 84 : results of soil investigation, courtesy E. Guegan (2012)

The profile of the coast includes a gentle 5% slope from the land to the shore, abruptly ended by a 1m vertical cliff. Then a slope varying from 15° to 45° plunges into the sea. The profile can be seen in figure 83.

The soil is mainly constituted of crushed rocks. Below a thin organic layer, one find a 3 m thick layer of Quarternary sediments, under the form of medium to poorly sorted gravel, alternated by thin layers of sand or pebbles. Below, there is a strong bedrock of shale. Fragments of the gravel layer detached from the crest cover the steep slope on the shore. Results of the soil investigations conducted by E. Guegan are displayed in the figure 84.

No investigation to measure the water content has been done. However, due to the presence of the close water table and the high porosity of the soil, it is safe to suppose that water shall play an important role in the thermal simulations.

The snow cover start from October. During wintertime, little to no heat flux should cross the snow to hit the shore. However, this protection has two features : on the shore (below the crest), the snow cover end in may, while on the land (above the crest) it last until the beginning of July. This creates a big difference between the surface temperatures of the two areas.

10.2. field investigations

The field investigations consist of three elements. First, a geological investigation to know the composition of the soil and the topography. The results are exposed in figure 84. Second, an investigation of erosion rates via satellite pictures, completed by a time-lapse camera shall show the erosion mechanisms. Third, thermal strings grounded in the soil shall measure the temperature repartition.

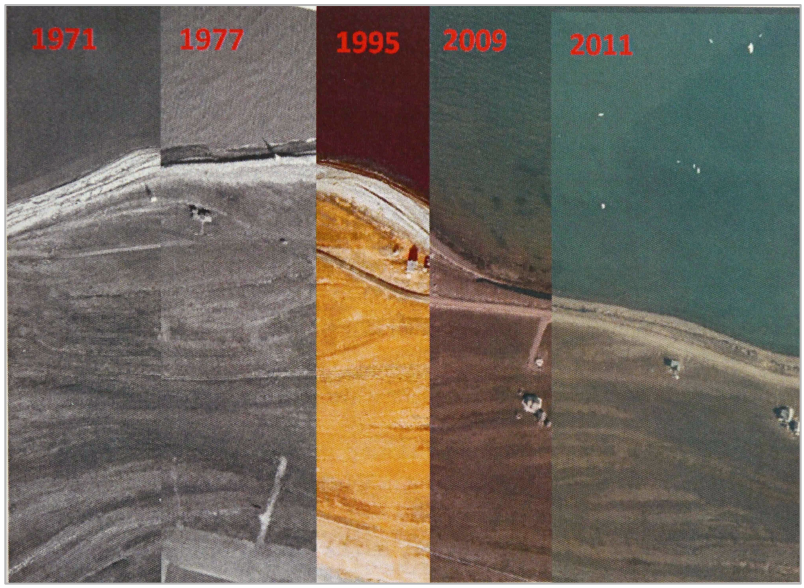

fig. 85 : simplified illustration of Remote Sensing Analysis ; All the aerial photographs from different years are georeferenced and therefor can be compared within the same coordinate system, courtesy E. Guegan (2012)

The figure 85 shows the ArcGIS analysis conducted by E. Guegan (2012). This study is based on aerial pictures of the coastline from 1969 to 2012. The line described by the bluffs or cliffs are used for clear identification, and compared picture after picture. The retreating distance is divided by the time between the photographs. The results evidenced a mean erosion rate of 0 and 75 cm per year (Guegan, submitted).

In 2012, E. Guegan installed 7 thermistor strings, along with two piezometers and a camera. Scheme of the installation is provided in figure 83. The thermistor strings provide the temperature distribution on the shore, into the bluff at the edge, 2 m and 4 m away and into the land at 10,5 m, 28 m and 58 m from the cliff top. Most thermistors are completely operational since spring 2012, providing one and a half year of data.

String number	Distance to the cliff top (m)
1	≈ 0
2	2
3	4
4	10,5
5	28
6	58

tab. 9 : position of the thermistor strings

10.3. Measurements

The main measurement is the temperature profile in the soil. It is provided by the seven thermistor strings. The data appears as a record of temperatures at different time intervals and different depth corresponding to the thermistors.

10.3.1. Thermal strings

The thermal string is composed of thermo-resistors (aka thermistors), whose electric conduction is affected by the temperature. This permits a very accurate measure of the temperature of the device, which is supposed to be that of the surrounding ground.

Thermistors are placed on a wire (string) at regular intervals. The string is then fitted into a drilled hole in the ground, supposedly vertical, so that the depth of every thermistor is known.

On the shore, the string is simply unrolled on the ground, giving the surface temperature for known positions.

10.3.2. Treatment of the data

Results have to be downloaded on-site, which proves to be rather challenging in winter or even in the beginning of spring because of the harsh climate. But the accessibility of the site at Vestpynten is not as challenging as most of the arctic shores.

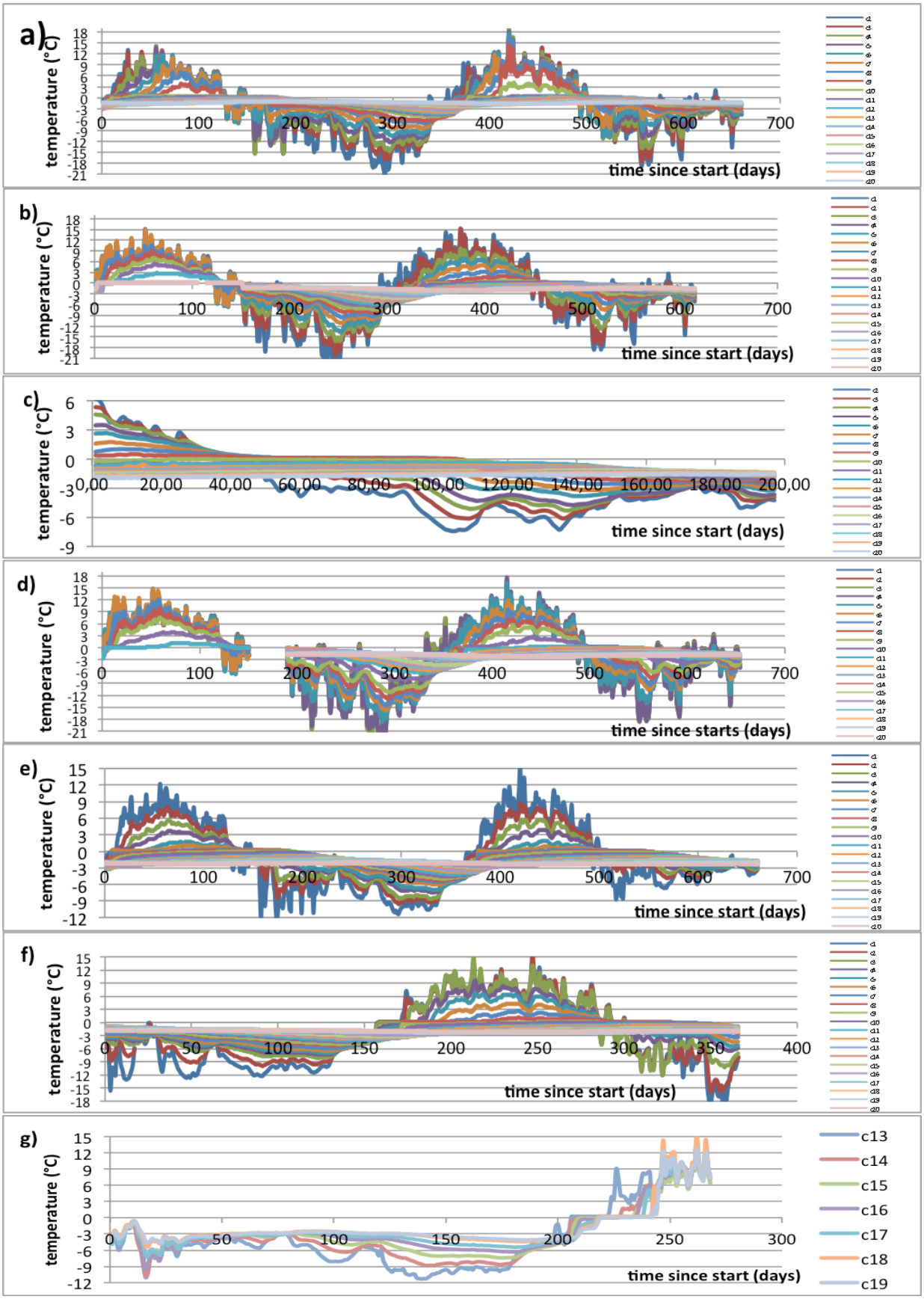

fig. 86 : results of thermistor strings 1 : a) ; 2 : b) ; 3 ; c) ; 4 : d) ; 5 : e) ; 6 : f) and bluff : g), results c) starts 1,5 year after because of a technical problem, courtesy E. Guegan and T. Dormoy (2014)

Once the data is downloaded, the most important thing to do is to check the depth of the first thermistors in the ground. Because of practical reasons, the position of the first thermistor does not coincide with the surface, so the measurement is very important to accurately know the position of every sensor into the ground.

Temperature measurements are taken at different time lapses. In order to have homogeneous data, it shall be formatted such as only daily mean temperatures are displayed.

Finally, some accidents appears to bias the data, notably the string Vest 3 that had to be replaced. In addition, the drilling of the hole, necessary for the installation, appears to affect the local ground temperature during the first year of the measure. Such bias have to be handled carefully before submitting the final temperature profile.

10.3.3. Results

The treated data is presented in the figure 86. Daily mean temperatures seem to form a nice sinusoidal-like temperature with a 1-year period, which suggest that a sinusoid approximation could be made. Beside, the temperature profile defined by the extreme temperatures shows features very similar to the full-scale model presented in the chapter 9.

10.4. Construction of the thermal model

The following analysis is a reproduction of the actual shore of Vestpynten (Svalbard). It has two layers of soil, a very significant water content, many different slopes including a vertical cliff and a surface temperature affected by snow.

The very main factor is the climate, so it is convenient to assume it will rule the full-scale model, along with the thermal diffusivity, which combines easily with it. The effects of water shall appear mostly in high-porosity and low-conductive soils, while slope geometry most of the time shall have a local effect, although binding the isotherms parallel to the surface slope even at big depth.

There is no way to simply hand-calculate such a complicated model, so the only comparison shall be with actual behavior of the coast at Vestpynten.

10.4.1. Climate design

The climate is supposed to be the most determining factor of the simulation. For so, the very first step shall be to design a climate model sufficiently close to the actual annual temperature of the surface. This can be done trough a simple excel table, with a σ-minimization method.

An important factor to consider is the choice of a thermistor representative to the surface temperature. Indeed, no thermistor is placed exactly at the surface. But even if that were the case, its temperature would not be representative. The surface roughness and sensitivity implies a very instable profile rather hard to handle. In addition, the installation itself has an significant local impact upon the temperature that should decrease quickly after the first few centimeters. After several experiments, a thermistor situated at 45 cm depth has been chosen for being the representative of the surface temperature. Examples of experiments to find the correct surface temperature model are exposed in Appendix A.

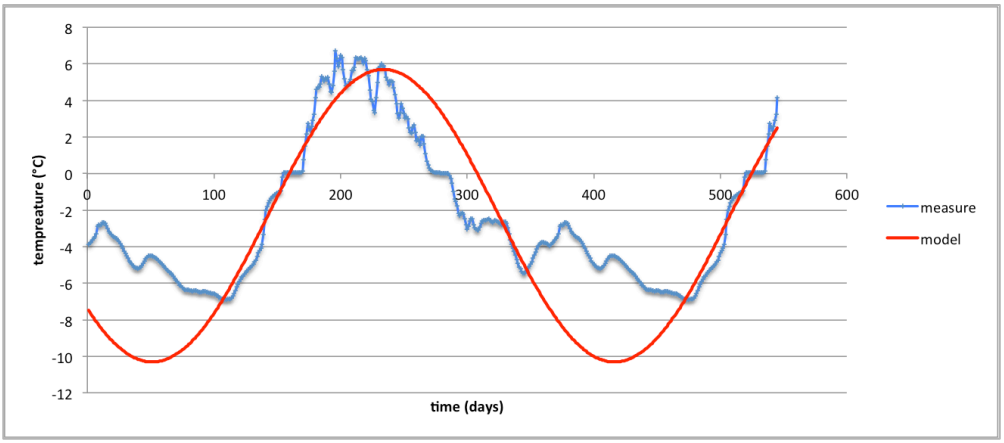

fig. 87 : modeled sinusoidal surface temperature versus results from Vest 6

10.4.2. Thermal diffusivity estimation

Thermal diffusivity is not a parameter difficult to measure, but no such measurements have been done in Vestpynten. However, clever back calculations using the theoretical model in chapter 6 combined with temperature measurements permit to estimate it rather accurately.

Given the theoretical calculations explained in the chapter 6, the analytical way to get the thermal diffusivity from the data at Vestpynten, and in particular those from Vest 6 because of the near-horizontal profile, is to overturn the formula (6.1 – 3) :

$$\alpha = \frac{p}{\pi} \cdot \left[\frac{z}{\ln\left(\frac{A_S}{A}\right)} \right]^2 \qquad (10.4.2)$$

- α : thermal diffusivity ($m^2.s^{-1}$)
- z : depth (m)
- A_S : amplitude of the surface temperature plot (°C)
- A : amplitude at depth z (°C)
- p : period of a cycle, so 1 year = 365x24x3600 = 31 536 000 s

Of course, this shall be calculated at many a depth. The Appendix C shows the main process of the calculation. Each virtual thermal diffusivity is result of the calculation between a certain depth and a “reference” depth.

In order to account for the change in diffusivity during freezing/thawing, the calculations shall be separated between winter and summer, with semi-amplitudes.

At last, when divergent thermal diffusivities have been eliminated, the chosen thermal diffusivities shall be tested by building a temperature profile, both from hand calculation and from TempW simulation. This profile shall be compared with the data from Vest 6, to check if the match is satisfying. The figure 90 shows the comparison between profiles build with the final set of diffusivities and the measurements from Vest 6.

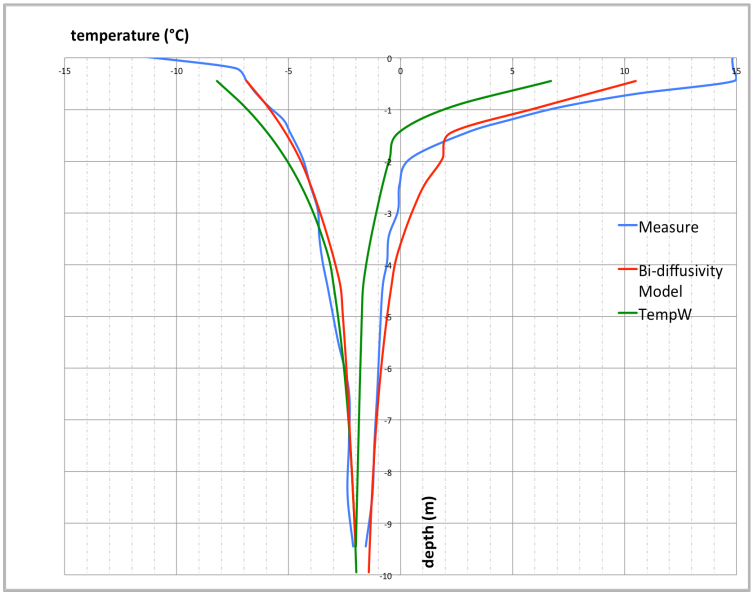

fig. 88 : temperature profile at Vest 6 (70 m from shoreline), comparison between measures and results from "bi-diffisivity" model and TempW simulation

Material	Unfrozen thermal diffusivity	Frozen thermal diffusivity
Gravel (0 to 3 m)	$1{,}3 .10^{-7}$ (m^2/s)	$6{,}0 .10^{-7}$ (m^2/s)
Bedrock (3 to 10m)	$1{,}3 .10^{-6}$ (m^2/s)	$1{,}3 .10^{-6}$ (m^2/s)

tab. 10 : results of thermal diffusivity estimation

10.4.3. Used geometry

Although geometry is not supposed to play a big role outside of binding the isotherms, it is convenient to adjust it early, for it is the most easy parameter to measure, and the most reliable.

The following geometry is used in the simulation :

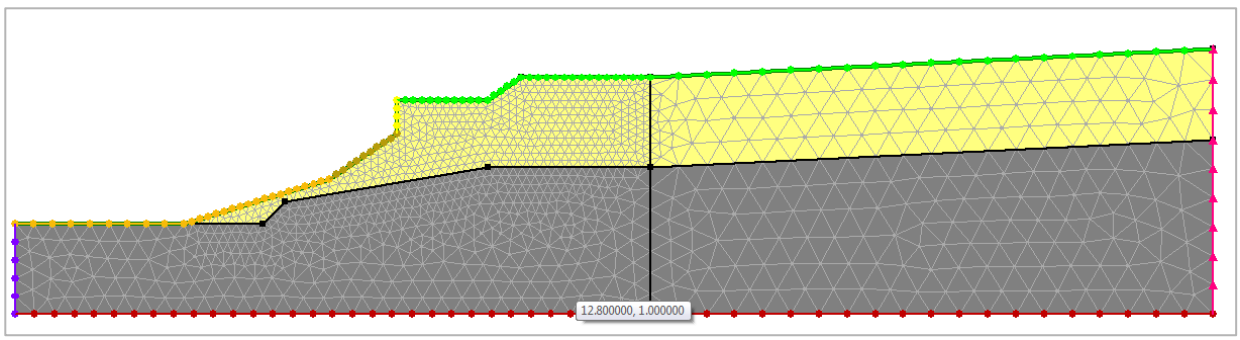

fig. 89: geometry and mesh used for Finite Element Method simulations at Vestpynten

10.4.4. Water content estimation

In Vestpynten, thermal diffusivity is high enough for the water enthalpy to have little effect. The water content is therefor not easy to estimate.

Later during the study, as a “dry” soil model seemed to match pretty well the experimental measurements, the effect of water enthalpy has been decided to be neglected, and the water content be put to zero.

NB : That does not mean the water has no effect. It appears under the variation of thermal diffusivity during freezing/melting, which is rather high.

10.5. Thermal simulations

After the model is build, a first simulation has been run. In order to verify the adequacy with the site, the thermal string 2 has been chosen for comparison with the calculation results.

10.5.1. First simulation, adjustment of bottom boundary conditions

With the parameters defined in table 10, the first simulation was rather straightforward and the results did fit rather well. The figure 90 shows a comparison of the temperature profile measured by the thermal string Vest 2 and a measurement at a corresponding location in the numerical model. The figure 91 displays the annual temperatures at different depths.

The first important result is the poor fitting of the temperature profile at depths below 5 m. The temperatures displayed by the measurements seem to converge toward -1,5°C instead of the -2°C of the bottom boundary condition. A small adjustment of the last was therefor necessary. The figure 92 shows the new temperature profile.

The left boundary condition, representing the sea also has been tested, but seems to have little to no effect upon the temperature below the cliff.

The temperature profile shows a very good fit for summer temperatures, but react poorly in winter, especially the first three meters. This could suggest an influence of the surface conditions on the slope, those are way more affected by snow in winter. The second simulation will try to handle this problem.

10.5.2. Second simulation, adjustment boundary conditions on the shore

Thanks to the thermal string deployed on the shore, it is rather easy to adapt the boundary conditions. Indeed, the temperature displayed is rather different from the surface temperature measured on the land side.

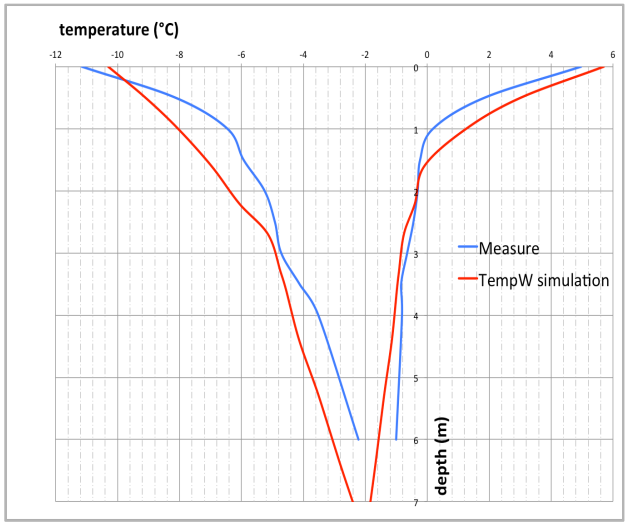

fig. 90 : temperature profile after first simulation at Vestpynten

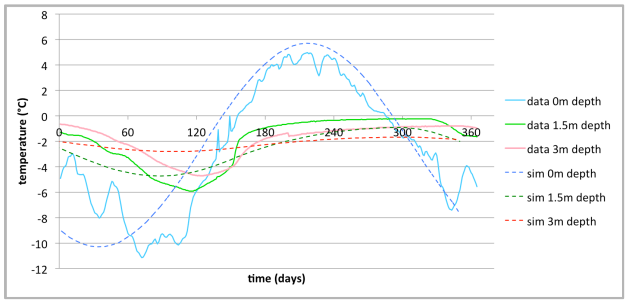

fig. 91 : annual temperatures after first test at Vestpynten

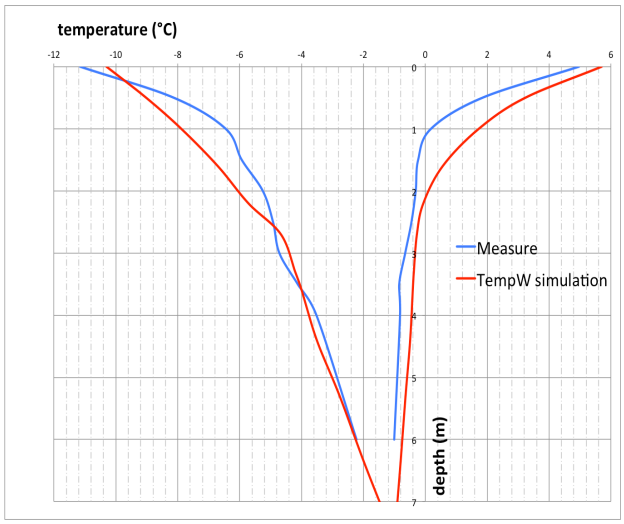

fig. 92 : temperature profile after first simulation and adjustment of permafrost under the beach

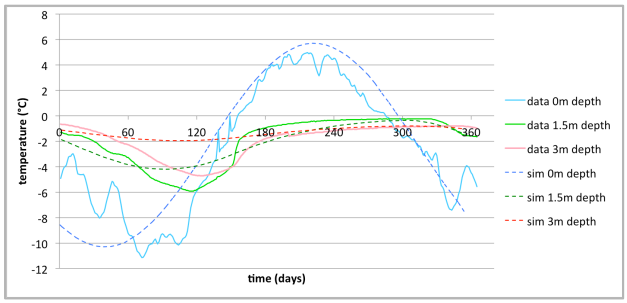

fig. 93 : annual temperatures after adjustment of permafrost under the beach

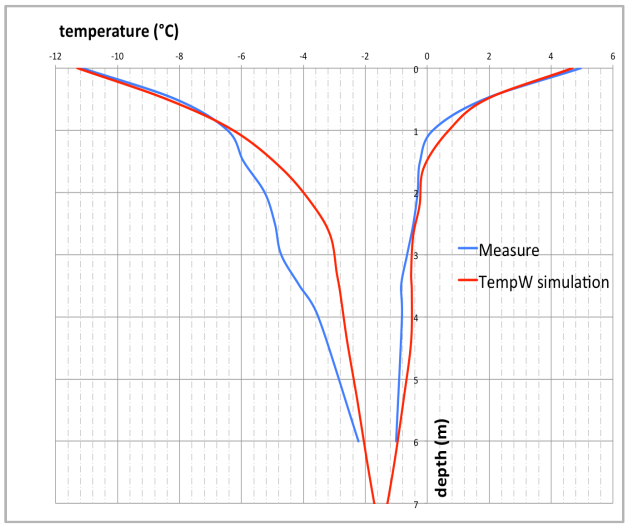

fig. 94 : temperature profile after second simulation, adding bluff boundary conditions

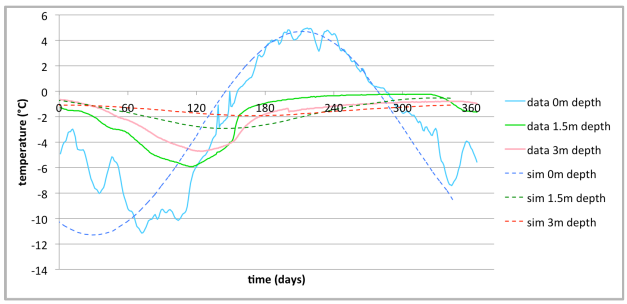

fig. 95 : annual after adding bluff boundary conditions

It has been decided to divide the shore surface in three parts, corresponding to the three different slopes, for practical reasons.

Several models for bluff surface temperatures where tested, including sinusoidal and crenel approximations. They are displayed in Appendix B. Finally, a sinusoidal approximation based on the mean annual temperature and amplitude did present the best match and was kept for further simulations. The modification of bluff surface condition seems to greatly improve the precision for the first meter below the surface (see figure 94). This is not surprising, considering the 1 m vertical cliff, and the great influence it shall have according to the "corner" model . However, after 1 m the slope decreases to 45°, and according to the formula (9.4), its influence is affected by a factor : $1 + a.\cos(\theta) = 1{,}86$.

Therefore, the curve still fits very poorly in winter for depth 1 m to 5 m.

10.5.3. Third simulation, addition of a virtual layer

As the results kept being surprisingly poor-fitting for minimal temperature between 1 and 5 m depth, a close observation of the measurement shows that the inflexion of the temperature profile characteristic of a brutal change in thermal conductivity is situated at 1 m below the surface, in the midst of the gravel layer. However, as the influence of the cliff explain pretty well this behavior in summer, it seems not sufficient in winter.

Those results suggest that in winter, the local thermal diffusivity of the gravel layer between 1 m and 3 m depth increases much more than what has been previously thought, becoming very close to that of the bedrock below. Hand calculations based on the inclination of the temperature profile between 1 and 3 m depth lead to a frozen conductivity of 2,6.

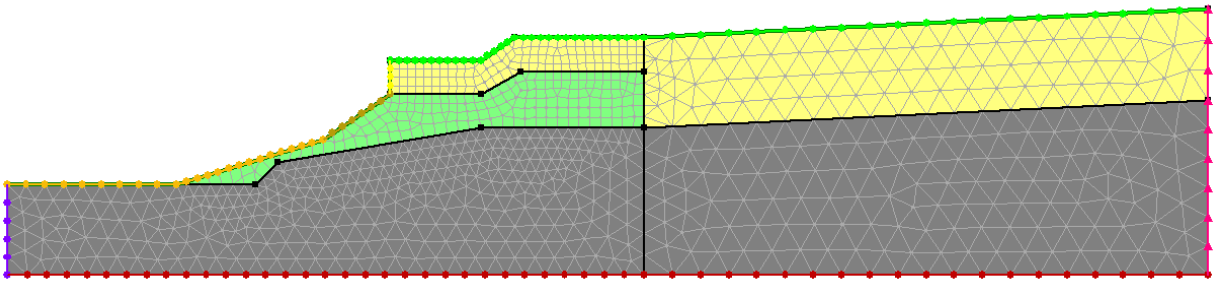

fig. 96: geometry and mesh used for Finite Element Method simulations at Vestpynten, after addition of a new layer (in green)

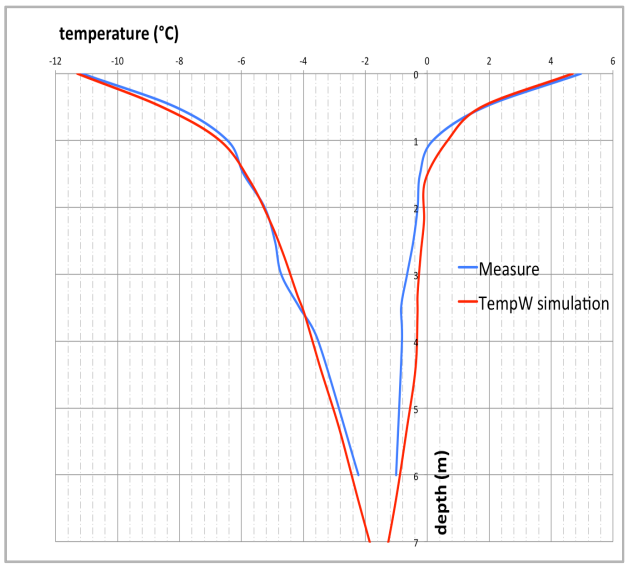

fig. 97 : temperature profile after third simulation, addition of a new layer under the bluff

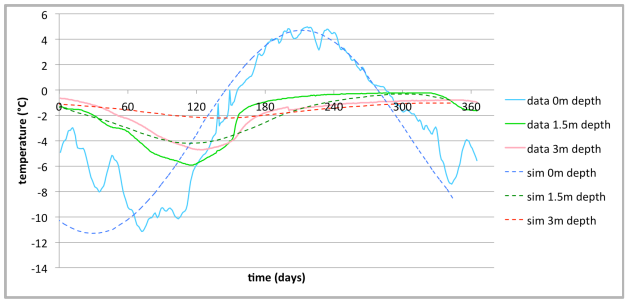

fig. 98 : annual temperatures after addition of a new layer under the bluff

In order to verify this hypothesis, a new material has been designed. Its unfrozen conductivity stays at 1,3 $.10^{-7}$ m^2/s, but the frozen diffusivity is set to 1,04 $.10^{-6}$ m^2/s. The position of this new layer is designed according to the figure 96. The resulting temperature profile and annual variations are displayed in figures 97 and 98. They seem to fit very closely to the measurements.

10.6. Conclusion

The final version of the model has a very satisfying match (see fig. 97) with the measurements from the field. However, they shall be taken carefully, for many a physical phenomenon does not have been taken in account.

First, the effects of water enthalpy have been neglected. It would seem that, with the thermal properties that have been calculated, its effects can be assimilated as an increased heat capacity. However, it is hard to tell only from temperature measurements which part is due to the material heat capacity and which is due to the latent heat.

Second, non-conductive like water displacement into the ground have been neglected. Such movements could disturb the results in summer. In particular, it is a possible explanation of why the temperature in summer between 1 and 5 meters is slightly below that of the model. The melting ice, at 0°C, transport its heat while leaving this layer. This possibility is reinforced by the suggestion that the “new layer” introduced in 11.5.3 has huge changes in water content.

The most surprising suggestion coming from this study is the existence of an area near the shore, where the thermal diffusivity varies enormously (1,3 $.10^{-7}$ m^2/s to 1,3 $.10^{-6}$ m^2/s) between summer and winter. Conductivity and heat capacities changes because of the freezing of porous water is not uncommon, but are of a limited extend : ice heat capacity is only twice smaller than that of water, and its thermal resistance is about twice that of water also. Thus, even a material that is almost only water should have a diffusivity variation above 300% by freezing.

The study in 3.2 suggests that such a difference could be explained by a change in water content. During summer, the gravel would be near dry and have a low thermal diffusivity (1,3 $.10^{-7}$ m^2/s), and in winter be saturated with a thermal diffusivity boosted. This paper shall not explain how such a variation in water content is possible in this situation. However, the huge variation of permeability that goes with the freezing of the water content, in particular in very permeable soils like the poorly sorted gravel present at Vestpynten, could be a good start point.

Those simulations also tell a bit about the role of the snow cover. The difference between the temperature profiles before and after the addition of particular boundary conditions on the shore (protected by the snow cover) shows that it prevents positive temperatures to be reached below 1 m depth. Thus a 1 m thick layer near the surface is prevented to melt completely in summer. Given the influence of the active layer depth suggested by McRoberts and Morgenstern (see chapter 5), this could have a huge impact upon the slope stability and the erosion rate.

The geometry also has a strong influence. The curves show a very different behavior in the first meter below the surface corresponding to the vertical cliff, and the second meter that correspond a gentler slope. Even without the snow cover, the shore materials act as a partial protection against thawing for the 2nd and 3rd meters of the gravel layer. The expected effect is rather similar to that of the snow layer. A coast with a higher vertical cliff would therefor probably experience thawing at a bigger depth, leading to an increased erosion rate. A complete study of the thermal process should therefore account for the evacuation rate of the scrap materials ripped from the cliff, and the resulting slope on the shore.

Yet another suggestion of this study is the impact of the warming of the permafrost. This is plainly showed by the difference between the temperature profiles in 11.5.1. At Vestpynten, the permafrost's temperature is higher than the surface temperature, meaning that it introduces a thermal gradient rather similar to the geothermal gradient (see 4.9). This can shifts the entire profile toward positive temperatures. That is why the temperature profile calculated with a -2°C

permafrost seems shifted to the left (lower temperatures) compared to the actual profile. Therefore, a complete study of the erosion rate should account for the warming of the permafrost, which is evidenced by the difference in its temperature near the shore and deep in the land.

11. Conclusion

11.1. Achievements

Trough this thesis, a toolbox has been constituted for thermal analysis of arctic shores, with a special focus on soil characteristics that are easy to measure in the field and monitor for a special interest area. Those tools have been specifically designed for handling thermal abrasion problems on the Arctic shoreline. They also aims at enabling a better understanding of the parameters ruling heat transfer in those soils.

A special interest has been observed in thermal conductivity estimation. Although it could be far more convenient to measure in the field, the study (Farouki, 1981) shows that huge variations, both in space and time, makes measurements hard to interpret. Meanwhile, the critical factors for thermal diffusivity calculations, namely the frozen and unfrozen water contents, are hopefully rather easy to obtain, for basically it needs nothing but an oven and a weighting scale to get. Thus, a quick estimation based on data at hand and a good knowledge of the models available could be far more profitable and cheap.

Moreover, the understanding of the mechanisms behind the soil thermal diffusivity highlights the critical factors that make every shoreline different. Not only will that help a geotechnical engineer to quickly grasp the potential for heat transfers in his shore area, but it can also be used to design innovative materials able to control the soil temperature.

The toolbox developed trough this thesis contain simple and precise numerical models that have been successfully tested and calibrated. The purpose is not to replace a powerful finite element software such as TempW, that shall appears as a straightforward way to design a shore installation. But trough the simple theoretical models, a clever geotechnical engineer shall get a wider view of the processes at work and the critical parameters. This understanding is at the basis of a complete thermal analysis and enables innovative designs.

Finally, the confrontation of the toolbox to an actual coastal area at Vestpynten, in addition to verify its adequacy, provides powerful insights of the mechanisms at work in this place. This suggests that those tools can help geologists and coastal engineers to have a better understanding of the impacts of different factors upon the coast, such as human activities and climate changes. For example, the conclusion of the case study highlights the increased depth of thawing due to permafrost warming.

11.2. Further work

It cannot be emphasized enough that those models have to be handled in complement of a true slope stability analysis. Although a thawing soil is by nature very vulnerable, the extend of this vulnerability depends widely on the soil nature. Thus, the development of a Thermo-Hydro-Mechanical Coupled analysis is of a crucial importance. Two approaches are currently in development at the Norwegian University of Science and Technology (NTNU), Trondheim, using Finite Element Method, one trough the software Plaxis and the other with Isogeometric Finite Element Method (IFEM).

As a sedimentary coast is in constant balance between sea actions and slope stability, a complete analysis shall also include a proper erosion model. Fortunately, this work is also undergoing into the SAMCoT group, and should allow for proper modeling.

Finally, one of the ultimate purposes of the study of erosion processes is to prevent or control them. That is a part of the Work Package 6 of SAMCoT, and hopefully the people facing this challenge will be able to rely on this toolbox.

12. References

Alter A. J., 1969, *water supply in cold regions,* U.S. Army Cold Regions Research and Engineering Laboratory, Monograph 11-C5A

Andesland B. and Ladanyi B., 2004, *Frozen Ground Engineering*, 2nd ed., Wiley, USA

Bahrami M., 1980, *Natural Convection*, Simon Fraser University, ENSC 388 (F09)

Bourbonnais J. and Ladanyi B., 1985, The mechanical behavior of a frozen clay down to cryogenic temperatures, 4th International Symposium on Ground Freezing, Sapporo, Japan, ed. Balkema, Vol 2, pp. 237-244

Caline F., 2010, *Coastal sea-ice action on a breakwater in a microtidal inlet in Svalbard*, Norwegian University of Science and Technology, PhD thesis

Crory F. E., 1973, Settlement associated with the thawing of permafrost, *Proceedings 2nd International Conference on Permafrost*, Yakutsk, U.S.S.R., North American Contribution., Washington D.C., National Academy of Sciences, pp. 599–607.

Davidson-Arnott R., 2010, *Introduction to Coastal Processes and Geomorphology,* Cambridge University Press

De Vries D. A., 1966, Thermal Properties of Soil, chapt. 7 in *Physics of plant environment*, ed. W. R. Van Wijk, Amsterdam

Fourier J., 1822, *Théorie Analytique de la Chaleur*, Firmin Didot, Paris

Farouki O., 1981, *Thermal Properties of Soils*, U.S. Army Cold Regions Research and Engineering Laboratory, Monograph 81-1

Farouki O., 1982, *Evaluation of Methods for Calculating Soil Thermal Conductivity*, CRREL report 82-8

Gemant A., 1952, How to compute thermal soil conductivities, *Heating, Piping and Air conditioning*, vol. 24, no 1, pp. 122-123

Guegan E.B.M., Sessford E.G. and Schomacker A., (submitted), Time-lapse aerial photography reveals significant coastal erosion on Svalbard, Norwegian high Arctic

Johansen O., 1977, *Thermal Conductivity of Soils*, Cold Regions Research and Engineering Lab, Hanover

Johnston G. H., 1981, *Permafrost Engineering Design and Construction*, Wiley, Toronto

Jorgenson M. T. and Brown J., 2005, Classification of the Alaskan Beaufort Sea Coast and estimation of carbon and sediment inputs from coastal erosion, *Geo-Marine Letters*, vol. 25, pp. 69-80

Kane D. L., Hinkel K. M., Goering, Hinzman L. D., Outcalt S. I., 2001, Non-conductive heat transfer associated with frozen soils, *Global and Planetary Change*, vol 29, no 3-4, pp. 275-292

Kanevskiya M., Shura Y., Jorgenson M. T., Pingc C. L. Michaelson G. J., Fortierd D., Stephania E., Dillona M., Tumskoye V., 2013, Ground ice in the upper permafrost of the Beaufort Sea coast of Alaska, *Cold Regions Science and Technology,* vol. 85, pp. 56–70

Kersten M. S. 1949, Laboratory Research for the determination of the thermal properties of soil, ACFEL Technical Report 23

Konrad J. M. and Morgenstern N. R., 1981, R*evue Canadienne de Géotechnique*, vol 18 no 4, pp. 482-491

Kunii D. and Smith J. M., 1960, Heat transfer characteristics of porous rocks, *American Institute of Chemical Engineers Journal,* vol. 6, no 1, pp. 71-78

Lantuit H., Overduin P. P., Couture N., Wetterich S., Atkinson D., Brown J., Cherkashov G., Drozdov D., Forbes D., Graves-Gaylord A., Grigoriev M., Hubberten H. W., Jordan J., Jorgenson T, Ødegård R. S., Ogorodov S., Pollard W., Rachold V., Sedenko S., Solomon S., Lim M., Rosser N. J., Allison R. J., Petley D. N., 2012, Erosional processes in the hard rock coastal cliffs at Staithes, North Yorkshire, *Geomorphology*, vol. 114, pp. 12-21

Lantuit H. and Pollard W. H., 2008, Fifty years of coastal erosion and retrogressive thaw slump activity on Herschel island, southern Beaufort Sea, Yukon Territory, Canada, *Geomorphology*, vol. 95, pp. 84-102

McGaw R., 1969, Heat conduction in saturated granular materials, Effects on Temperature and Heat on Engineering Behavior of Soils, Highway Research Board special report 103, pp. 114-131

McRoberts E.C. and Morgenstern N. R., 1974, The stability of thawing slopes, *Canadian Geotechnical Journal*, vol. 11, no. 4, pp. 447-469

Mickley A. S., 1951, The thermal conductivity of moist soil, *American Institute of Electrical Engineering Transactions*, vol. 70, pp. 1789-1795

Morgenstern R. and Nixon J. F., 1971, One-dimensional consolidation of thawing soils, R*evue Canadienne de Géotechnique*, vol 8, pp. 558-565

Nixon J. F. and McRoberts E. C., 1973, A study of some factors affecting the thawing of frozen soils, R*evue Canadienne de Géotechnique*, vol 10, pp. 439-452

Pullman, E, Jorgenson, M. T. and Shurt, Y., 2007, Thaw Settlements in Soils of the Arctic Coastal Plain, Alaska, *Arctic, Antarctic and Alpine Research*, vol 39 no 3, pp. 468-476

Rodzik J. and Zagorski P., 2009, Shore ice and its influence on development of the shores of south-western Spitsbergen, *Oceanological and Hydrobiological Studies*, vol. 38, pp. 163-180

Smith W. O., 1942, Thermal conductivity of dry soils, *Soil Science*, vol. 53, pp. 435-459

Steenhuisen F., Streletskaya I. and Vasiliev A., 2012, The Arctic Coastal Dynamics Database: A New Classification Scheme and Statistics on Arctic Permafrost Coastlines, *Estuaries and Coasts,* vol. 35, pp. 383-400

Taylor G. S. and Luthin J. N., 1978, A model for coupled heat and moisture transfer during soil freezing, R*evue Canadienne de Géotechnique*, vol 15, pp. 548-555

Teixeira S. B., 2006, Slope mass movements on rocky sea-cliffs: A power-law distributed natural hazard on the Barlavento Coast, Algarve, Portugal, *Continental Shelf Research,* vol. 26, pp. 1077–1091

Varnes D. J., 1958, Landslides types and processes, *Landslides and engineering practice*, ed. Eckert E. B., Highway Research Board, Special Report no 29, pp. 20-45

Woodside, W. and Messmer, J. M., 1961, Thermal Conductivity of Porous Media, *Journal of Applied Physics*, vol. 32, no 9

Appendix A : establishment of a climate model

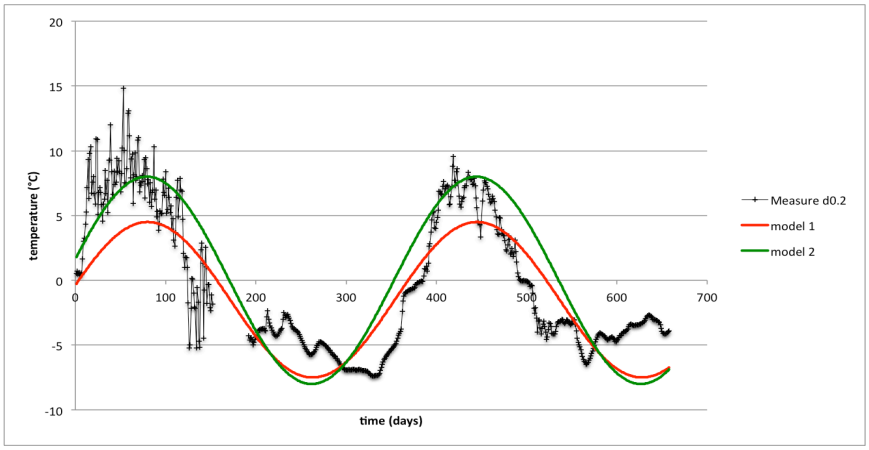

Measurements from string 6 at 20 cm depth, along with sinusoidal attempts to model it. The model 1 is based on the lowest amplitude, the model 2 on the highest amplitude.

Standards deviation with measurements is of 6,1 for M1 and 10,6 for M2.

These models were finally discarded because of the high standard deviation the measurements have when compared with the model.

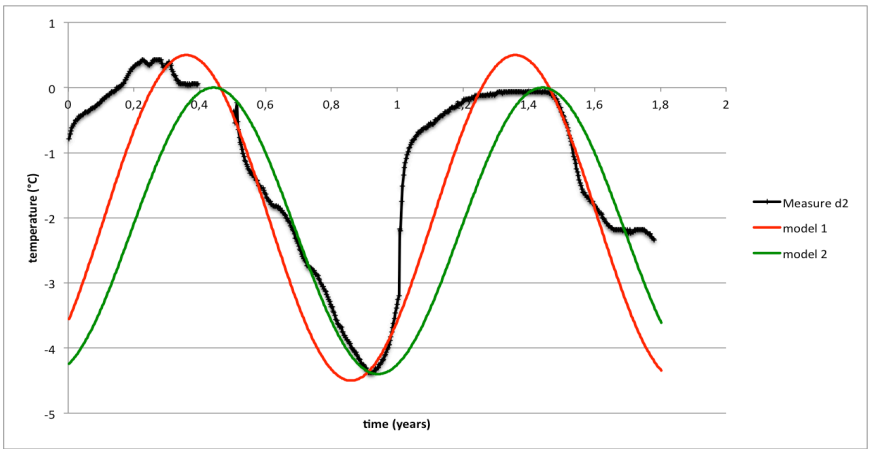

Measurements from string 6 at 2 m depth, along with sinusoidal attempts to model it. The model 1 is based on the highest amplitude, the model 2 on the lowest amplitude.

Standards deviation with measurements is of 0,04 for M1 and 0,06 for M2.

These models were finally discarded because a boundary condition based on the 2 m deep measure would impeach the modeling of the first layer.

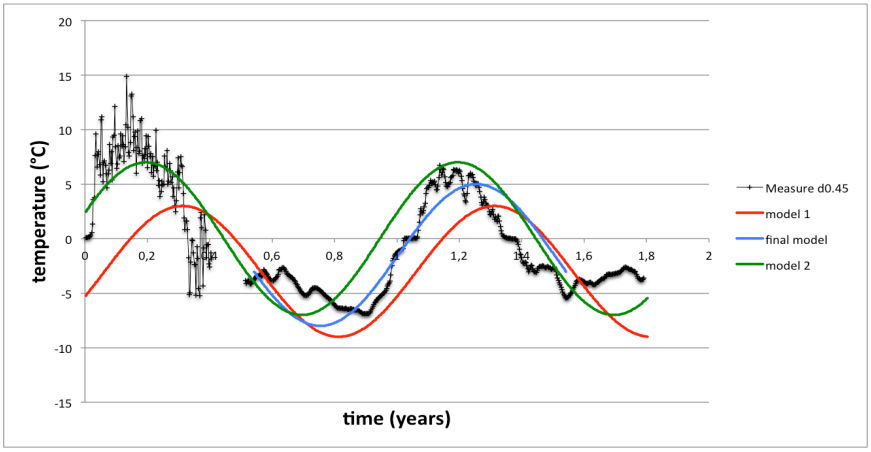

Measurements from string 6 at 45 cm depth, along with sinusoidal attempts to model it. The model 1 is based on the lowest temperatures, the model 2 on the maximum temperatures. The blue curve represents a mean of the two and was the final choice.

Standards deviation with measurements is of 0,16 for M1 and 0,16 for M2.

The final model, in blue, was chosen for its low standard deviation (0,12) when compared to the measurements, and its flexibility of use.

Appendix B : models for bluff boundary condition

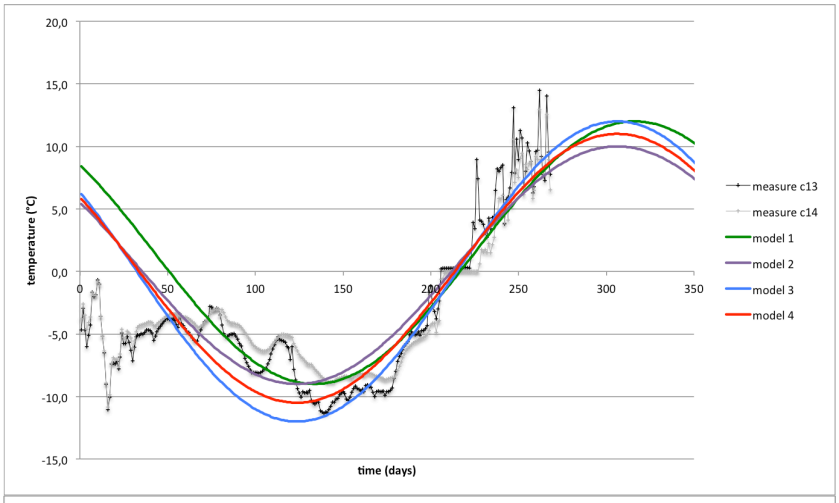

Measurements from the thermistor string deployed on the beach, against models that shall be tested as boundary condition.

This representation concerns the vertical cliff.

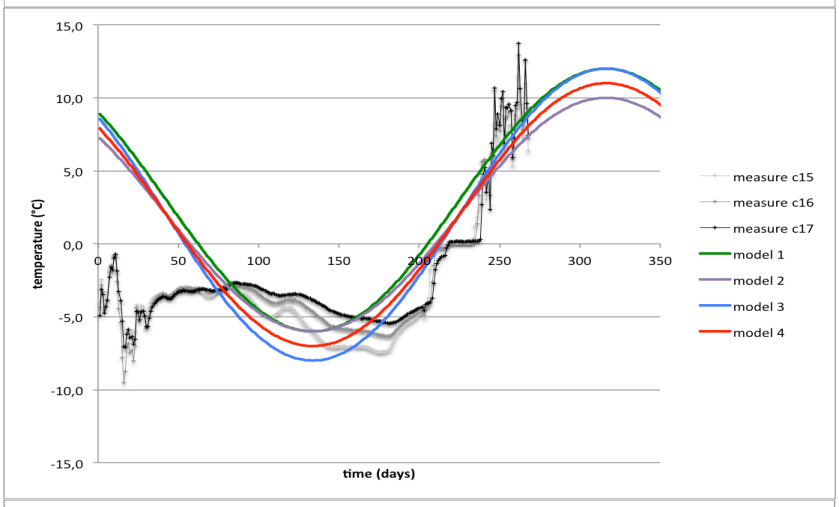

Measurements from the thermistor string deployed on the beach, against models that shall be tested as boundary condition.

This representation concerns the slope at the foot of the vertical cliff.

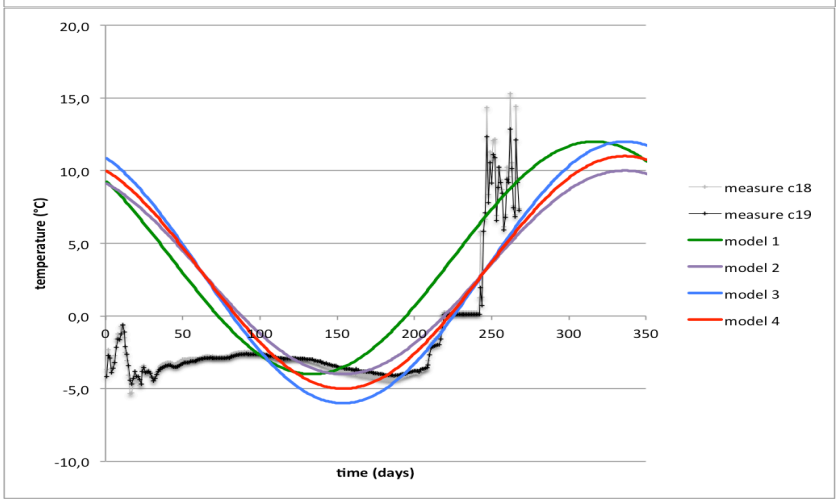

Measurements from the thermistor string deployed on the beach, against models that shall be tested as boundary condition.

This representation concerns the beach near the sea.

Appendix C : thermal diffusivity calculations

Measures

Max	13,903	15,495	14,8725	9,5425	6,715	4,37	2,56	1,075	0,1	-0	-0,5	-0,68	-0,915	-1	-1,18	-1,37	-1,37
Mean	-1,4489	-1,496	-1,6652	-1,7317	-1,5999	-1,7399	-1,5702	-1,744	-2	-2	-1,8852	-1,9267	-1,9525	-1,7926	-1,9471	-2,1183	-1,8547
Min	-18,733	-15,9	-11,948	-7,385	-6,885	-6,43	-5,87	-5,2325	-5	-4	-4,045	-3,6975	-3,635	-3,4825	-3,25	-2,81	-2,31
depth	-0,2	-0,45	-0,7	-0,95	-1,2	-1,45	-1,95	-2,45	-3	-3	-3,95	-4,45	-5,45	-6,45	-7,45	-8,45	-9,45

reference depth		Upper layer						mean
ref 0.2	unfroz	4,15E-06	6,47E-07	1,30E-07	1,30E-07	1,27E-07	1,67E-07	1,38E-07
	froz	3,54E-05	1,27E-07	6,20E-08	1,38E-07	2,54E-07	5,09E-07	2,18E-07
ref 0.45	unfroz	9,16E-06	5,12E-07	2,47E-07	1,75E-07	1,71E-07		1,98E-07
	froz	1,23E-06	1,90E-07	2,63E-07	3,65E-07	5,47E-07		5,18E-07
ref 0.7	unfroz	1,86E-06	4,36E-07	2,52E-07	2,20E-07			2,36E-07
	froz	3,76E-07	4,76E-07	6,34E-07	8,79E-07			5,91E-07
ref 3.95								
ref 4.45								
ref 5.45								

Result Max	1,3 e-07
Result Min	5,5 e-07

	Lower layer						mean
unfroz	2,01E-07	7,82E-07	9,61E-07	1,74E-06	2,71E-06	1,79E-06	1,36E-06
froz	1,87E-08	1,70E-07	5,23E-07	1,05E-06	1,93E-06	4,13E-06	1,30E-06
unfroz	7,11E-07	9,62E-07	1,96E-06	3,24E-06	1,93E-06		1,76E-06
froz	5,81E-08	2,54E-07	5,86E-07	1,14E-06	2,42E-06		8,90E-07
unfroz	3,42E-07	1,22E-06	2,51E-06	1,50E-06			1,39E-06
froz	5,42E-08	2,22E-07	5,41E-07	1,27E-06			5,22E-07

Result Max	1,3 e-06
Result Min	1,3 e-06

example : this cell is the diffusivity calculation between the depth 1,2 m (above the cell) and the "reference"depth 0,2 m (to the left). And it is a frozen diffusivity.